uOttawa

L'Université canadienne
Canada's university

FACULTÉ DES ÉTUDES SUPÉRIEURES ET POSTOCTORALES

u Ottawa

L'Université canadienne
Canada's university

FACULTY OF GRADUATE AND POSDOCTORAL STUDIES

Michael Fancy
AUTEUR DE LA THÈSE / AUTHOR OF THESIS

M.A.Sc. (Mechanical Engineering)
GRADE / DEGREE

Department of Mechanical Engineering
FACULTÉ, ÉCOLE, DÉPARTEMENT / FACULTY, SCHOOL, DEPARTMENT

Design, Analysis, and Fabrication of a Prototype Non-invasive System for Assessment of Biological and Synthetic Tissues

TITRE DE LA THÈSE / TITLE OF THESIS

A. Fahim
DIRECTEUR (DIRECTRICE) DE LA THÈSE / THESIS SUPERVISOR

R. Munger
CO-DIRECTEUR (CO-DIRECTRICE) DE LA THÈSE / THESIS CO-SUPERVISOR

EXAMINATEURS (EXAMINATRICES) DE LA THÈSE / THESIS EXAMINERS

M. Labrosse

J. Sasiadek

Gary W. Slater
LE DOYEN DE LA FACULTÉ DES ÉTUDES SUPÉRIEURES ET POSTDOCTORALES /
DEAN OF THE FACULTY OF GRADUATE AND POSTDOCORAL STUDIES

Design, Analysis, and Fabrication of a Prototype Non-invasive System for Assessment of Biological and Synthetic Tissues

Michael A. Fancy

A thesis submitted to the Faculty of Graduate and Postdoctoral Studies
in partial fulfillment of the requirements of the degree of
Masters in Mechanical Engineering

Ottawa-Carleton Institute for Mechanical and Aerospace Engineering
University of Ottawa
Ottawa, Canada

Supervisors: Dr. Atef Fahim and Dr. Rejean Munger

Your file Votre référence
ISBN: 0-494-11267-0
Our file Notre référence
ISBN: 0-494-11267-0

To my Wife Karen Louise Fancy and Daughter Sarah Elizabeth Fancy

Acknowledgements

The author would like to thank Dr. Fahim for his valuable engineering insight that was used in the design. Dr. Munger provided the author with not only a thorough understanding of optical instrumentation, but also an excellent learning environment through his visual optics lab at the University of Ottawa Eye Institute. The author would also like to thank Dr. May Griffith for the use of lab space and equipment provided, as well as the assistance of many of her staff members. The author would also like to thank Dr. Heather Sheardown for the engineered samples for optical testing. Dr. Jacob Sivak provided valuable feedback related to his knowledge of testing bovine ocular lenses. Additional feedback was also provided by Mr. David Priest, Dr. Linda Marchese, Dr. Neil Lagali and Mr. Malik Hakim. Assistance in preparing biological samples was provided by Dr. Sandy Vascotto, Ms. Donna Bueckert and Ms. Cecilia Becerril. Mr. Brent Cotter at the University of Ottawa Mechanical Engineering machine shop also provided high quality machined parts, which aided in the overall system quality.

Most of all, I would like to thank my wife Karen and daughter Sarah for their patience and support over the last several years, without which this work would not have been possible.

Abstract

A new instrument system for the non-invasive assessment of biological systems has been designed, built and validated. This system utilizes the optical characteristics of a biological system to assess both its static and dynamic response over time. The changes in the optical properties can then be used to quantify the response of the biological system to external or internal stimuli. This new system incorporates an efficient light delivery system, as well as a novel light collection system to provide high repeatability, reproducibility, sensitivity, and detection thresholds. The system incorporates simultaneous measurement of transmitted light, forward scattered light, specularly reflected light, and non-specularly reflected light in across the visible spectrum, to provide flexibility in the biological systems that can be measured. It is shown that typical values are 0.02% for repeatability and 0.15% for reproducibility. Sensitivity in transmission and backscatter measurements was improved by a factor of 20 compared to a previously built instrument, which was the basis for the new design. The system is capable of detecting light attenuated down to 0.0063% of the maximum intensity, resulting in a superior threshold. The system was then validated by measuring the optical properties of various biological samples, both natural and engineered. These samples include bovine, porcine, and human corneas and lenses, as well as synthetic materials. Biological sample testing were consistent with published results on the back vertex distance (BVD) test (bovine lenses), the bovine corneal opacity test (BCOP, bovine corneas), and published results obtained with the precursor to the new device.

Table of Contents

List of Figures

List of Tables

Acronyms

ACRONYM	MEANING
DVM	digital volt meter
FSL	forward scattered light
POC	proof of concept
NSRL	non-specularly reflected light
SRL	specularly reflected light
TL	transmitted light

Metrological Terms

TERM	DEFINITION
Accuracy	the closeness of the agreement between the result of a measurement and a true value of the measurand [24].
Drift	slow change of a metrological characteristic of a measuring instrument [24].
Measurand	a particular quantity subject to measurement [24].
Measurement	a set of operations having the object of determining a value of a quantity [24].
Precision	the closeness of agreement between independent results of measurement obtained under stipulated conditions [24].
Repeatability (of results of measurements)	(qualitative): the closeness of the agreement between the results of successive measurements of the same measurand carried out under the same conditions of measurement. (quantitative): the standard deviation (σ) of the measurement results [24].
Reproducibility (of results of measurements)	(qualitative): the closeness of the agreement between the results of measurements of the same measurand carried out under changed conditions of measurement. (quantitative): the standard deviation (σ) of the measurement results [24].
Sensitivity	the change in response of a measuring instrument divided by the corresponding change in the stimulus [24].
Threshold	the limit below which a stimulus causes no reaction [25]

Glossary

TERM	DEFINITION
entrance pupil	see Appendix B: Optical Concepts
exit pupil	see Appendix B: Optical Concepts
intensity	the power per unit solid angle of a source [23]
irradiance	the power per unit area or flux density on an illuminated surface [23]
radiance	the power per unit solid angle per unit projected area [23]

1 Introduction

1.1 Biological and Non-biological Systems

In industry and research, there is a demand to expand the available testing capabilities to monitor the change in health of biological and non-biological materials. As the cost related to improper assessments can be significant, high performance measurement systems are required. These testing capabilities can be based mechanical, electrical, or optical technologies, to name a few. One rapidly expanding technology is in the area of biophotonics, which can be defined as the application of photonics for synthesis, diagnosis, or treatment of biological or medical problems. There are also many examples of optical technologies in use for both biological and non-biological applications. Some of the optical technologies include fluorescence detection, surface plasmon resonance detection, raman spectrography, and near-infrared absorption.

1.2 The Need for Monitoring

The optical system developed in this thesis can be applied to a wide range of applications covering many industries. Tissue engineering is "expected to be one of the two largest growth areas in engineering" [1]. It follows that with development in this area, that there will be a corresponding increase in demand for new diagnostic tools. Toxicology is another area requiring improvements in available testing protocol, particularly because of the European Union Parliament decision to ban animal testing over the next five years [2]. One example of toxicology testing is the Draize test where substances that may prove harmful to humans are placed in the eye of a live rabbit with the physiological response converted to a test score, for which researchers have been trying to replace for decades [3, 4]. Water quality, is even more broadly accepted, even by the general public, as an area requiring the best diagnostic tools available [5]. Turbidity (relative clarity of a liquid) is one area of water quality as well, as the food packaging industry, that is a potential application for the system presented herein. Agriculture industries use light-based applications

to measure the optical properties of leaves [6]. In the automotive industry, where paint quality standards are very important to overall quality of the product, there is a high demand for non-invasive real-time screening systems [7].

An often-desired feature of a testing system is its non-invasive or non-destructive testing of the sample. By leaving the sample intact, it is available for any follow-up testing. As well, the same sample is used repeatedly, requiring a smaller number of samples, which in turn reduces testing costs. An assumption with destructive testing at multiple time points is that all of the samples would have produced similar results if measured following the same conditions, which is not necessarily true.

Monitoring techniques, from a biological point of view, can be classified as either *in vitro*- or *in vivo*-based. In vitro testing places fewer demands on the instrument system design, resulting in fewer regulatory issues and a reduction in development costs, and thus is the approach taken for the proposed system.

1.3 Attributes of the Proposed New System

The new optical measurement system will be presented that combines a number of key features, and can be used in many biological and non-biological applications. The system is non-invasive, manufactured with off-the-shelf components, and incorporates multiple tests, producing high quality objective results.

1.4 Organization of the Thesis

Firstly, a review of some of the optically based assessment systems currently available, including a summary of the limitations of working with biological systems is presented in Chapter two. The theoretical basis for the new system as well as its specifications are presented in Chapter three. The validation of the as-built design against specifications is presented in Chapter four. As the intended use for this system is biological applications, a series of tests on a selection of biological

samples to demonstrate its abilities is presented in Chapter five. Finally, a conclusion to this work in Chapter six provides a basis for subsequent research possibilities.

2 Literature Review

2.1 Introduction

There are many techniques available to analyze biological systems to determine their status or to measure the change in status. A mechanical system can be used to measure strain or fluid flow. Electrical technology could be used, for example, to measure ion count to indirectly determine the pH level. Optical measurements can be used to sense changes in colour, intensity, or shape. Chemical-based systems can be used, for example, to measure the reaction of biological samples to a known reagent. Furthermore, techniques may also be classified by their impact on the system during or after testing, or by their degree of invasiveness. An invasive test in one in which there is a measurable change in the sample after the test, such as with a dye, ionized molecules, or a change in organization. A test may also be classified as either *in vivo*, which is performed in the living body or organism, or *in vitro*, which is performed outside the living body.

This review focuses on biological assessment techniques that are optically based, as that is the basis for the system developed. Both invasive and non-invasive techniques are reviewed, noting that non-invasive techniques can be more difficult to develop due to the requirement to keep the biological system intact.

2.2 Bovine Corneal Opacity Test

The bovine corneal opacity (BCOP) test was developed by Gautheron *et al* in 1992 as an invasive test of various ocular irritants [8]. Bovine corneas are placed in a specially designed holder, which allows light to pass directly through the sample. The holder has two chambers that allow an irritant to be in contact with both the anterior (front) and posterior (back) surface of the cornea. Two separate optical tests are performed on the cornea: opacity and permeability, each performed on a separate sample. The opacity test compares the amount of light transmitted through the cornea to a control sample. The permeability test measures the uptake of a

fluorescein-based solution using the bovine cornea. A total weighted-score based on the individual scores of the two tests determines the relative impact of the irritant. In 1994, Gautheron *et al* further validated the test protocol by testing 52 substances at each of 12 European labs [9]. As a more complete assay-based test, the test goal was to develop an equivalency to an invasive live subject based irritancy test known as the Draize test. The BCOP test accurately correctly predicted that a sample was either an irritant or non-irritant for 96% of the tests. In 1996, Casterton *et al* introduced a test that modified three BCOP test parameters: a different instrument to measure opacity, a revised method for calculating the irritancy score, as well as a modified technique for dealing with solid irritants [10].

As two separate samples are tested, one for the opacity test and one for the permeability test, an assumption is made that both samples would have reacted similarly, which is not necessarily true. In addition, the initial conditions of the tissue are not used as a relative indicator. Again, as the initial condition of each sample is different, the final test results are therefore less reliable. A scale of 1-100 [8, 9] was created and then converted to a second scale of just three ranges to allow comparison to the Draize test. This final grouping improved their accuracy in predicting equivalency to the Draize test more easily, but at the cost of a coarser scale. The reliability of their data is also questioned based on their statement that similar results are obtained from fresh tissue, and tissue that is preserved for 48 hours [9]. As will be presented herein, optical properties of corneas change noticeably in the first 24 hours, post mortem. The results of this BCOP testing also indicated that as the toxicity levels increased, the variability between labs also increased. The revised technique used by Casterton *et al* did address the lack of comparing optical properties of the cornea prior to toxicity exposure. The opacity testing is performed at only one wavelength, namely 570nm [10]. By doing so, the test results do not consider any possible light tissue interaction at different regions of the visible spectrum (380 nm to 780 nm). Measurements were limited to only one point in time, and thus did not measure any temporal dependence on the optical properties, possibly resulting in variability in the irritancy score.

2.3 Flow Cytometry

Flow cytometry (FC), also referred to as microfluidics, is a newly emerging invasive test which measures the various properties of fluid as is forced through a thin wall measuring only tens of microns in diameter, with flows as low as a few nanolitres per second [11]. Examples of properties can include particle count, optical properties, or chemical properties. The driving force to move the fluid is often achieved with pneumatic pressure. Detection can be achieved using electrodes, fluorescence, scatter, UV-absorbance, electrochemicals, luminescence, or Raman spectroscopy. A multifaceted test assay is achieved by deflecting portions of the fluid down separate chambers, and can even include supplying a control substance for calibration purposes.

One example of flow cytometry takes advantage of the directional characteristics of the scattering of light when directed towards the cell. The quantity of light fluoresced in the same direction as the excitation source, known as forward angle light scatter (FALS), is proportional to the size of the cell contained within the fluid stream. The quantity of light scattered at right angles is proportional to the granularity of the cell [12].

FALS, although promising, has a number of issues to consider. Firstly, cell shape as well as cell homogeneity will affect FALS, requiring either the application of a correction factor, or a limitation of the cell size to be tested [12]. Secondly, a database of immunotoxins must be established before for full implementation. Finally, the ability to perform a number of simultaneous tests on single technology is limited by the degree of cross in the detected signal, which greatly reduces the specificity of the test [13].

2.4 Polarized Light Scattering Spectroscopy

Polarized light scattering spectroscopy (LSS) is a non-invasive technique that utilizes the light polarization characteristics from reflected surfaces of a test sample. When polarized light is directed towards a target sample, the spectrally reflected

light can be distinguished from non-specularly reflected light, as it undergoes multiple surface reflections. The non-specularly reflected light is eventually randomly polarized, distinguishing it from the specularly reflected light. Using this data, the cell size and degree of mutation can be calculated with further analysis, making it ideal for detecting cancerous cells. One such approach developed by Gurjar *et al* directs collimated light from an arc-lamp source through a series of spectral filters redirecting the reflected signal to a charged coupled device (CCD) [14]. The spectral filters provide an analysis across the visible spectrum of 450-750 nm enhancing the capabilities of the system.

This technique focuses solely on the scattering properties of the sample substance. Effective implementation is dependent on knowing the refractive index of the target cell, and that it remain constant over time. A tolerance analysis of this dependent variable was not provided. As well, the raw data must be analyzed using Mie Scattering Theory, adding a level of complexity, time, and cost to the procedure. In order to compare the two signals, separate images are required both with and without a second polarizer (analyzer) in place. The resulting time lapse between two measurements could affect measurements.

2.5 Back Focal Distance

The back focal distance test (BVD) used by Sivak *et al* is an irritancy test that utilizes the change in focal pattern of bovine lenses when exposed to an irritant. The tests maintain the tissues in a liquid medium until testing, which is 10 minutes in duration. For each of 22 points along the lens (across the equatorial axis), collimated light from a laser (615 nm HeNe) is directed at the lens and the resulting focal lengths are measured. Measurements are made before the irritant is applied and afterwards, up to 4 days. The BVD test has been utilized by several researchers [15-17] and has be used to test the impacts of dozens of irritants on the bovine lens. Results demonstrate the initial changes in optical properties, as well as near full recovery of the optical properties to the untreated state.

This test is based on refraction, and as such, only a tissue such as the crystalline lens can be used. The system utilizes a fixed-wavelength laser as its light source and in using such a narrow spectrum, as there may be a false change in signal due to a molecular interaction, for example. In addition, testing other wavelength ranges in the visible spectrum may reveal additional light-tissue interaction characteristics. It is also known from the results of other papers that scatter does vary by wavelength [18, 19]. Additional post-testing processes, such as video digitization, add to the time, complexity, and cost of the system. The method is based on the assumption that all irritants change the refraction of the lens. However, it is possible that an irritant could affect the strength of the light without impacting the refractive nature of the lens resulting in a false negative. As the measurement is performed in lasting about 10 minutes, the impact of hydration, which affects opacity and scatter of the light, cannot be neglected. The level of hydration can also impact on the overall shape of the lens, which in turn affects refractive power.

2.6 Corneal Instrument (U/O Eye Institute)

A system was developed at the University of Ottawa Eye Institute to measure the transmitted light and non-specularly reflected light form artificial corneas. This system is periodically referred to in this report as the predecessor to the system developed herein. Light from a halogen light source is directed through a user-selectable spectral filter and focused onto the sample. The transmitted light is compared to the signal with no sample present and the non-specular light from the sample is compared to the signal from a control with a known light scattering value. The system is able to monitor the changes in both optical properties of human and animal corneas over time and also proved beneficial in comparing optical properties of corneal constructs used in research in developing the artificial cornea [20]. The testing also revealed that there was a variation in optical strength as a function of the wavelength.

There are a several key issues regarding this design. Firstly, light is delivered

to the sample focused, not collimated. By focusing the light, the maximum light possible is concentrated in a small area, but the axial location must be positioned at a precise distance from the focusing lens to focus the maximum light unto the sample. Secondly, the non-specularly reflected light is measured using a ring of eight Si photodiode detectors that sense light at a specific azimuth above the sample. As well, there is no light captured in between the each of the eight detectors. As a result, there is no integration of the full non-specularly reflected light from the sample. The system does not measure the light that is scattered in the forward direction nor the light specularly reflected from the sample. The drift of the light source is accounted for and applied to the transmitted light but not to the non-specularly reflected light. The measured accuracy of the transmitted light is 5% and is not stated for the non-specularly reflected light.

2.7 Biological Materials: Working Limitations and Requirements

A review of some of the optically based biological assessment techniques has revealed some of limitations of these designs. As a result, a list of requirements can be generated for any new measurement system. Biological samples are very often spatially heterogeneous. As a result, the system should be designed to eliminate or reduce the impact of sample heterogeneity, if required. Even under ideal conditions, no two biological samples are unique. Thus, any testing system intended for biological samples must have a precision in measurements that exceeds the across-sample variation. Biological samples require a healthy environment to both survive and thrive. Although few testing methods can maintain a perfect living environment, every attempt should be made to provide the tissue with a medium that sustains such a healthy state. Basic cell/tissue survival leads directly to the requirement for a non-invasive testing protocol, that neither kills the sample outright, nor leaves a remnant of the testing procedure. The impact to tissue health can also be minimized by reducing the handling of the tissue, preventing or eliminating both mechanical damage as well as contamination concerns. By proper selection of a sample holder that is commercially available and approved for biological applications and incorporating it into the design, the long-term health of the tissue can be improved.

Many of the systems described here use a variety of optical techniques. An optimal design would incorporate many of these properties in a single testing system. As many possible light tissue interactions can occur, inclusion of multiple bulk measurements should be included in the design. Therefore, transmitted, forward scattered, specularly reflected as well non-specularly reflected light should be measured. The signal from any of these four signals can be weak, requiring that the new system detect very low light signals as well as maximum possible intensity levels. The measurement should be automated so that a preset test frequency can be implemented and a resulting peak temporal signal can be determined. Some papers have produced final optical test data using scales of 1-100 and some have used scales of 1-4. Therefore, the system should have a resolution of better than a scale of 1-100 to avoid being classified as qualitative.

With a review of various optical systems completed and knowledge of some of the limitations and requirements of working with biological samples in mind, a new system design is herein presented.

3 System Design

3.1 Theoretical Basis of the Optical Design

3.1.1 Optical Measurements

The result of light striking a transparent material can be a combination of transmittance (including refraction), reflectance, and absorbance. The transmittance can be composed of both transmitted and forward scattered light. Likewise, reflectance can be composed of specularly and non-specularly reflected light. The system described herein measures the bulk properties of transmitted, forward scattered, specularly reflected, and non-specularly reflected light, whether that light interaction occurs on the surface or inside the sample.

The transmitted light (Tr), as defined herein, is the percentage of incident light that passes perpendicularly through a sample. In general, the thicker the material, the lower the transparency for a given sample. Both the molecular structure and the bulk structure will also impact the transparency.

The forward scatter (FSc), as defined herein, is percentage of incident light that passes perpendicularly through a sample, and deflected to by 5° to 20° from the normal. Forward scatter in a transparent media is a function of the particle size. As the particle size approaches the wavelength of the light source, scatter increases in the forward direction. This effect, known as Mie scattering, is observed first with shorter wavelengths (i.e. 450nm) and increasingly so with longer wavelengths (i.e. 650nm). Therefore, for complete characterization, scatter must be measured as a function of the wavelength.

Specular reflection (RSp), as defined herein, is the ratio of light that when directed towards a smooth surface, reflects, according to Snell's law of reflection, at an angle equal to the angle of the incident light (for this system, perpendicular).

Non-specularly reflected light (RNSp) is all reflected light, which is not specularly reflected.

Fluorescence is the emission of light at a higher wavelength than the incident light, and while it can be measured is possible, is not part of the focus of this research.

Refraction of light through a medium is a function of the angle of incidence and the respective indices of refraction of two media. The curvature of a medium can refract rays either away from or towards a focal point. Refraction is not measured as part of this research, and as such, its impact is minimized by design.

The interaction of light with a biological media can be complex. It can be evaluated on a nanometer scale utilizing individual frequencies of light, or on a larger scale, which instead considers the bulk effect of these interactions. An ideal measurand of the light tissue interaction is irradiance, as it is direct, relatively easy to implement and does not require a complex analysis. Irradiance is the power per unit area projected on a surface. All the detectors measure irradiance, and as such, a ratio or normalized value will be calculated for each of the four above-defined optical properties.

3.1.2 Detailed Design Specifications

The detailed design specifications are the lower level design requirements that ensure that the system is effective for the intended application. These requirements stem partly from knowledge gained from other researchers as well as possible improvements to their work.

Four optical properties, or signals, are incorporated into the design: transmitted, forward scattered, specularly reflected, and non-specularly reflected light. These four optical properties are measured simultaneously, adding to the

flexibility of the design and the sum of these four signals, along with any absorption, is ideally unity. Therefore, if one of the signals from a sample is high, the others must be low. The expected operating range was chosen based on the immediate need to measure corneal tissues within the lab. Consequently, the system is designed for transparent tissues with the operating ranges as shown in Table 3-1.

Table 3-1: System Expected Operating Range

Optical Property	Expected Operating Range
Transmitted Light	60 – 100% of maximum illumination/intensity
Forward Scattered Light	2 - 10% of maximum illumination/intensity
Specularly Reflected Light	1 - 5% of maximum illumination/intensity
Non-specularly Reflected Light	5 – 20% of maximum illumination/intensity

For each of the four optical properties, the uncertainty of the measurements must be much less than the variability of the biological materials to ensure that the system is not the limiting factor. Based on previous experiments at this lab and by others (Gautheron 1994), the optical measurement variability across identical samples base is expected to be as high as 5%. The repeatability and reproducibility specification for each of the four optical properties is summarized in Table 3-2.

System sensitivity must be good enough to differentiate not only the changes between two different samples, but must also be able to track small relative changes in optical properties of a sample over a period of minutes. The target was established at the design phase, to exceed the performance of a system previously built at this lab (Priest, 1998), and improve on the scale of 1% used by Gautheron (Gautheron, 1994).

Table 3-2: System Repeatability and Reproducibility specifications

Optical Property	Repeatability (over expected operating range)	Reproducibility (over expected operating range)
Transmitted Light	< 1% of maximum intensity	< 1% of maximum illumination/intensity
Forward Scattered Light	< 2% of maximum intensity	< 2% of maximum illumination/intensity
Specularly Reflected Light	< 2% of maximum intensity	< 2% of maximum illumination/intensity
Non-specularly Reflected Light	< 2% of maximum intensity	< 2% of maximum illumination/intensity

The threshold, or minimum detectable light level, of the system follows from the expected operating ranged defined above, with the exception of the transmitted light, as it is much stronger than the other three signals. Therefore the threshold for each of the properties is set as such: 1% of maximum transmitted light, 2% of maximum forward scattered light, 2% of maximum specularly reflected light, and 5% of maximum non-specularly reflected light.

To calibrate the system, individual control targets are used for each of the four optical measurements. Controls are placed in the system, and therefore, their size and anchoring as well as their optical characteristics must be considered in their implementation in the system. The complete calibration of the system is described in Section 3.3.

The system is designed with the ability to measure across the visible spectrum in equal bandwidths for each of the four optical properties. Previous work on the BCOP test (Gautheron 1992, -1994, Casterton 1996) and on the BVD test (Sivak 1997, Hartwick 1997, Bantseev 2003) did not utilize the wavelength variation in their testing, but it is known that light/tissue response for transmitted light and

non-specularly reflected light varies by wavelength (Priest 1998). Therefore, in the present design, all properties are tested at five 40nm-wide spectral ranges centered at 450 nm, 500 nm, 550 nm, 600 nm, and 650 nm as well for the complete visible spectrum (approximately 380 nm to 780 nm).

The design incorporates a broadband incandescent light source (halogen) and not a laser for several reasons. Firstly, using a single wavelength laser could result in an interaction not typical of broader range. Secondly, incorporating lasers would require one unit for each of the ranges, and would not provide an evenly distributed spectral testing range, based on the available laser lines. Conversely, a singe broadband source, in conjunction with neutral density filters, can be readily implemented for a reasonable cost, and it can accommodate testing of different spectral regions within the visible spectrum.

The design uses a non-imaging illumination system. An imaging system forms an image (the light source, in this case) of the object at the sample plane, or image plane. A non-imaging system places the sample at the exit pupil and results in a less intense, but more uniform light distribution at the sample plane and is presented in more details in Appendix B: Optical Concepts. By delivering collimated light, there is less variation in the optical signal with small changes in tissue placement in the axial direction.

In utilizing a non-stabilize (low-cost) light source, fluctuations can occur in the illumination intensity of 1.5% to 10% depending on the source. As this system primarily targets small changes in irradiance at the detector, it is important to remove any impact of the variation in the source intensity. Therefore, the source intensity is continuously monitored so that all measurements are taken relative to source intensity, effectively eliminating the impact of source stability. By implementing this feature, there no need to wait for the system to warm up.

This system can be used for a variety of biological samples and therefore is

able to sample the optical properties inside a target area from 2 mm to 6 mm in diameter. A smaller diameter allows smaller samples to be tested, but in addition, smaller sections of larger samples can be tested to detect local variations. This variation is accomplished by changing the illumination area without changing the level of irradiance on the sample. The design incorporates a separate aperture that independently controls the beam irradiance on the sample. More details are provided in Section 3.1.3.

The sample will be placed on an aperture to allow passage of light and may not be able to structurally support itself. Vertical orientation of the sample would eliminate this sag but would also require an attachment point, which would place a strain on the tissue due to its own weight and therefore would change its optical properties. By aligning the tissue horizontally, an attachment point is not required thus adhering to the non-invasive design requirements. The new design has a series of interchangeable adaptor plates, depending on the application, with the first two plates designed to hold commercially available transparent culture chambers (trays). For optimal portability and space requirements existing within a lab, it is important to keep the footprint of the system less than $0.1m^2$ (~1 ft^2) and a height of less than 0.4m (~16").

Refraction errors in reading are reduced or eliminated by ensuring that a curvature is not introduced in the sample (located at the exit pupil) while under test. Any curvature in the sample can affect all of the measured optical properties, adding an additional, unwanted variable to the testing process.

By incorporating a holder that can contain a fluid, it is easier to maintain the health of the biological samples. Ideal conditions include adequate hydration levels and nutritional (growth mediums). The samples can be directly moved from the growth chamber to the instrument, without handling the tissue. The holder also ensures that the tissue is flat, minimizing the aforementioned refraction errors. The effect of the holder is compensated and described in more detail in Section 5.1.

3.1.3 Proof of Concept (POC) Design Process

The design process utilized optical knowledge, modeling of the collecting mirror optical efficiency using optical design software, and finally, verification using the as-built design (bench top) to achieve the same or similar results. The data from the bench test results were then analyzed for improvements as necessary.

A primary specification of this system is to increase the sensitivity of the measured light signal after it interacts with the sample, relative to previously designed system. This light is then emitted, collected, and detected. Design improvement can consider light collection, light detection, or both. A common method to detect light is by use of a standard photodiode. While increasing the area of this component is possible, there are a number of drawbacks. Most notable is the cost of such a device: the cost increases dramatically with area, to the point where it can be prohibitive. Another approach to improving the detected signal is to increase the collection efficiency of the system to bring more light to the detectors. The forward scattered and non-specularly reflected light are ideal candidates to apply improved optical collection efficiency, as they have a large angular spread in two dimensions, and for most samples, low signals. This optical method to improve collection efficiency can be implemented using a focusing/collecting mirror, or a lens. While, in general, both the electronic and optical methods can achieve the desired results, there are advantages in using a collecting mirror for this design. For a given size, a curved mirror is much lighter than a lens. Spectral flexibility is easier to implement with a mirror than with a lens, as chromatic aberrations must be considered in the lens selection. A mirror as a reflective device, can more easily fold or redirect optical paths, resulting in a more compact instrument. Before purchasing a reflecting mirror, a readily available (RA) mirror from the lab with a parabolic shape was used. Comparing the surface area of this mirror of 167 cm^2 and the surface area of the photodetector of 1.79 cm^2, results in a theoretical 93-fold increase in the capture area.

The mirror was then modeled in Zemax© optical simulation software (Zemax)

to determine the impact of tilting the mirror, as tilt is required to avoid obstruction of the incident on the sample from the source, and impact of location and required size (minification/magnification of the "object") of the detector. Using paraxial optics formulae and terminology, the illuminated sample is modeled as the "object" and the detector is modeled as the "image". The scattered light from the illuminated sample is redirected towards the detector in this model. The results of the simulation using Zemax are shown in Figure 3-1. An ideal pattern is represented by a series of tightly grouped concentric markers. With these results, the mirror was then placed in a setup that allowed for axial adjustment, tilt of the mirror using an indexed scale, as well as the lateral movement of the detector. The light was directed towards a frosted glass "sample" that scattered the light to verify the collection efficiency of the mirror as shown in Figure 3-2. While not shown in this picture, the tight grouping of the image projected onto to the detector is very similar to the images predicted by Zemax in Figure 3-1. The relative changes in strength and shape from bench top testing considered only the forward scattered light; therefore, the final proof of concept would also need to verify that similar results could be obtained for non-specularly reflected light.

As these preliminary results were positive, more testing was completed to determine which type of conic (i.e. parabolic, elliptic, or hyperbolic) would be optimal for this design. A separate project to compare various conics is presented in the appendix of this paper and determined that the parabolic mirror is optimal for the design.

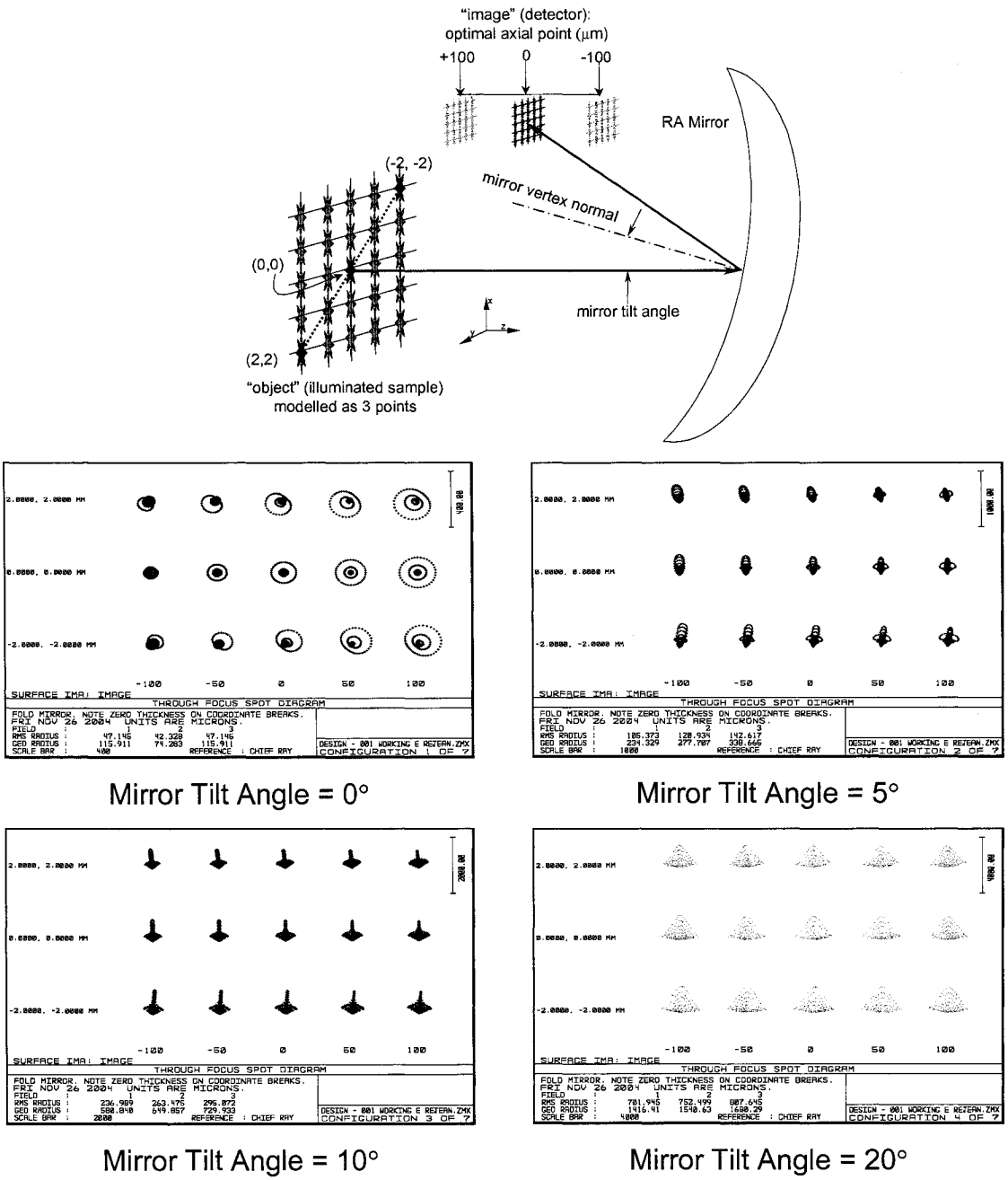

Figure 3-1: Impact of RA mirror tilt on Image - Zemax

The object (sample) is modeled as 3 coordinate points (-2, -2), (0,0), and (2,2), and are represented by three rows of spot patterns in each of the four tilt diagrams (i.e. 0°, 5°, 10° and 20°) above. The 5 columns represent focus in front of (-100, -50), at (0), and behind (50, 100) the optimal point for the modeled detector along the z-axis, for each of the four tilt angles. As the RA mirror is tilted away from the axis (from 0° to 20°), the light rays are less concentrated and therefore reduce the collection efficiency of the mirror.

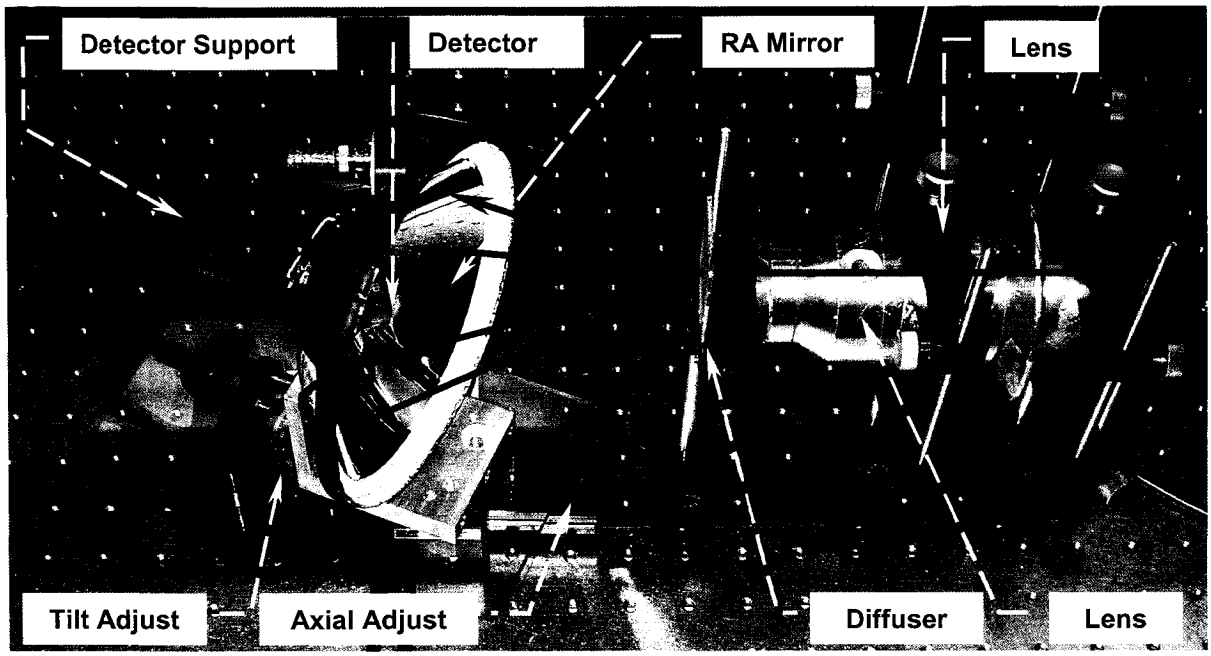

Figure 3-2: Impact of tilt on image quality – Actual setup

The scattered light is collected by the RA mirror and focused onto a target sample mounted on the tip of the detector support.

The preliminary data on the light gathering capability of the RA mirror resulted in procurement of a parabolic mirror or proof of concept (POC) mirror. However, additional engineering specifications for the new mirror were also established. Although the shape of the mirror was verified both with Zemax and on the bench top, the focal length, maximum and minimum diameters had yet to be defined. The focal length of the mirror is bounded by the physical geometry of the setup. The distance between the sample and the vertex of the mirror, (object length), and the distance between the detector and the vertex of the mirror (the image length) are related by the paraxial optics formulae. For a given mirror focal length, excessive reduction of the object distance prevents access to the sample, and excessive reduction of the image distance results in the detector blocking the incoming light path. Both of these distances could be increased simultaneously by choosing a larger focal mirror length resulting in a much larger instrument. Another constraint on mirror selection is the magnification of the object size (the diameter of the illumination spot on the sample) on to the image plane, which must be smaller than the detector area. This relationship is also defined by the paraxial mirror equation. Finally, there are only

discrete sizes of mirrors available from suppliers. The maximum diameter could have been modeled on Zemax, but was completed instead using the bench top setup. The maximum possible exterior diameter is 160 cm permitting access to the test sample while an inner diameter of 16 cm allows the incident light to pass through the vertex of the mirror to the sample. This latter criterion is a function of the mirror tilt angle of 5°, and was determined using the RA mirror. The surface finish of the mirror is also important resulting in a smoothness specification of $\lambda/4$, which is sufficient to prevent scatter generation from the mirror surface. The coating is electrodeposited rhodium, which provides reasonable abrasion resistance while maintaining the optical reflection qualities over the visible spectrum.

The optical design incorporates a three-lens system with the first lens collimating the light and the other two lenses working as a two-lens relay system to magnify the light from the 2 mm ∅ fiber to a 6 mm ∅ spot size. See Appendix B: Optical Concepts - 3 Lens System for supplemental information.

Two types of lens designs can be considered for the system. Condenser lenses are those that have a larger diameter for a given focal length compared to other designs. The advantage of these lenses is their ability to collect and refract a larger amount of light, at the expense of an increase in optical aberrations. Although this light gathering property is important, the chromatic error is of greater concern, such that achromatic condenser lenses are used in the design.

An additional feature to this three-lens system is that two apertures can be added that will separately control the spot (beam) size and irradiance (intensity) at the sample plane. The impact of these two variables was verified in Zemax and the simulated effect is represented in Figure 3-3 as well as in Appendix B: Optical Concepts - Figure "3 Lens System", "Changing beam size using Aperture 1", and "Changing Intensity using Aperture 2". The first aperture (A1) is located at the rim of the collimating lens (lens 1) and the second aperture (A2) is located at the focal plane of the telescoping lenses where an intermediate image of the source is

formed. By placing the sample at the exit plane (secondary focal plane of lens 3) the size of the exit plane is controlled by changing the size of A1. By changing the size of A2 the amount of light is varied which controls the intensity per unit area on the sample. The change in intensity and beam size was consistent with the bench top setup observations. This optical portion of the design with the as built lenses was modeled in Zemax and the 2D layout from this model is shown in Figure 3-4.

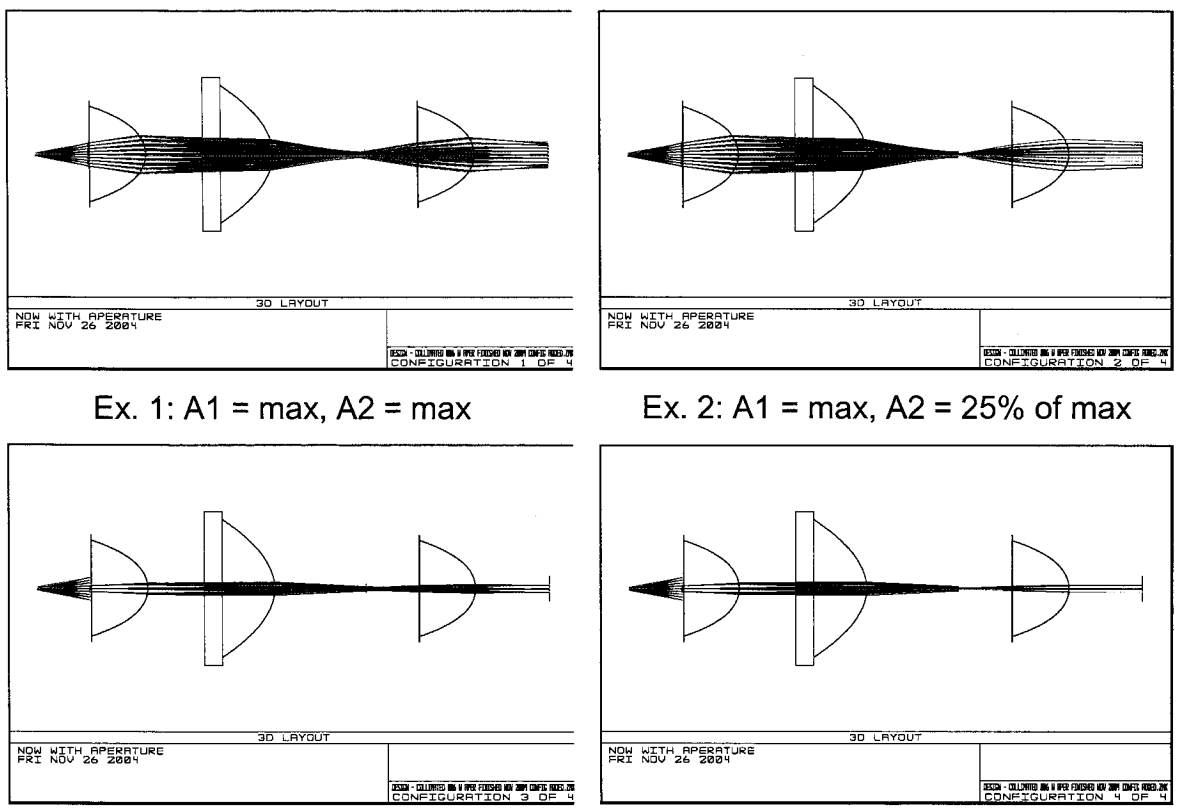

Ex. 1: A1 = max, A2 = max

Ex. 2: A1 = max, A2 = 25% of max

Ex. 3: A1 = 25% of max, A2 = max

Ex. 4: A1 = 25% of max, A2 = 25% of max

Figure 3-3: Impact of varying apertures – Zemax

Impact of separately varying aperture A1 on spot size and A2 on irradiance.

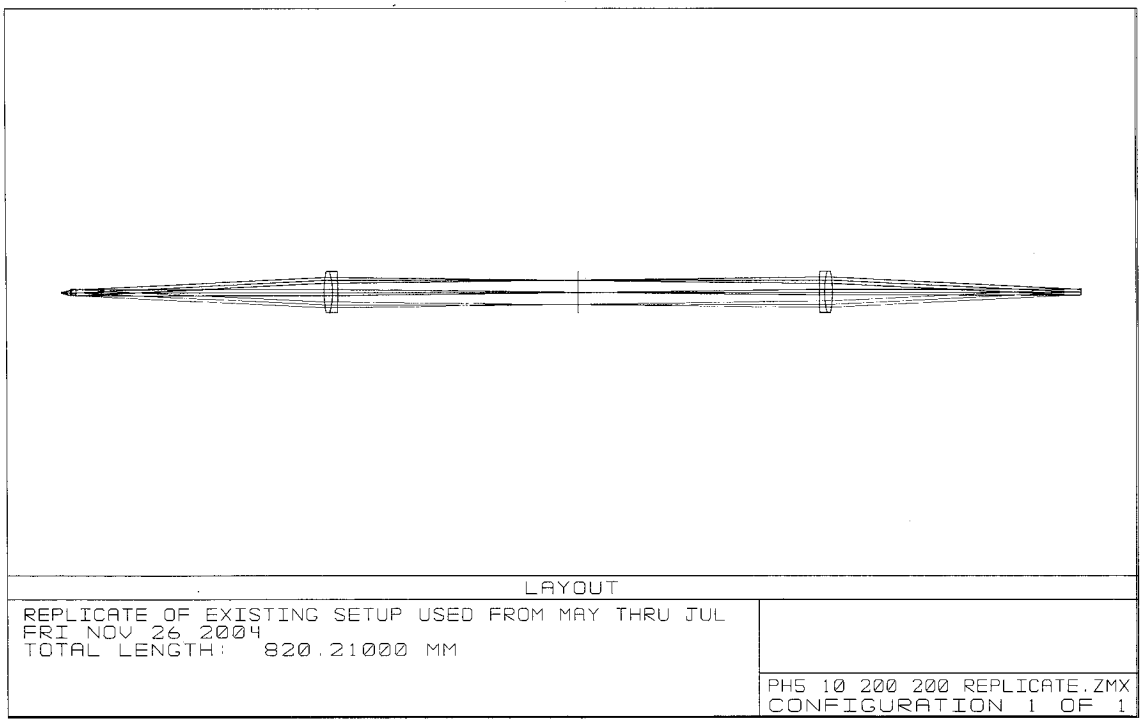

Figure 3-4: Optical Design - Before size Reduction

From left to right: fiber tip, followed by lens 1 (collimating lens), lens 2 (relay lens), aperture 2 (middle of figure), lens 3 (relay lens), and, finally the sample plane.

3.2 System Component Selection

3.2.1 Light Source Selection

Various light sources could be considered for this application based on their associated characteristics. A flatter spectral distribution of intensity across all wavelengths ensures that optical signals are of the same magnitude for each wavelength range. Five 40 nm-wide FWHM (full width half maximum) spectral filters will permit sufficient illuminance over the visible spectrum to be measured at the detector. The total power for the visible spectrum is much higher than that of the 40 nm–wide spectrums. Therefore, a neutral density filter is used when testing in the visible spectrum to keep the detector response in the same range. Reduction of the impact of light source fluctuations (short-term change) is also important during the time that all five optical measurements are taken, as the relay-controlled detectors

require a finite operating time. Drift is a long-term change in light, which can negatively impact the signal interpretation, and must be minimized to improve the reliability of the measurements. The overall power or intensity of the light increases the optical operating range of the system: if the light source power is too low, the signals from the samples are too weak to be measured reliably. This design uses a 15-Watt halogen light as it meets many of the above characteristics, while keeping costs low.

3.2.2 Final Collecting Mirror Selection

To help collect more light, two convex mirrors (collecting mirror) separately capture the forward scattered light and the non-specularly reflected light as described in Section 3.1.3. As such, the outstanding parameters to define are: external mirror diameter, sample to mirror distance, and detector to mirror distance. The final external diameter was determined by empirically testing the POC mirror. This test required the construction of several annular blocking cones that are designed to seat recessed into the mirror for optimal comparison, to simulate use of smaller mirrors using the full-size mirror. From preliminary testing, five cones were constructed with diameters of 4 cm, 5 cm, 6 cm, 7 cm, and 8 cm and the detector response was measured for each. Three separate scattering elements, an opal diffuser, frosted glass, and white card stock, were each tested at 450nm and 650nm for a total of six tests to obtain a broad range of possible operating conditions and are presented in Figure 3-5. Reduction of the mirror diameter from 16 cm to 8 cm maintained 98% of the signal obtained with the full-size mirror. Thus, an 8 cm diameter mirror was used in the final, as-built design (model PB-117 by Perkin Elmer).

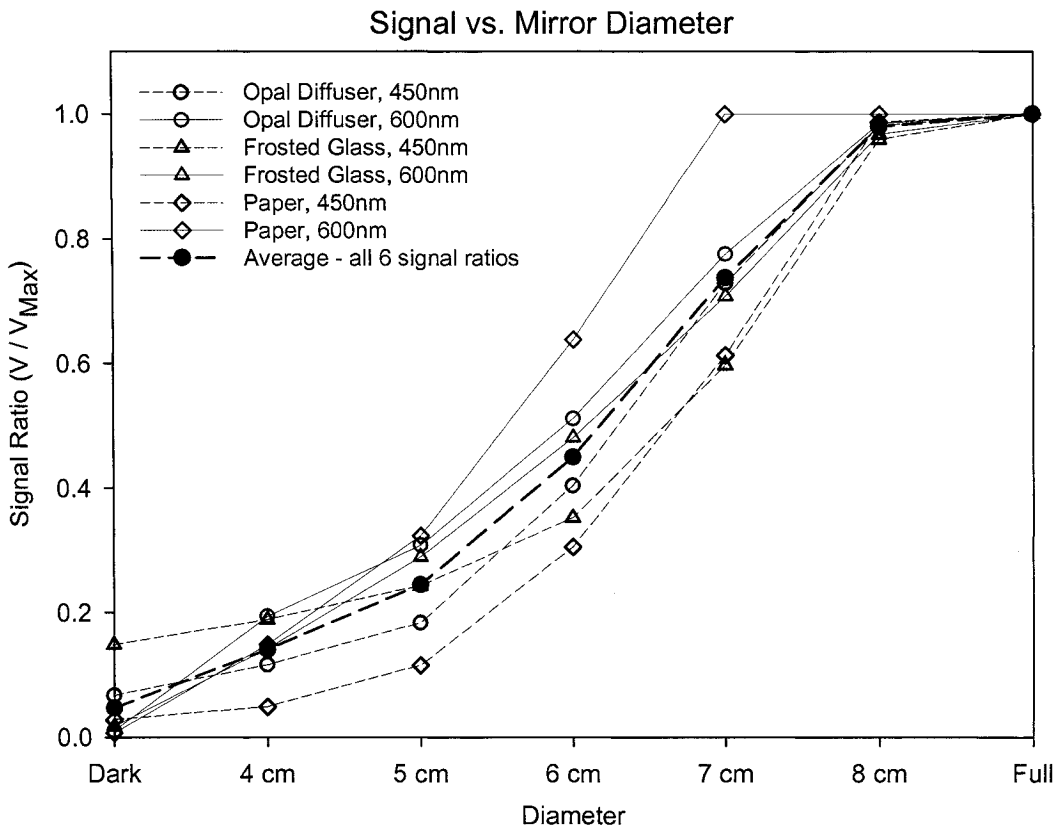

Figure 3-5: Optimal Mirror Size

Using the oversized POC mirror, reduced sizes are simulated using annular blocking cones from 4 cm to 8 cm.

3.2.3 Mechanical Component Selection

The first bench top design used optical components that were easy to adjust (i.e. tilt, x-, y-displacement) and replace. Once the POC data was collected, the instrument was reduced in size in order to meet design specifications. Those criteria that can possibly impact on the repeatability of the system are herein reviewed.

A size reduction ratio of 2:1 of the optical elements achieves the desired layout specifications and is shown in Figure 3-8 and an optical layout drawing with optical dimensions is included in Appendix E: Optical Layout Drawing. This size reduction is aided by optically "folding" the system at 45° in two locations using flat mirrors. In reducing the size of the setup, the physical limitations and the requirement to both measure the reference signal and redirect the specularly

reflected light from the sample required that the beam splitter be placed between lens 3 and the upper collecting mirror as shown in Figure 3-8. Its placement requires that a very small beam splitter be used, resulting in additional reflections from the edge of the mirror, which were subsequently corrected for, with the application of flat black paint. With the design reduced in size and folded, the angle between the marginal ray (the ray which goes the rim of the aperture) and the z-axis using Zemax at the sample plane increased to 5° and is represented in Figure 3-6. This value represents an increase from the POC design and any impact to the precise sample location in the z-axis will be presented later in the validation portion of this report.

A number of custom mechanical mounts were designed and built to hold the detectors and collecting mirrors to allow for final positioning. A support structure was also designed to hold the interchangeable sample adaptor plates.

To improve both the sensitivity and repeatability of the design, a cover and baffle system (cover) was constructed to isolate the various optical light paths from each other as well as isolate all detectors from ambient light. To verify the impact of using this cover, the detector voltage for each detector was measured with and without covers in place and with the lab lights off. Using a variable electric controller, the ambient light was gradually increased from dark to full intensity with no resulting change in the detector voltage.

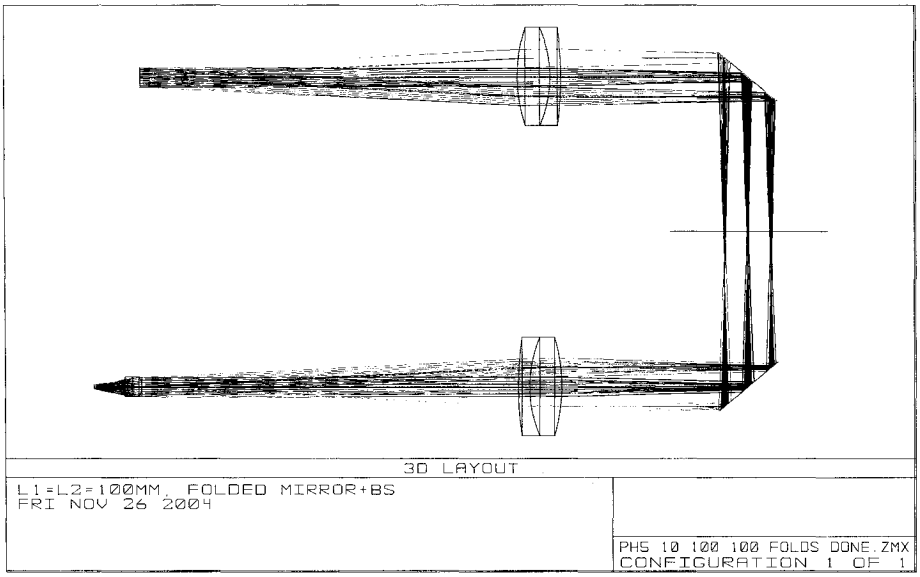

Figure 3-6: Final Design - angle of collimation with the z-axis

The final, "folded" design using two mirrors (fiber tip at lower left, sample plane at upper left).

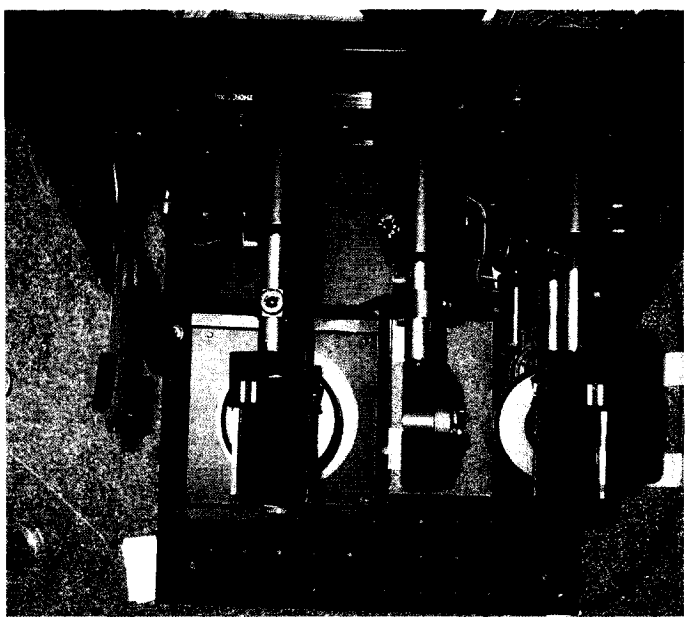

Figure 3-7: The Final As-Built Instrument (Top)

The final design with cover removed. All optical components (identified in the next figure) are located the same distance from the back plane (top of picture).

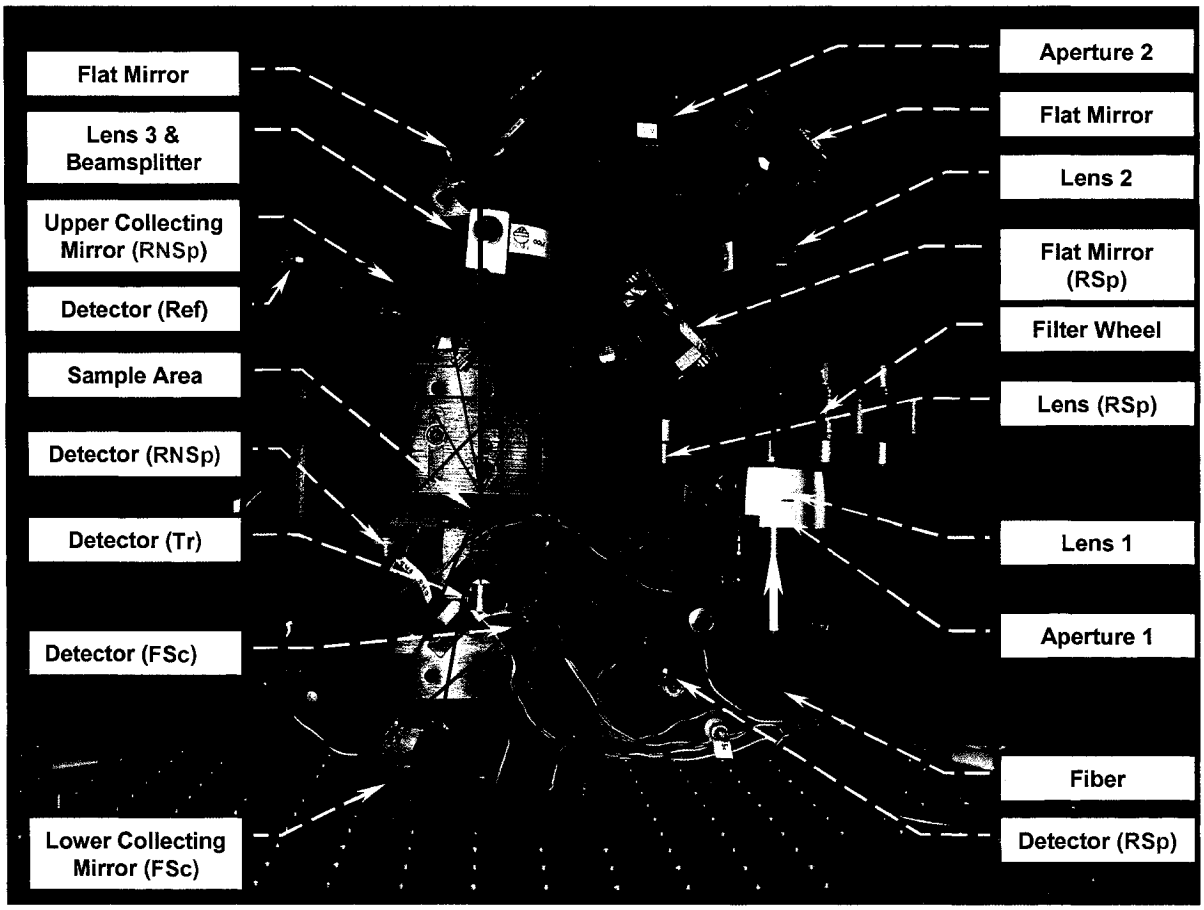

Figure 3-8: The Final As-Built Instrument (Side)

The final design with cover removed and is a 90° CCW representation of the design schematic shown in Figure 3-6.

A 633 nm HeNe laser was used in a standard alignment technique for system x-y alignment to the optical axis as it effectively amplifies any errors much more than the extended source can. To verify the final z-axis placement of the optical components, a small object was placed at the object plane before the first (lens #1) and was successfully imaged at the sample plane. A complete parts list used in this design is included in Appendix A: Equipment List

3.2.4 Electronic Component Selection

Three key issues are important in the implementation of the electronic components of the system design: sensor selection, sensor conditioning, and sensor placement.

Sensor selection must consider the intended wavelength and the expected light irradiance/power levels. There are many types of detectors available including photo-multiplier diodes, avalanche photo-diodes, vacuum photo diodes, and semi-conductor diodes (Si). An array detector was not considered, as these detectors increase the noise at a disproportionately higher rate, based on Poisson's statistics, by distributing the same signal across multiple detecting elements. An Si detector was chosen as it operated over the intended wavelength and at a reasonable cost. The optimum detector area was chosen based on the sample size illumination area of 28 mm^2, a collecting mirror magnification ratio of 1:1, the requirement to for the focused light should overfill the detector area, and the fact that a smaller detector reduces the obstruction to the optical path. A Hamamatsu (model S2386-45K) that detects light from 320 nm to 1100 nm was used for all five measurements.

The next step in incorporation of the electronic components is the conditioning of the signal from the sensor. The sensor produces an output current proportional to the photon energy incident on the active area of the photodetector. There are many circuit application possibilities to amplify the current signal from the detector, such as charge digitizing A/D, switched integrator, and transimpedance amplifier. The selected design incorporates a transimpedance amplifier as it is one of the simpler designs and, that there are no requirements for high frequency measurements. The transimpedance amplifier design uses a photovoltaic (PV) mode and not a photoconductive (PC) mode, as this sensor design is not exposed to high frequency changes, and is operating in low light conditions. The feedback resistance is different for each optical measurement as the irradiance levels vary and each must be kept low to keep the circuit as linear as possible.

The final consideration of the sensor design is the placement of the various detectors. There are a total of five detectors in the system: one to monitor the light source (Ref), and one for each of the four optical signals measured off of the sample as shown in Figure 3-8 and in Appendix E: Optical Layout Drawing. The detector for

transmitted light is placed in line with the sample and incident light. There is some flexibility in the exact placement, but if it is placed too close to the sample, the detector will block out forward scattered light. If placed too far back from the sample, the signal can be too weak to detect. As well, a small tilt is required in the detector, such that the protective glass on the front of the detector does not reflect light back in to the specular reflection pathway. The placement of the detector for forward scatter is partially defined by the focal length and tilt of the forward scatter-collecting mirror. See Appendix D: Detector Mounting Details. The system uses a single beam-splitter that diverts the reflected specular light and diverts a portion of the reference (incident) light to their respective detectors. By choosing one and not two beam splitters, and by calculating the ideal transmitted/reflected ratio of the beam splitter, the signal to the weakest detector is maximized. The calculation optimizations are shown in Appendix F: Beam Splitter Optimization. The detector measuring specularly reflected light utilizes a beam-splitter to remove the detector from the incident beam path. The detector placement for non-specularly reflected light is also defined by the focal length and tilt of the mirror. Both collecting mirrors must be tilted by an amount that allows for the physical placement of the detector out of the beam path while minimizing aberrations associated with a larger tilt angle. A schematic of the optical beam paths, the collecting mirrors, and the detectors is shown in Appendix C: Design Schematic.

3.2.5 System Automation

The automation process incorporates a number of benefits including increasing the speed of operation, reducing the chance of operator error, and using a predefined automated measurement of all five signals.

A scaling calibration is incorporated into the automation by establishing the minimum (0% intensity) and maximum (100% intensity) values for each of the four optical properties for each session. Automation is used to ensure each calibration control is placed into the instrument in series, and ensures that sample testing cannot be completed ahead of this step. Both the normalized and the raw data

signal are recorded for future diagnostic evaluations, along with wavelength tested, date and time of test, and warm-up duration. The data is stored in ASCII format to provide a simple importing process for further evaluation.

A separate, less-frequently used, calibration routine is also incorporated into the system to account for the non-linear relationship between the detected intensity and the true intensity across the full scale of the measurements. A flow chart is included in Appendix H: System Calibration Flow Chart. This procedure is not required each time the instrument is turned on, but allows for the collection of actual-sample changes in the non-linear detector response. Neutral density (ND) filters with calibrated attenuation values are placed in the instrument reducing the incident light by known amounts, the response is recorded, and a calibration curve is generated by a polynomial curve fit constants across the intensity response curve.

Visual Basic® 5.0 software is used as the front-end application to automate the testing process. The output from each sensor is connected to an individual transimpedance amplifier and is then connected to the 10-channel data acquisition card (DAC) of a digital multimeter operating in voltage mode (DVM). The DVM is connected to a computer using a GPIB cable and GPIB card. One advantage of this setup is that measurements can be taken for each of the 5 detectors rapidly in series, limited only by the relay speed (3.5 ms) of the DAC.

3.3 Calibration of System Components and the Integrating Sphere

3.3.1 Selection and Testing of the Controls

Before samples are measured, the scale (0-100%) must be established for each of the four optical properties. The minimum level is established for each property by measuring the electrical signal with the light source turned off. The maximum is established by placing one of the calibrated controls in the instrument that is uniquely maximized for each of the four optical measurements. Numerous potential controls were tested to determine which one produced the maximum signal

for each of the selected optical properties. Unlike biological samples, these controls are stable, homogeneous, have associated engineering specifications for verification, and have better coverage for the expected operating range. The optical properties were measured for each of the controls and results are presented in Figure 3-9. It is important to consider that no one single control is ideal, as there is a wide and variable operating range for each of the optical properties as summarized in Table 3-1.

For transmitted light, the control selected is an empty path as it directs the maximum possible light to the Tr detector.

Four holographic diffusers were considered with scattering angles 10°, 15°, 20°, and 25°. An angle of 20° is consistent with the geometry of the mirror as an angle greater than 20° subtended to the vertex of the mirror exceeds the mirror diameter and an angle smaller than 20° increases the ratio of light redirected from the sample to the 16 mm opening at the vertex of the mirror. Thus, based on the test results and the geometry, the selected control for forward scatter is a 20° holographic diffuser. For consistency and to reduce the specular reflection, the holographic diffuser is utilized with the dull side as the incident surface.

A flat mirror was selected as the control for specular reflection. As the measurement of this property is very sensitive to angle of incidence, the tilt of the mirror is critical. Preliminary testing confirmed that utilizing a larger mirror, which straddled the adapter plate and the base, resulted in high repeatability errors. Consequently, a smaller mirror is utilized that could rest entirely on the adaptor plate.

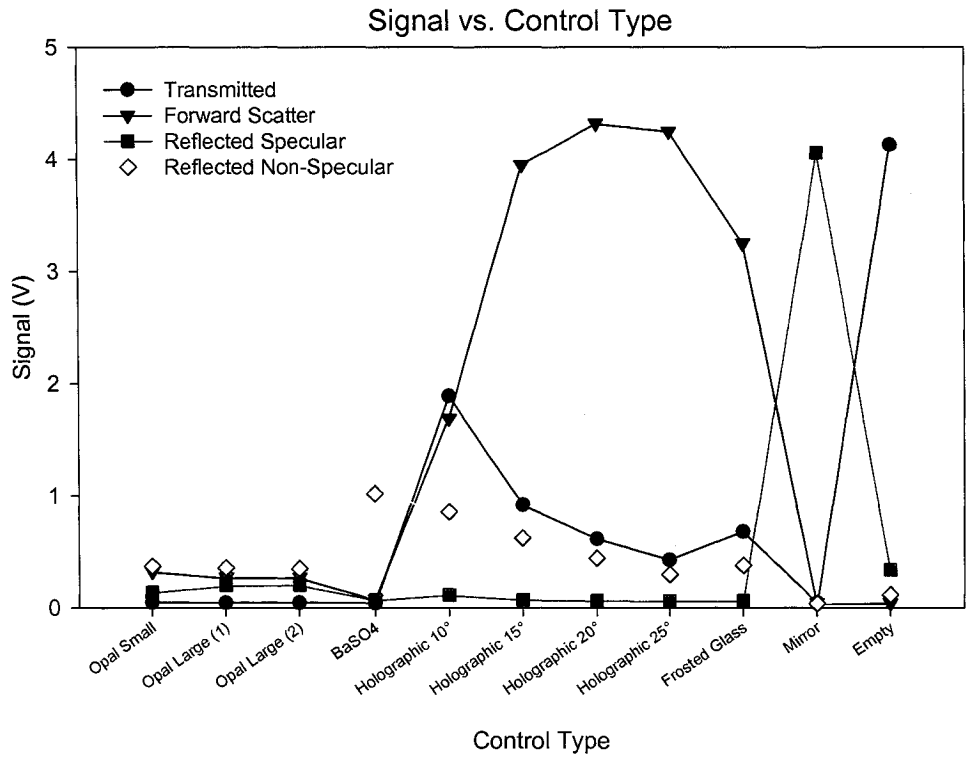

Figure 3-9: Optical Properties of Potential Controls

Potential controls are tested to determine which has the strongest signal strength for each of the four optical properties.

$BaSO_4$ is used as an ideal non-specular material as it produces a near-Lambertian reflection, but due to the integral mounting of the component available in the lab, an opal diffuser was used. The effect of improperly placing the opal diffuser can cause errors as a small tilt redirects light away from the vertex of the mirror, although less dramatic than with specular reflection described earlier. It is also be important to place a flat black material to form a skirt around the opal diffuser to prevent any lateral leakage of light directly to the intended detector. For consistency, the opal diffuser is placed with the glass-backed surface face up as the incident surface.

3.3.2 Selection and Calibration of the Neutral Density Filters

It is not sufficient to define the operating range of each control, using minimum and maximum points alone. The relationship at various intermediate

points must also be defined. From previous testing, it was established that the relationship between the expected and measured signal could be non-linear. Therefore, neutral density (ND) filters are used in the system to produce a calibrated signal over the entire expected operating range. By choosing enough intensity points over the range of intended use, and by combining no more than two ND filters simultaneously to reduce multiple interface reflections, a calibration curve of signal intensity vs. detector response is generated and written into the software controlling the DVM.

The selection of ND filters must consider the supplier availability as well as the intended specified range for each of the four optical measurements as defined in Table 3-1. By choosing more ND filters in the appropriate range, a resulting non-linear regression more closely approximates the interpolated signal. As a result, the nominal ND filters in Table 3-3 are used.

The optical density of the ND filters is a nominal value only, and determined at the time of inspection by the manufacturer. In addition, there are differences across the visible spectrum. A spectrophotometer was used to calculate the actual optical density of each ND filter at the five spectral ranges, as well as the peak wavelength value for each range. The ND filters are calibrated with the same light source used for the system to take into account its spectral dependence. The results of this test are presented in Table 3-4.

The ND filters are placed within the instrument, with several considerations in mind. Firstly, the light must make a single pass through the ND. Secondly, they must have a consistent tilt angle, if any, with respect to the optical path as a small variation in tilt will affect the attenuation of the signal and specular reflections from the filter can invalidate the experiment.

Table 3-3: Optical Property and Corresponding ND Filters

Item	Transmitted Light (Nominal OD / %)	Forward Scattered Light (Nominal OD / %)	Specularly Reflected Light (Nominal OD / %)	Non-specularly Reflected Light (Nominal OD / %)
1	0.00 / 100.0	0.00 / 100.0	0.00 / 100.0	0.00 / 100.0
2	0.04 / 91.2	0.04 / 91.2	0.04 / 91.2	0.04 / 91.2
3	0.10 / 79.4	0.20 / 63.1	0.10 / 79.4	0.20 / 63.1
4	0.20 / 63.1	0.30 / 50.1	0.30 / 50.1	0.30 / 50.1
5	0.24 / 57.5	0.50 / 31.6	0.50 / 31.6	0.50 / 31.6
6	0.30 / 50.1	0.70 / 20.0	1.00 / 10.0	0.70 / 20.0
7	0.40 / 39.8	0.80 / 15.8	1.20 / 6.3	0.80 / 15.8
8	0.60 / 25.1	1.00 / 10.0	3.00 / 0.10	1.00 / 10.0
9	1.00 / 10.0	1.20 / 6.3	-	1.20 / 6.3
10	-	1.30 / 5.0	-	1.30 / 5.0
11	-	1.50 / 3.2	-	1.50 / 3.2
12	-	2.00 / 1.0	-	2.00 / 1.0

Optical density and transmittance for the ND filters used for each of four optical properties. OD = -log(T). T is the fraction of transmitted light through a substance.

3.3.3 Design of the Integrating Sphere

The controls for non-specular reflection (opal diffuser) and forward scatter (20° holographic diffuser) are used to calibrate the system prior to a testing session. However, these are not calibrated controls from the factory, and they are not perfect diffusers. Therefore, an integrating sphere is utilized to measure and calibrate these two controls.

Table 3-4: Measured Optical Density of each ND filter

Filter Type	Nominal OD	Visible Spectrum	450 nm (461.8 nm)	500 nm (519.2 nm)	550 nm (569.5 nm)	600 nm (615.5 nm)	650 nm (635.1nm)	Mean
n/a	n/a	100%	100%	100%	100%	100%	100%	100%
C	0.1	87.31%	88.64%	88.72%	89.24%	87.73%	88.06%	88.28%
C	0.2	65.33%	66.16%	66.40%	67.38%	65.68%	66.14%	66.18%
C	0.3	50.50%	52.78%	51.57%	52.08%	51.85%	50.70%	51.58%
C	0.4	38.44%	40.40%	39.24%	38.75%	39.22%	38.50%	39.09%
C	0.5	31.41%	33.33%	32.15%	32.19%	31.85%	31.70%	32.11%
S	0.04	89.81%	90.91%	90.41%	91.81%	89.93%	90.34%	90.54%
S	0.1	80.45%	78.66%	80.17%	81.30%	80.87%	79.03%	80.08%
S	0.3	44.53%	51.89%	50.93%	50.30%	49.29%	49.05%	49.33%
S	0.5	33.79%	36.24%	33.60%	33.61%	32.45%	32.97%	33.78%
S	1	11.68%	13.13%	12.50%	12.22%	12.17%	12.20%	12.32%
S	1.2	6.31%	6.02%	6.77%	6.38%	6.91%	7.19%	6.60%
S	3	0.10%	0.12%	0.07%	0.07%	0.09%	0.10%	0.09%

Measured optical density of each ND filter used in eventual calibration of the system measured at the peak transmittance in braces (C = Circular, S = square).

An integrating sphere can separately capture the transmitted, forward scattered, specularly, and non-specularly reflected light from the two controls. Knowing the absolute intensity incident on the sample, each control can then be used in the instrument to calculate relative signal of a test sample.

The principle of an integrating sphere is that light directed into the sphere is reflected off of the internal surfaces an infinite number of times such that any one point on the surface will be typical of the radiance for the entire internal surface; it spatially integrates the complete flux from the target. Therefore, by placing a

detector of a known small area on the surface of the sphere, the total input flux can be determined. The following section derives the mathematical statements used later in this research. The full development of the spatial integration can be found from LabSphere Inc. [21].

The internal surface radiance of an integrating sphere for an input flux, Φ_I, is defined by:

$$L_S = \frac{\Phi_i}{\pi \cdot A_S}\left[\frac{\rho}{1-\rho\cdot(1-f)}\right] = \frac{\Phi_i}{\pi \cdot A_S}\cdot M \quad [\text{W / m2 / sr}] \tag{3-1}$$

$$f = \frac{A_i + A_e}{A_S} \tag{3-2}$$

$$M = \frac{\rho}{1-\rho\cdot(1-f)} \tag{3-3}$$

where: Φ_I is the input flux to sphere
ρ is the reflectance of the sphere, which is a function of wavelength, λ
f is the port fraction, representing the ratio of access ports to the total internal surface area of the sphere
A_e is the total area of exit ports of sphere [m^2]
A_i is the total area of input of sphere [m^2]
A_S is the area of sphere [m^2]
and M is the sphere multiplier, which is a function of wavelength, λ

The flux incident on the photodetector is defined by:

$$\Phi_D = L_S \cdot A_D \cdot \Omega \quad [\text{W}] \tag{3-4}$$

where: Ω is the projected solid angle
and A_D is the active area of the detector [m^2]

The projected solid angle can be approximated by:

$$\Omega = \pi \cdot \sin^2\theta \quad [\text{sr}] \tag{3-5}$$

If the detector is mounted flush with the internal surface of the sphere, then the acceptance angle is defined by:

$$\theta = \pi/2 \quad \text{[rad]} \tag{3-6}$$

Therefore, the flux incident on the photodetector can be defined by:

$$\Phi_D = L_S \cdot A_D \cdot \pi \quad \text{[W]} \tag{3-7}$$

Rearranging Equation 3-1leads to:

$$\Phi_i = \frac{L_S \cdot \pi \cdot A_S}{M} \quad \text{[W]} \tag{3-8}$$

Therefore, the ratio of incident flux on the detector to that entering the sphere is:

$$\frac{\Phi_D}{\Phi_i} = M \cdot \left(A_D / A_S \right) \text{[-]} \tag{3-9}$$

The input flux to the detector is converted to a current defined by:

$$\Phi_D = \frac{i_D}{R_D} \quad \text{[W]} \tag{3-10}$$

where i_D is the current measured at the photodetector as a result of light entering sphere
and R_D is the responsivity of detector [A/W], which is a function of wavelength

Rearranging Equations 3-9 and 3-10 results in:

$$\frac{i_D}{\Phi_i} \cdot \frac{A_S}{A_D} = M(\lambda) \cdot R_D(\lambda) \quad \text{[A / W]} \tag{3-11}$$

The variables on the left side of Equation 3-11 are known. The value of R_D as a function of wavelength is provided by the manufacturer of the detector and is verified in-situ using several lasers, each with a measured input flux. Then, by

measuring a number of points within the spectrum, R_D is determined, resulting in a single unknown M, which is a function of f and ρ. The latter value is a function of λ and is known as the spectral flatness. Measuring M completes the calibration of the sphere and allows for calibration of the controls.

3.3.4 Construction of the Integrating Sphere

Integrating spheres are commercially available but as the cost of such devices is high, and mounting the selected controls would likely be more difficult, an integrating sphere was constructed in the lab.

The sphere must measure the total flux for holographic diffuser (forward scatter) and opal diffuser (non-specularly reflected). Each control is tested separately, and requires different setup conditions but uses the same sphere with a reflectance, ρ.

The determination of the diameter of the sphere is governed by several factors. Firstly, the sphere diameter has to be large enough that the detector port is no more than 5% of the total sphere area, as a rule-of-thumb [21]. This latter guide ensures that there is sufficient integration of the incident light inside the integrating sphere, and that both the diameter and the reflectance of the internal sphere surface be large enough. Secondly, the diameter has to be small enough to measure a reliable signal at the detector. A smaller size also makes construction and mounting for testing more manageable. Using Equation 3-1, the following relationship can be stated:

$$L_S \propto \frac{M}{D_S^2} \tag{3-12}$$

where: D_S is the internal diameter of the sphere
and M is the sphere multiplier

The sphere is constructed out of common plaster of Paris, as it is easy to form a smooth mold, retains its shape, cures in less than five minutes, and is

inexpensive. There are two molds, an exterior mold defining the exterior shape, which is important only to maintain a flat bottom for the mounting of the sphere, and a mold defining the interior radius of the sphere. As well, the sphere is created in two hemispheres so that the interior mold can be removed after curing is completed, with alignment pins set in the two halves ensuring that the ports are accurately and consistently aligned with respect to each other. All the required port mounts are placed on the interior mold rather than at post-curing, for simplicity of construction. See Figure 3-10 for mounting details.

The sphere must also have the best scattering possible inner surface coating. If the reflectance is too low, much of the light is absorbed from the sample resulting in a small dynamic test range of the sphere. Commercially available spheres have a minimum reflectance of 85%, and can reach close to 100% depending on the coating and wavelength [21, 22]. A flat white paint obtained from a local paint store is used for the internal coating of the laboratory-constructed integrating sphere.

Another important consideration is the construction and placement of internal baffles that ensure that any light impinging on the detector surface is indirect light after multiple scattering inside the sphere. The baffles are made of the same material as that of the wall and are tested for line-of-site-impact from light.

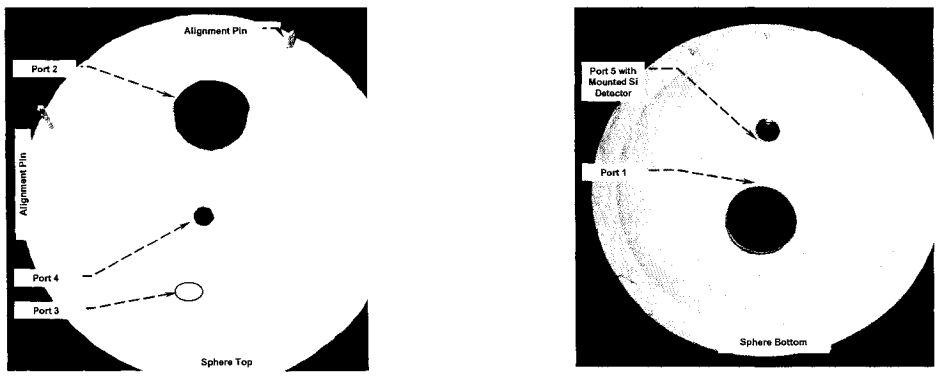

Sphere: Top Half Sphere: Bottom Half

Figure 3-10: Integrating Sphere Details

The smaller ports (3, 4, and 5) are for detectors while the larger ports (1 and 2) are for mounting of the controls (opal and holographic diffuser).

3.3.5 Calibration of the Integrating Sphere

Using light source (halogen) used for the system and the same five spectral ranges into a fiber from the and then collimated using a 10 mm aspheric lens and directed into the integrating sphere. The input flux (Φ_i) is measured at the fiber tip using a Laser Check model by Coherent Instruments Division and the current (i_D) from this light is measured using a Hamamatsu model S2386-45K Si photodiode mounted on the inner sphere surface. With the area of the detector (A_D) and sphere (A_S), and the responsivity of the detector at each wavelength known, the sphere reflectance can be calculated. While the filtered sources provide a wider spectral range for the sphere reflectance, the Laser Check is more accurate with line lasers than with a spectrally filtered source. Therefore, the light source and fiber are then replaced with three lasers (500 nm, 540 nm, and 630 nm) and the process repeated. The result for both the halogen light source and the line lasers are presented in Table 3-5. As this mean sphere reflectance of 0.828 is comparable to commercially available spheres (LabSphere, 2004), this lab integrating sphere is acceptable to measure the absolute optical properties of the opal diffuser and holographic diffuser.

Table 3-5: Integrating Sphere Calibration Data

Wavelength λ [nm]	Input Flux (Φ_i) [W]	Detector Current (i_D) [A]	Responsivity: calculated R [A/W]	Responsivity: using laser R [A/W]	Sphere Reflectance ρ [-]
450	609×10^{-06}	0.42×10^{-06}	0.24	n/a	0.854
500	1.20×10^{-03}	0.86×10^{-06}	0.30	0.42 (500nm)	0.829
550	1.77×10^{-03}	1.47×10^{-03}	0.36	0.34 (540nm)	0.824
600	2.11×10^{-03}	1.83×10^{-03}	0.41	n/a	0.811
650	1.81×10^{-03}	1.88×10^{-03}	0.45	0.43 (630nm)	0.824

The sphere reflectance using the halogen and laser sources.

3.3.6 Calibration of the Controls using the Integration Sphere

As the two collecting mirrors capture only a portion of the forward scattered and non-specularly reflected light, it is necessary to convert this relative signal to an absolute signal so that the measurand is more meaningful. The device utilized in this research to determine the absolute reflectance and transmittance from a material is the integrating sphere.

Using the sphere, the absolute non-specularly reflected light from the opal diffuser is determined by removing the specular component as presented in Figure 3-11. Specularly reflected light is contained to a small angular region (defined by laws of reflection) and as such, it can be "trapped" using a small flat black-painted material. By replacing the trap with a plug that matches the sphere, the total reflectance of the control can then be measured and is summarized in Table 3-6. The absolute non-specular reflection for the opal diffuser is 40.2% (mean) for the five wavelength ranges and is incorporated into the test system's software so that the measured signals are converted directly to absolute readings.

Before transmittance testing, it is important to determine if the degree of

collimation has any impact on the transmission through the 20°-holographic diffuser. Light is directed into the sphere using two methods: the first method used uncollimated light, and the second method used collimated the light.

The results shown in Table 3-7 lead to the conclusion that the degree of collimation has little impact on calibration of the total forward scatter of the holographic diffuser. The supplier of the diffusers confirmed that there should be no measurable difference between collimated light and uncollimated light when measuring the forward scattered light (Diaz, 2004).

Like the opal diffuser, the holographic diffuser is calibrated to determine the absolute forward scatter. The setup for testing is illustrated and described in Figure 3-12 and the results presented in Table 3-8. The mean forward scatter for all wavelengths is 91.5% and is incorporated into the system's software so that the measured signals are converted directly to absolute readings.

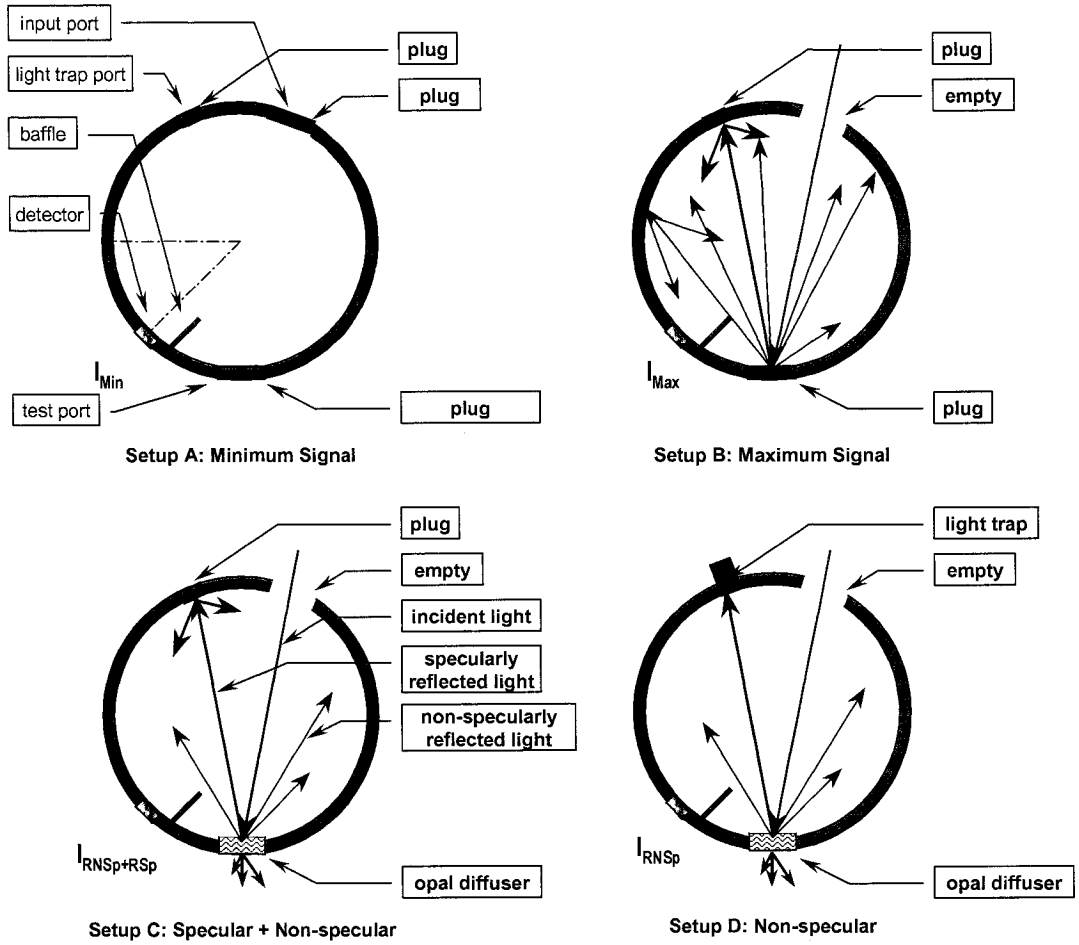

Figure 3-11: Measurement of Absolute Non-specular Reflected Light – Opal Diffuser

The sequence A, B, C, D describes the process for calibrating the opal diffuser in the integrating sphere.

Table 3-6: Absolute Specular and Non-specular Reflection of Opal Diffuser

Optical Property	450nm	500nm	550nm	600nm	650nm	Mean
Non-Specularly Reflected Light	51.4%	63.6%	37.5%	35.7%	28.2%	40.2%
Specularly Reflected Light	15.6%	0.0%	4.4%	3.6%	3.6%	10.8%
Total Reflectance	67.0%	63.6%	41.9%	39.3%	31.7%	51.0%

The absolute non-specular reflected light of the opal diffuser measured at the five spectral wavelength ranges.

Table 3-7: Impact of Collimation on Transmitted Light through Holographic Diffuser

Light Delivery	Detected Current
collimated	12.0 mA
uncollimated	12.1 mA

Results of launching both collimated light and uncollimated light through a 20°-holographic diffuser as measured at the integrating sphere surface.

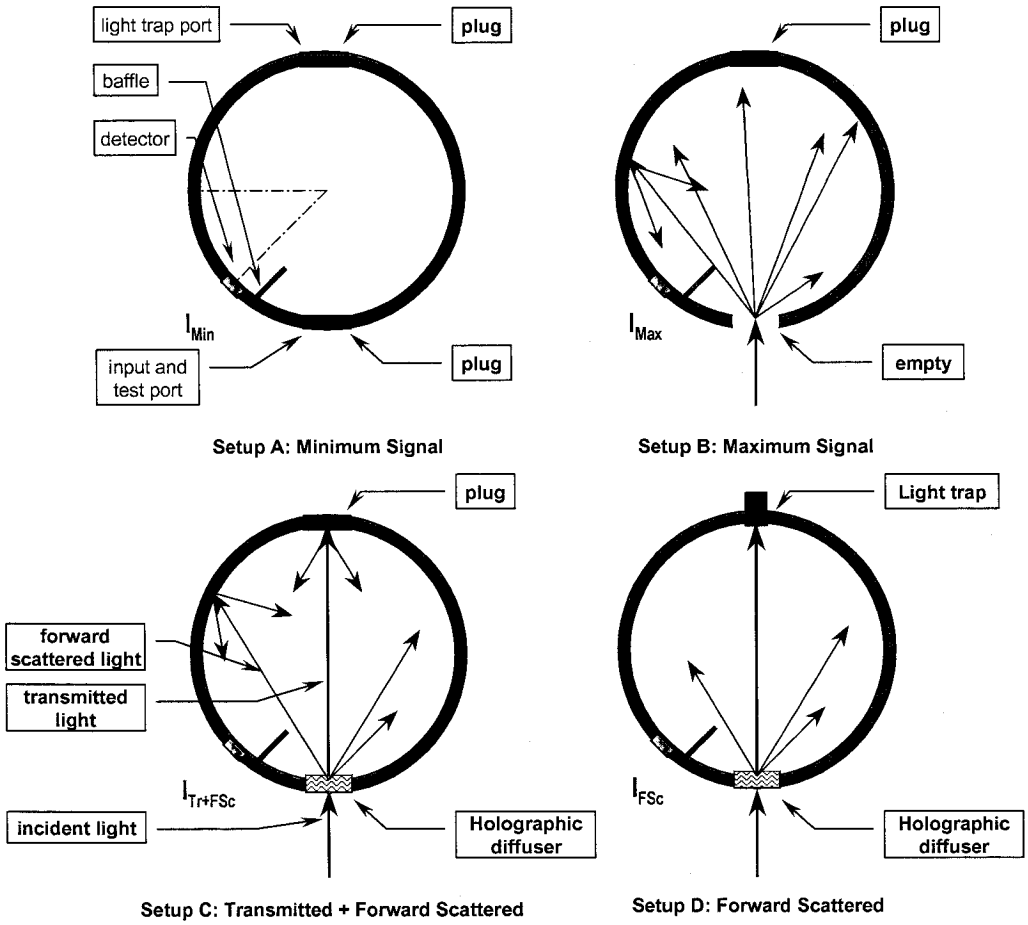

Figure 3-12: Measurement of absolute Forward Scattered Light – Holographic Diffuser

The sequence A, B, C, D describes the process for calibrating the holographic diffuser in the integrating sphere.

Table 3-8: Absolute Forward Scattered and Transmitted Light of the Holographic Diffuser

Optical Property	450nm	500nm	550nm	600nm	650nm	Mean
Forward Scattered Light	94.6%	91.9%	90.6%	89.1%	91.1%	91.5%
Transmitted Light	0%	0%	0%	0%	0%	0%
Total Transmittance	94.6%	91.9%	90.6%	89.1%	91.1%	91.5%

The absolute forward scattered light for the holographic diffuser at the five spectral wavelength ranges.

3.3.7 Calibration of the System

With the calibration of the ND filters complete and the absolute optical properties of the controls known, it is then possible to complete the system calibration. Software was written by the author to assist this calibration process to reduce both the time required and the probability of operator error occurring. The entire test is performed with the cover in place. The minimum signal from the detector is recorded with the light source off and the maximum signal is recorded while the control for one of the four optical properties is placed in the instrument. Using the optical density range specific to each optical property (Table 3-3), the system response is calibrated for the expected range of operation. The ND filters are placed in between the control and the appropriate detector, ensuring that the incoming beam path is not interfered with. Measurements are performed three times at each of the six spectral ranges and for each of the four optical properties. The irradiance is normalized to the maximum signal from the control as follows:

$$\frac{V - V_{Min}}{V_{Max} - V_{Min}} \tag{3-13}$$

where: V is the measured voltage for a given optical density
V_{Min} is the minimum signal, with light source off
V_{Max} is the maximum signal, with control in place

The measured normalized irradiance is plotted against the expected irradiance, both normalized to the maximum signal. The resulting non-linear response, likely due to the large range in optical signal and the large feedback gain in the signal amplifying circuit, was fitted to a 3rd order polynomial of the form:

$$f = y_0 + a \cdot x + b \cdot x^2 + c \cdot x^3 \qquad (3\text{-}14)$$

where: a, b, c, y_0 are constants determined from linear regression analyses
f is the calculated signal from regression analyses

Utilizing Equation 3-14 and the measured signal, the interpolated value is calculated in real time. Storing this regression data eliminates the need to calibrate the system, requiring only the maximum and minimum values for each session (each time the system is turned on). While the constants are not listed here they are stored in the software ready for sample testing, and the standard error of the estimate in using Equation 3-14 is listed in Table 3-9.

Table 3-9: Regression Analyses – R^2 using 3rd order polynomial

Optical Property	450nm	500nm	550nm	600nm	650nm	White
Transmitted Light	0.9997	0.9997	0.9996	0.9994	0.9989	0.9975
Forward Scattered Light	0.9978	0.9996	0.9995	0.9998	0.9995	0.9990
Non-specularly Reflected Light	0.9993	0.9991	0.9997	0.9998	0.9996	0.9989
Specularly Reflected Light	0.9997	0.9994	0.9982	0.9974	0.9974	0.9969

The results of regression analyses using the expected signal and the measured signal.

3.4 Summary

The theoretical design was developed from the high-level specifications down through the detailed specifications. At each stage, the design was rigorously tested using both simulation software as well as on using a bench top setup. The

calibration controls are a cornerstone of the design and, as such, much detail went in to their selection and testing. With these steps complete, the system was ready for validation testing.

4 System Validation

Before any sample measurements can be made, the performance limits of all the measurands must be established. This validation of the system implementation will include repeatability, reproducibility, sensitivity, threshold, light source drift and fluctuations, and vertical sample position sensitivity.

Some of the variables that can impact the validation of the system and are herein reviewed. The lab lights are left on, as the impact of external lighting with the cover in place had been previously tested and verified to have no impact on any of the five detectors. The DVM is also configured with the built-in scan time of the A/D relays set to 16.67 ms (medium) which provides a compromise between noise and speed as per the manufacturers specifications. Furthermore, the software written by the author enabled data collected from the DVM to be averaged for every 10 consecutive readings. Preliminary testing revealed that the opal skirt could actually protrude below the opal diffuser, raising one end causing it to tilt, resulting in variability of data, and was therefore accurately maintained for each test.

4.1 Repeatability of System Optical Measurements

The repeatability of the system evaluates the change in the measurand while nothing, including the sample, is changed between measurements and is defined as the standard deviation of three measurements, with a 67% confidence limit. These three measurements define 1 session and a session is performed for each of the four optical properties, at the each of the six spectral ranges previously defined, and for the range of intensities listed in Table 3-3. The target sample is the control appropriate to each of the measurements already specified.

The results of the system repeatability are presented in Figure 4-1 for transmitted light, Figure 4-2 for forward scattered light, Figure 4-3 for specularly reflected light, and Figure 4-4 for non-specularly reflected light. The mean range of repeatability (maximum variation) for transmitted light is 0.03% (of max. intensity),

which is better than the specification of 1%. Similarly, repeatability is 0.02% for forward scatter, 0.04% for specularly reflected light, and 0.02% for non-specularly reflected light and in all cases is better than the specification of 2%.

As nothing in the setup is modified between each of the three measurements of the session, any variation in the measured signal is a measure of the system limitations. Testing reported on in subsequent sections will consider these two variables separately to determine their impact on the overall system reliability. The results from this test of system *repeatability* will be important in the analysis of system *reproducibility*, which is described in the next section.

4.2 Reproducibility of System Optical Measurements

The reproducibility of the system is a measure of the difference in the measurand while the target sample (the control) is changed between each of three sessions, thus the additional variable introduced is the sample positioning. A session is the same as defined in the previous section and the target sample is the control appropriate to the measurement already specified. A mean is calculated for each of three sessions. The standard deviation of these three means defines the reproducibility of the system intersession variability with the instrument in the same state.

The results of the system repeatability testing are presented in Figure 4-5 for transmitted light, Figure 4-6 for forward scattered light, Figure 4-7 for specularly reflected light, and Figure 4-8 for non-specularly reflected light. The mean range of repeatability for transmitted light is 0.07% (of max. intensity) and is better than the specification of 1%. Similarly, the repeatability is 0.16% for forward scatter, 0.56% for specularly reflected light, and 0.18% for non-specularly reflected light and all are better than the specification of 2%.

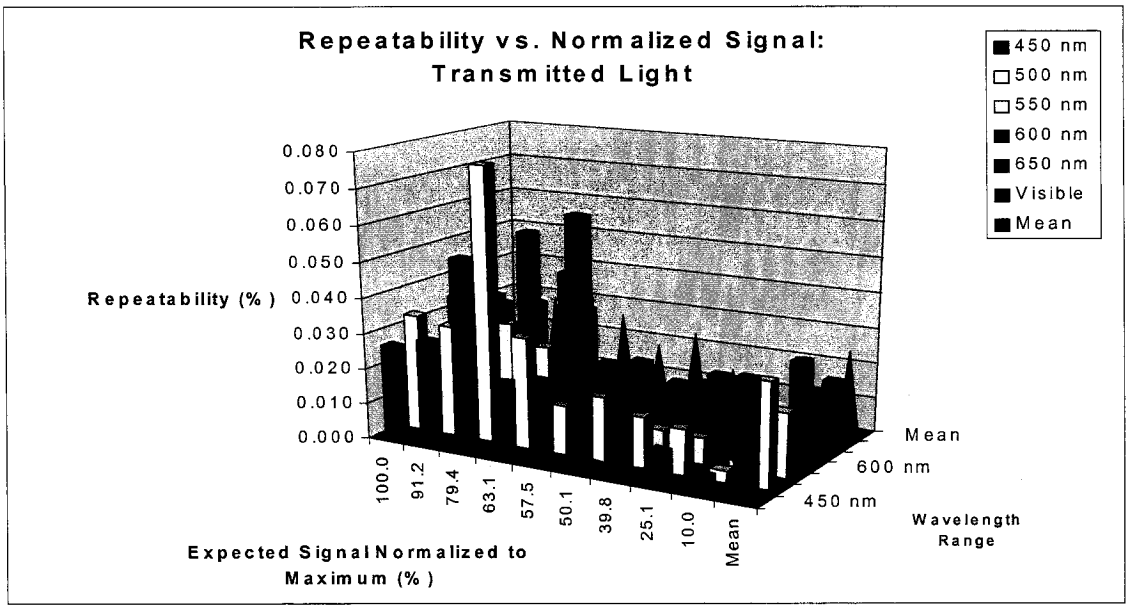

Figure 4-1: Repeatability - Transmitted Light

Mean system repeatability for transmitted light over five spectral bands and the visible spectrum are better than the specifications of <1% (of max. intensity).

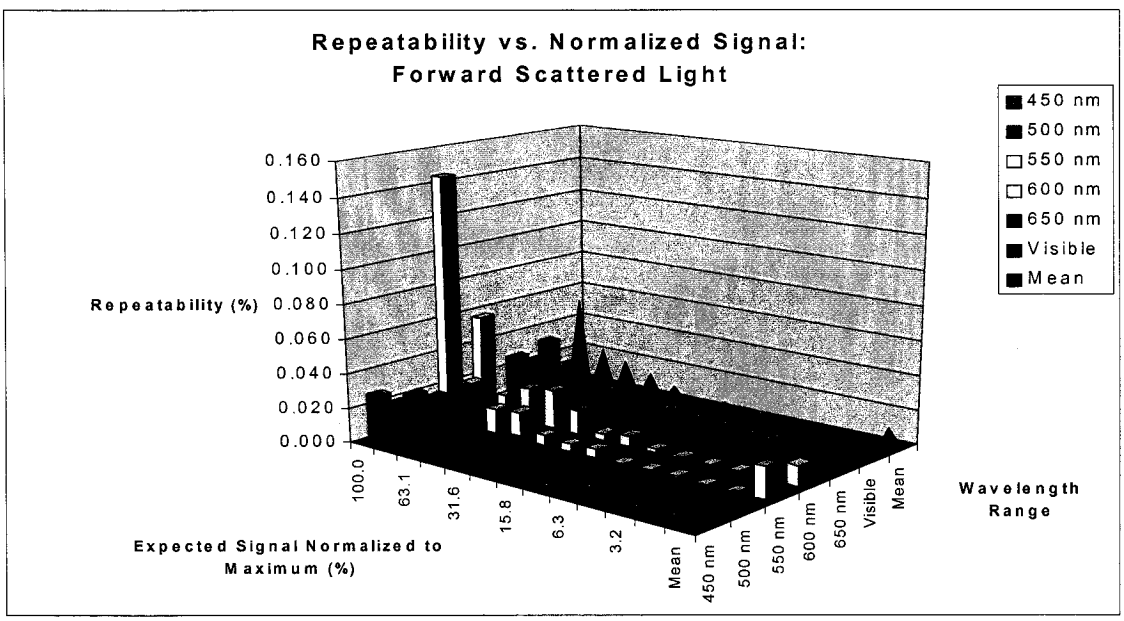

Figure 4-2: Repeatability – Forward Scattered Light

Mean system repeatability for forward scattered light over five spectral bands and the visible spectrum are better than the specifications of <2% (max. intensity).

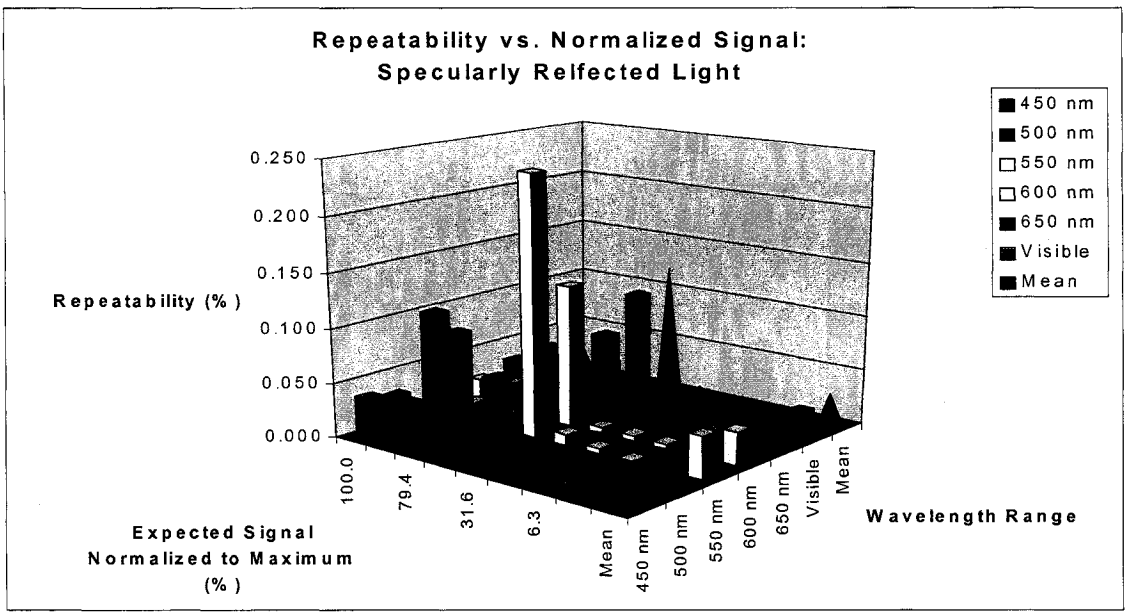

Figure 4-3: Repeatability - Specularly Reflected Light

Mean system repeatability for specularly reflected light over five spectral bands and the visible spectrum are better than the specifications of <2% (max. intensity).

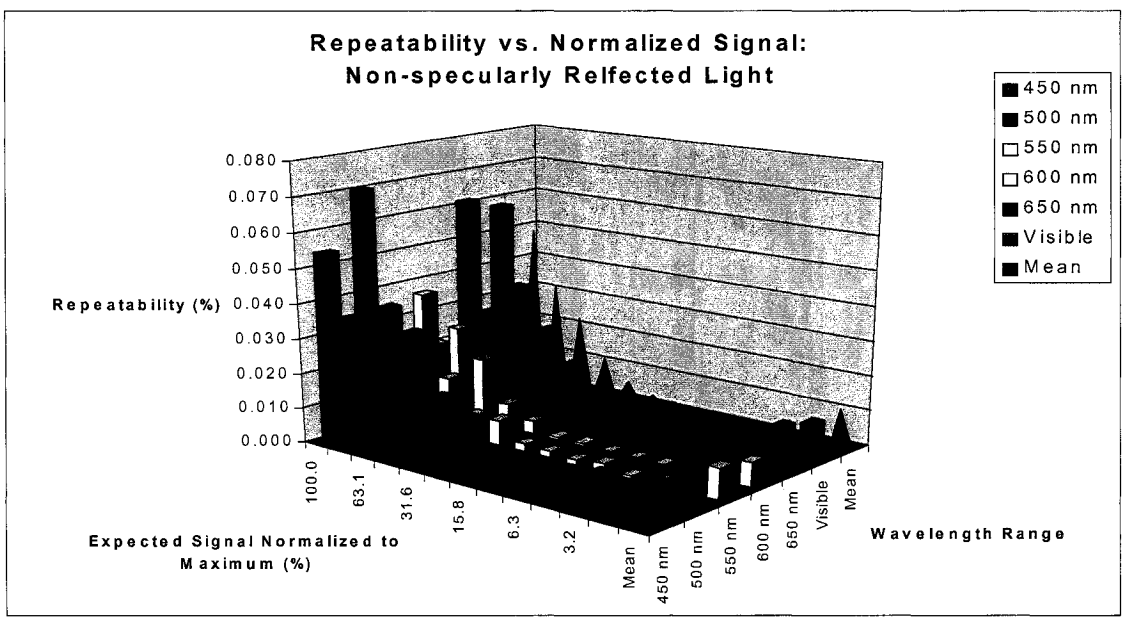

Figure 4-4: Repeatability - Non-specularly Reflected Light

Mean system repeatability for non-specularly reflected light over five spectral bands and the visible spectrum are better than the specifications of <2% (max. intensity).

The maximum values listed at the bottom of each table also meet the specifications noting that no data was excluded.

Based on the above results, the repeatability is better than the reproducibility for each of the four optical properties. Considering that the only variable introduced in the repeatability test is the placement of the control, it is likely responsible. Therefore, a separate test measured the optical properties as the control sample is moved laterally, 1 mm in the same direction between each measurement, and then when the sample is returned to the original location. The results demonstrate that the first and last measurements, which were taken at the same position (< 1 mm co-locating error), were closer than any other two readings. The system reproducibility is likely related to how precisely the control is placed in the same location between measurements.

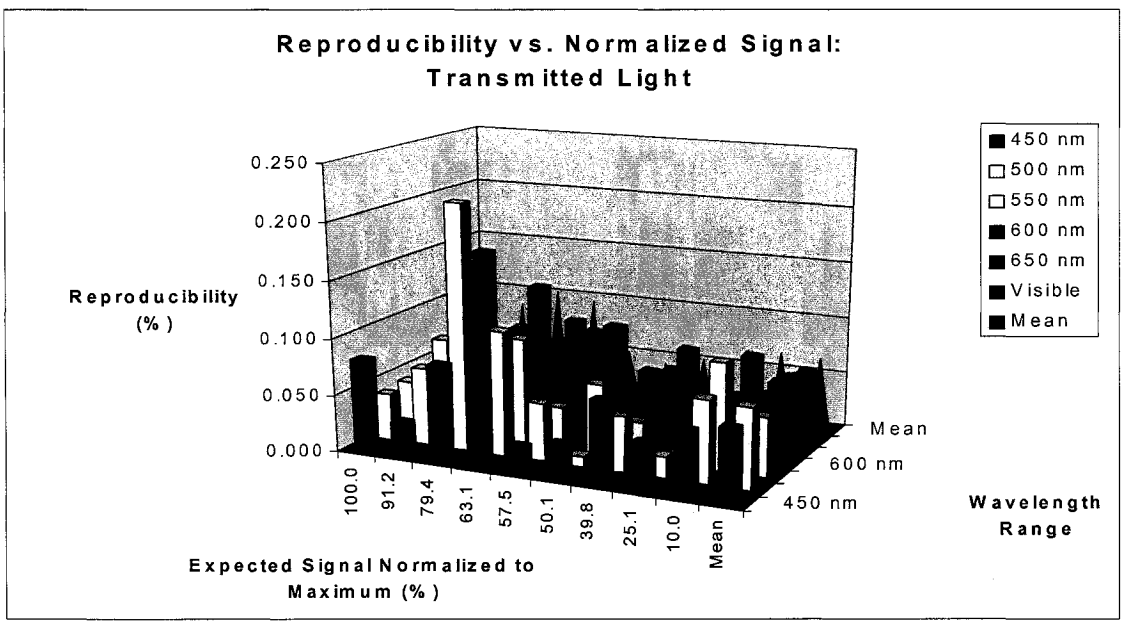

Figure 4-5: Reproducibility - Transmitted Light

Mean system reproducibility for transmitted light over five spectral bands and the visible spectrum are better than the specifications of <1% (max. intensity).

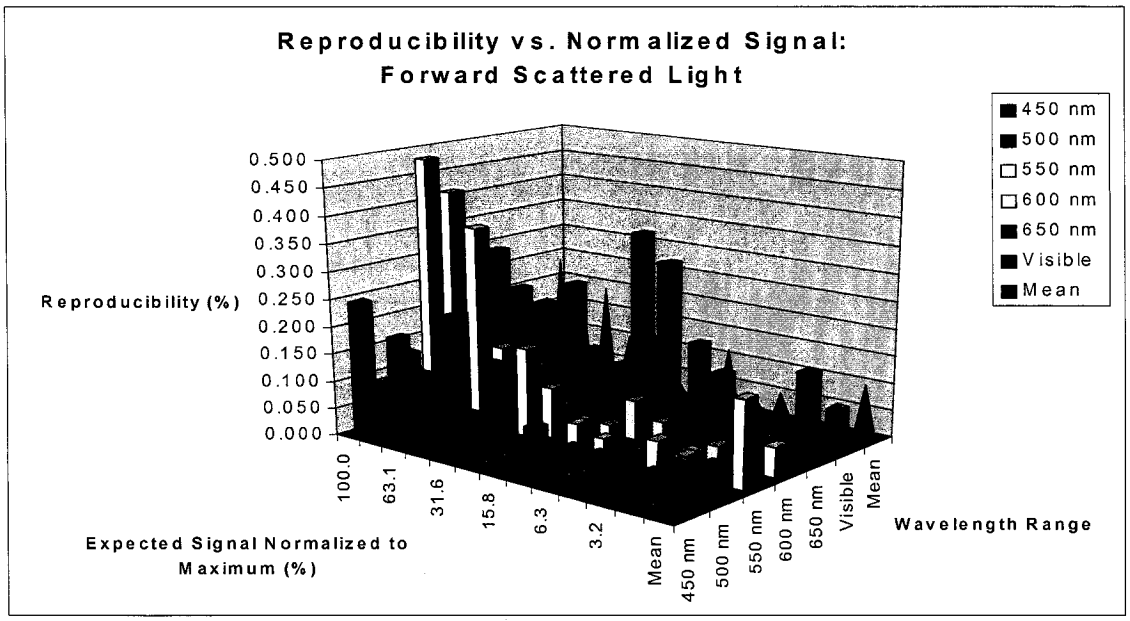

Figure 4-6: Reproducibility - Forward Scattered Light

Mean system reproducibility for forward scattered light over five spectral bands and the visible spectrum are better than the specifications of <2% (max. intensity).

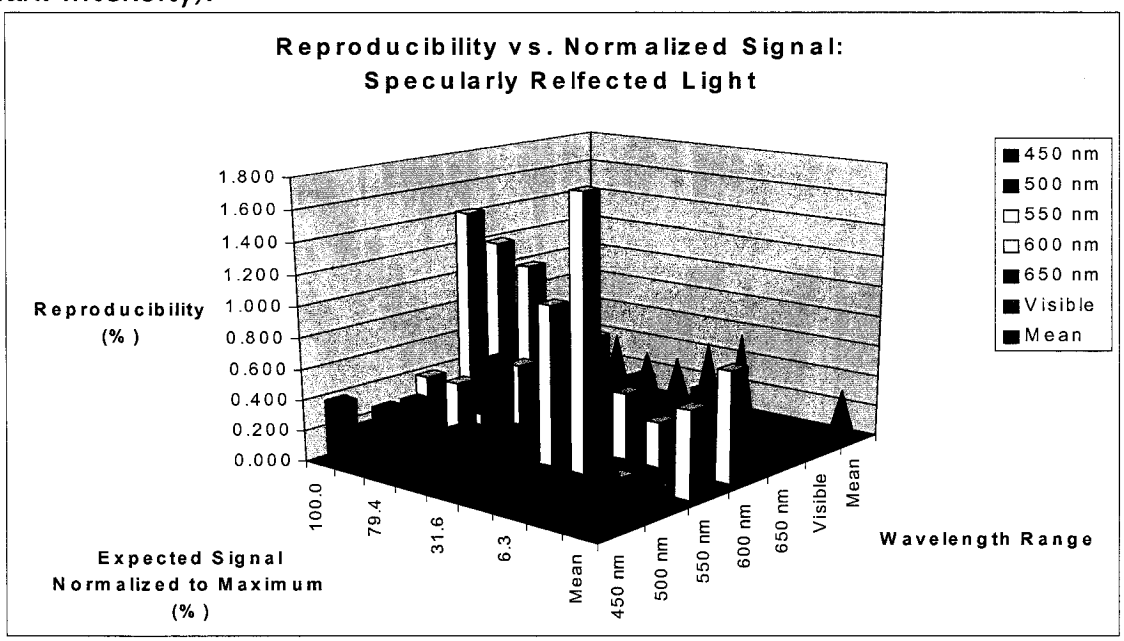

Figure 4-7: Reproducibility - Specularly Reflected Light

Mean system reproducibility for specularly reflected light over five spectral bands and the visible spectrum are better than the specifications of <2% (max. intensity).

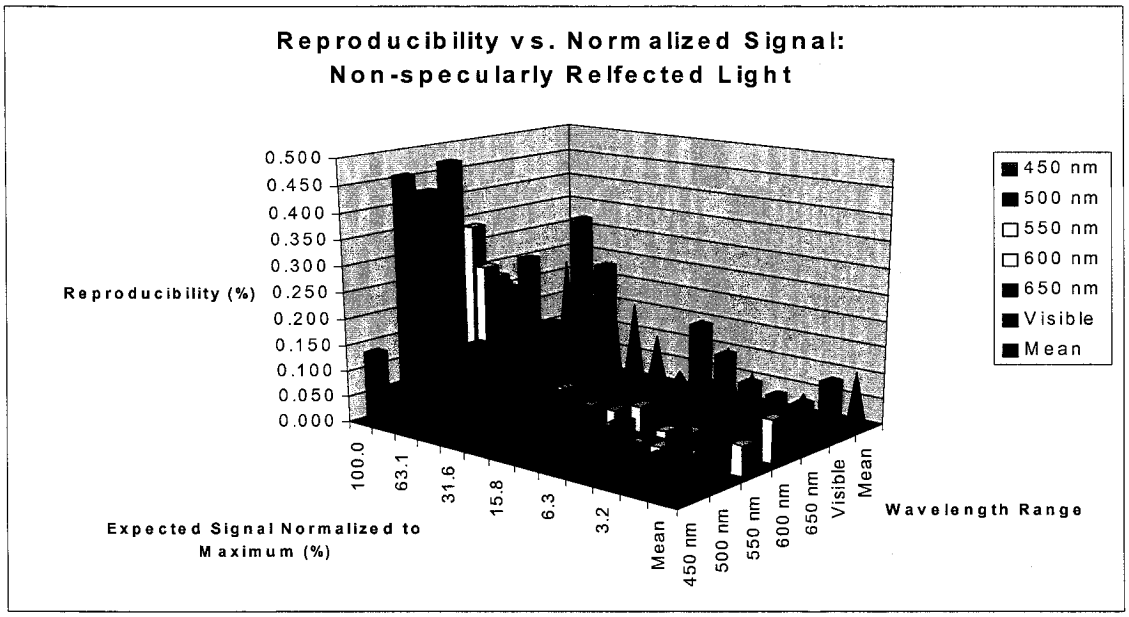

Figure 4-8: Reproducibility - Non-specularly Reflected Light

Mean system reproducibility for non-specularly reflected light over five spectral bands and the visible spectrum are better than the specifications of <2% (max. intensity).

4.3 Sensitivity of System Optical Measurements

The sensitivity of the system is the change in response of the optical property divided by the corresponding change in the input or stimulus. For this system, the sensitivity is particularly important for forward scattered and non-specularly reflected light and is one measure of the effectiveness of the parabolic collecting mirrors. Sensitivity is better represented for this research as a relative improvement in one technique over another. A test setup was designed to allow the collection and detection techniques of both the current system as well as that used in the older system (Priest, 1998) to be utilized simultaneously as shown in Figure 4-9. This approach removes all but the variable in question, which is the improvement in signal when using the collecting mirror. Two detectors are placed in the same optical system with the first, representing the older instrument, captures the light as it reflects off a control (opal diffuser) in the exact location as used in the older instrument. The second detector, representing the ideal location for this system,

detects light from the control *after* it is reflected off the collecting mirror.

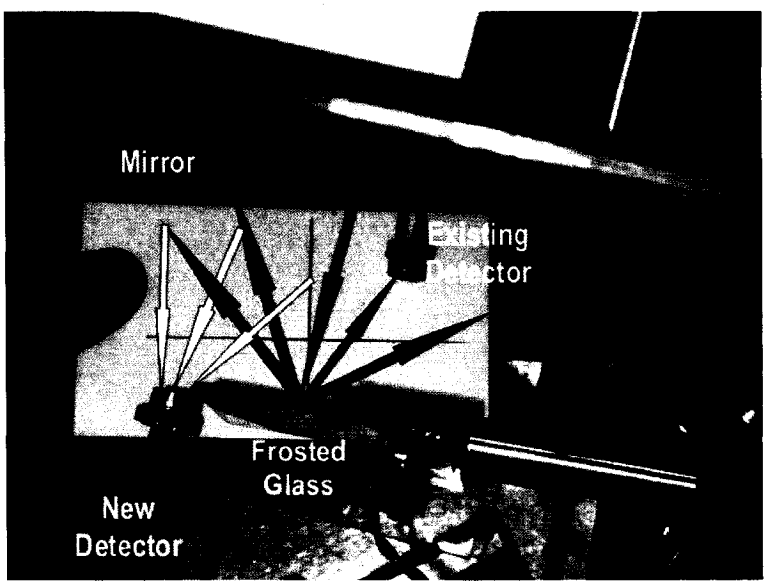

Figure 4-9: Sensitivity Setup

Scattered light from the sample (blue arrows) is directly measured by the existing detector and via the mirror (yellow arrows) to the new detector.

Both detectors measure the signal concurrently, and, other than the optical amplification of the "new detector", there are no other variables other than their placement that affect the sensitivity. The results of the signal measured in volts through a transimpedance amplifier circuit are represented in Figure 4-10. The graph demonstrates that there is a significant improvement in the sensitivity of the mirror compared with using no mirror at all and it is approximately 20 fold in range of 2% to 14% of maximum intensity. The data not only demonstrates a large improvement in sensitivity, but that the change in sensitivity is related to the change in incident intensity by a 3rd order polynomial fit. Results are similar for a qualitative test that compared the brightness at the location of the detector for the non-specularly reflected and forward scattered light.

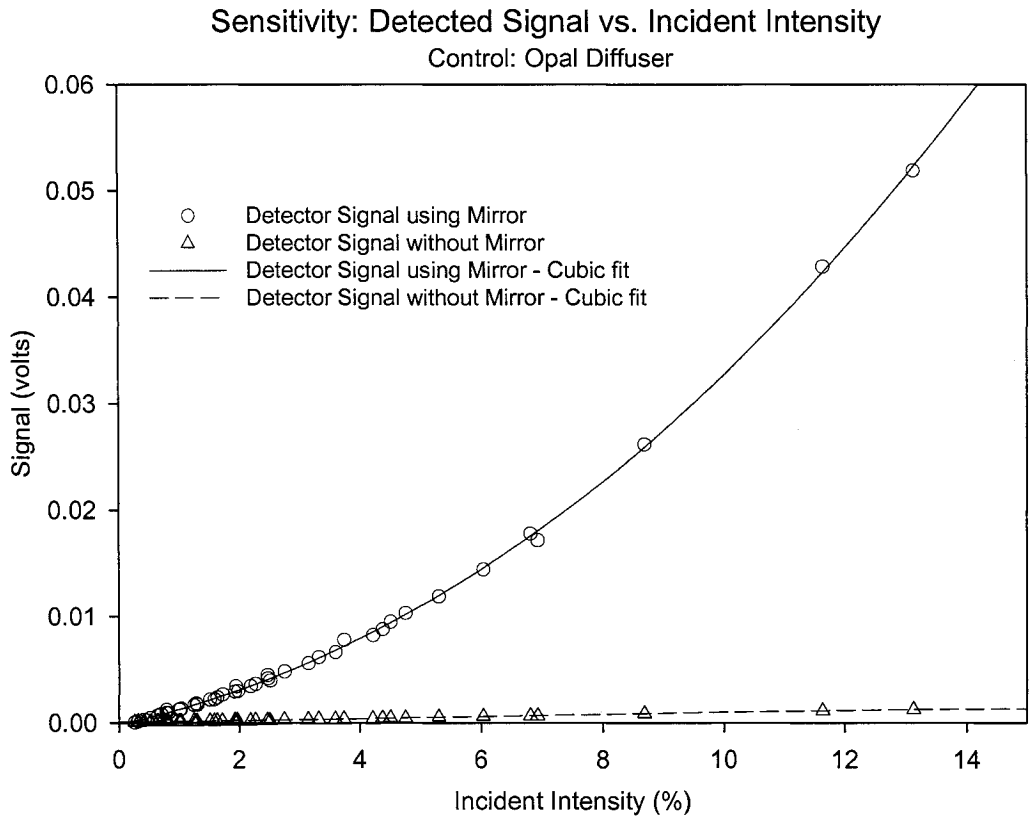

Figure 4-10: Relative Improvement in Sensitivity

The sensitivity of the two detectors, one measuring the signal reflected from an opal diffuser, and the other, the signal using the POC collecting mirror.

4.4 System Threshold Measurements

A threshold test determines the minimum signal that can be detected by the system. This test is limited by the availability of ND filters and based on preliminary testing, two optical densities are used: 4.24 (0.0063%) and 4.20 (0.0057%), both of which are outside the system specifications and are obtained by stacking three ND filters and two ND filters, respectively and are repeated for all four properties and at all six spectral ranges. A session includes three separate measurements with the ND filters undisturbed between measurements.

The paired t-Test as presented in Table 4-1 is used to test that a difference

between the measured values using the two optical densities is real. The value of P is less than 0.005 for all but three measurements (transmitted light 500 nm, forward scattered light 450 nm, and specularly reflected light 650 nm). For the remainder of the measurements the paired t-Test thus confirms that the system threshold is 0.0057% of maximum illumination.

Table 4-1: System Threshold

Wavelength	Nominal (% max. intensity)	Tr (% max. intensity)		FSc (% max. intensity)		RSp (% max. intensity)		RNSp (% max. intensity)	
		Measured	P	Measured	P	Measured	P	Measured	P
450 nm	0.0060	0.1579%	0.0023	0.4468%	0.1950	0.1299%	0.0019	2.2748%	0.0011
	0.0055	0.1569%		0.4460%		0.1281%		2.1608%	
500 nm	0.0068	0.0617%	0.0115	0.1274%	0.0010	0.0500%	0.0021	0.4116%	0.0011
	0.0061	0.0610%		0.1265%		0.0487%		0.3821%	
550 nm	0.0064	0.0430%	0.0019	0.0778%	0.0043	0.0361%	0.0039	0.1958%	0.0028
	0.0059	0.0426%		0.0766%		0.0352%		0.1824%	
600 nm	0.0069	0.0381%	0.0008	0.0651%	0.0001	0.0329%	0.0009	0.1496%	0.0013
	0.0062	0.0376%		0.0639%		0.0317%		0.1393%	
650 nm	0.0072	0.0381%	0.0010	0.0656%	0.0011	0.0340%	0.6235	0.1349%	0.0013
	0.0065	0.0377%		0.0645%		0.0340%		0.1254%	
White	0.0063	0.0412%	0.0077	0.0727%	0.0033	0.0373%	0.0010	0.1817%	0.0030
	0.0057	0.0407%		0.0717%		0.0361%		0.1732%	

The results of a t-Test and the probability (P) that data from testing 2 nominal intensities were obtained from different populations for all but 3 of the 24 tests.

4.5 Measurement of and Correction for Light Source Stability

One significant design feature of this system described earlier is that the light source is monitored in real time, and any changes are used to adjust the signal detected from the four optical properties. This specification is based partly on the fact that drift can occur with halogen light sources, because of either the electronics, or the bulb element. This test is used to confirm that drift exists, and to quantify it. A

preliminary test determined that the drift of the light source changed by 1% in the 2-minute period immediately after the source is turned on. The reference signal is obtained by using a beam splitter, which optically splits a small portion of the light towards the reference detector. As the software designed by the author utilizes a 1 second polling of the signals over a period of five minutes, the polling is started and the light source is then turned on.

The results compared both the raw signal and calibrated signal from the reference detector with both signals normalized to their respective signals at the 4-minute mark. This latter point is chosen, as it is more stable than at the initial point of turning the source on. The data in Figure 4-11 reveals that there is an 8% drop in the raw signal within the first 4 minutes of the source being turned on. At the one minute-mark, the signal decay appears to be more linear but continues to decrease even after 4 minutes. By contrast, the calibrated signal is stable after less than 20 seconds. The small variation is possibly the result of the ramping up of the light source using a rotary knob, and the non-linear relationship of the detectors at the instant the light is first emitted from the bulb.

4.6 Sensitivity of System Measurements due to Sample Height

As part of the design specifications, the system uses a collimated light delivery system. One of the advantages of this system is that there should be a reduced sensitivity to the sample height, or vertically. Ideally, the same results can be achieved regardless of the sample thickness or height. However, undesirable sensitivity to height is more prevalent in the final as-built system because of the size reduction and must be quantified.

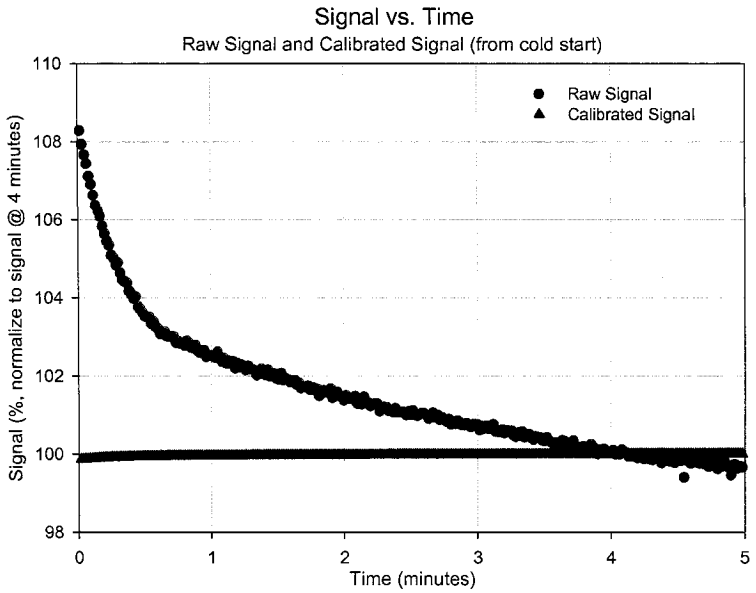

Figure 4-11: Light Source Drift Test

The above graph using white light demonstrates the need for the real-time reference detector for calibration, and the results of using the calibrated signal.

A test utilizing glass plates, each with a known and identical thickness, measures the relationship between each of the four optical properties, and sample height or thickness. Glass plates are well suited as they are transparent and enable the testing of all four optical properties. In addition, their optical properties are well known, and can therefore be compared to the theoretical results.

The glass slides are thoroughly cleaned before testing to ensure minimal impact of any deposits. Consequently, forward scatter remains almost inexistent, even as the number of glass slides is increased as demonstrated in Figure 4-12. Both the measured transmitted and specularly reflected light closely approximate the values predicted by the Fresnel equations when no forward scatter and non-specularly reflected light is assumed. As slides are added, there are additional interfaces introduced, resulting in a decrease in transmitted light and an increase in specularly reflected light. An equation representing glass that has 96.8% transmittance with neither forward scatter nor non-specular reflection is also plotted in Figure 4-12 with the measured transmitted light for comparison. This difference

between 100% and this latter value, 3.2%, is likely the amount of light absorbed by the glass slides.

A second test is used to better isolate the non-specularly reflected light as a function of sample height. A piece of glossy paper purchased from a local stationary store was placed at heights that increased by 0.040" (1.02 mm) to a maximum of 0.40" (10.2 mm). The data from the testing is presented in Figure 4-13, and it demonstrates that non-specularly reflected light *is* a function of sample height. As the reflected light is imaged onto a detector with a mirror of a given focal length, any change in the vertical sample position will impact the size of detector required to capture the light, and if the detector size remains the same, the signal will change. It is also relevant that the paper sample produced non-specular reflection that is well beyond the system limits. Nevertheless, any future sample testing will need to consider this variable.

4.7 Summary

Validating the system is primarily based on repeatability, reproducibility, sensitivity, and threshold testing. Results from this testing demonstrates that this new system meets or surpasses all specifications. Drift and fluctuations in the light source are both quantified and calibrated for in the design. Limitations to the sample height are also quantified. With the system validation process completed, biological sample testing can be performed. Therefore, in a perfect situation, the system outperforms our expectations except for non-specular reflection where object position (height) is critical.

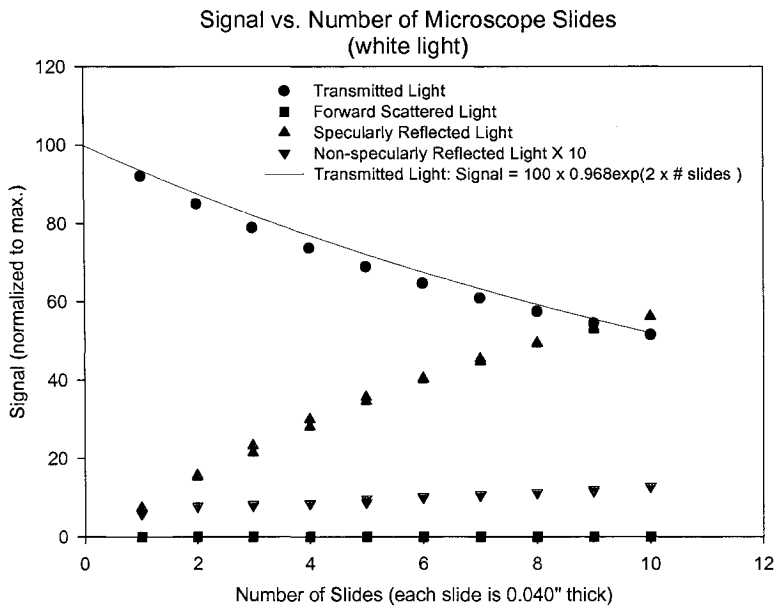

Figure 4-12: Variation of Signal with Microscope Slide-stack Height

The graph above shows how each of the four optical properties varies with sample height and thickness, measured twice at each height.

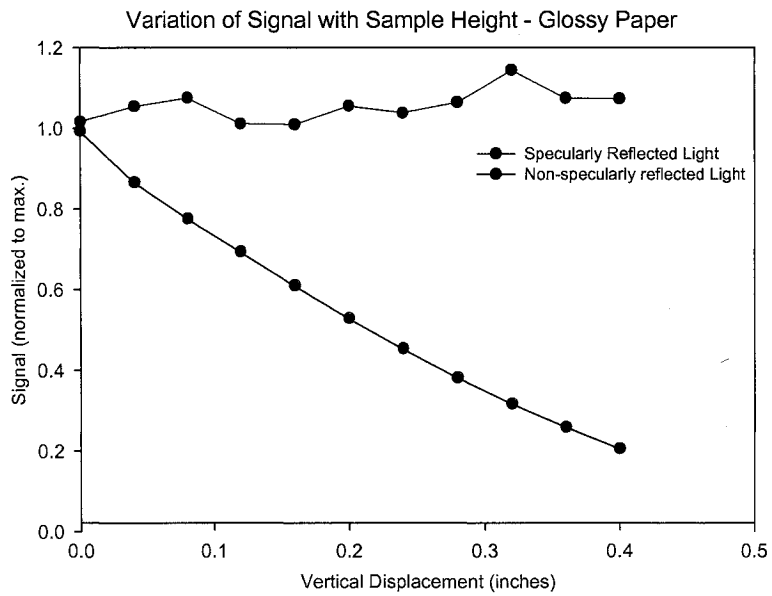

Figure 4-13: Variation of Signal with Sample Height

Using a sample of glossy paper, both specular and non-specular light characteristics measured with changing sample height.

5 Biological Application Testing

Final application verification requires that a measurement system be developed and tested with a real sample. Potential applications targeted by this device can be divided into two categories: synthetic biomaterials and natural materials. A brief statement on common protocols for each of the two categories is discussed, followed by details on methods and results of tests on actual materials of each type.

5.1 Measurement Technique using the Sample Holder

The samples are fully immersed in a tray and transparent fluid such as water, a saline solution, or a transparent growth medium for use with living tissue. The tissue needs to be measured in a neutral, or a buffered saline solution (BSS) to ensure that there are no osmotic changes, which could impact the tissue/sample correlation to changes in its optical properties. The solution must be pH balanced to the sample, maintaining the short-term health of that sample. As the measurands are no longer the result of the sample alone, but include the tray with the fluid, their impact must be quantified. The term "holder" will refer to the tray when filled with a fluid. Biological tissue can have lower specular reflection than the tray, and when placed in the holder, the tissue sample can reduce the specular reflection that is measured from the tray under the sample. Consequently, simple subtraction of the holder measurand would be incorrect. There are several possible methods to correct the measurand for the effect of the holder, depending on the measurand. The tray could be tilted such that the specular reflection from the tray is diverted away from the detector. This approach would also reduce the specular light from the sample, which is also parallel to the tray. The approach taken in this research is to model the light interaction with the various mediums using the Fresnel equations to theoretically account for the holder effects.

The Fresnel equations are used to model the percentage of incident light that is reflected and transmitted as shown in Figure 5-1.

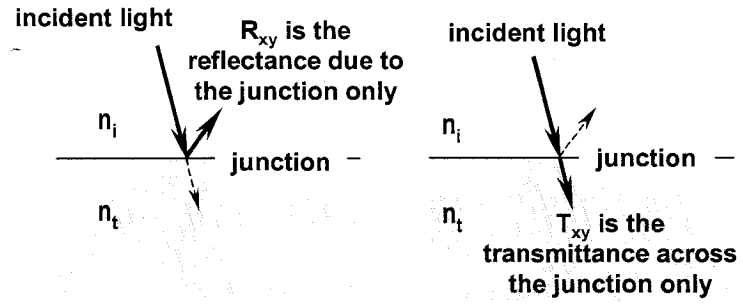

Figure 5-1: Transmittance and Reflectance

Assuming near normal incident light and that there is no non-specular reflection nor forward scatter, the reflectance at the junction of two mediums is,

$$R_{xy} = \frac{(n_t - n_i)^2}{(n_t + n_i)^2} \tag{5-1}$$

where: n_i and n_t are the indices of refraction of incident (x) and transmitted (y) mediums

With the same assumptions, the transmittance at the junction of two mediums x and y is given by:

$$T_{xy} = \frac{4 \cdot n_t \cdot n_i^2}{(n_t + n_i)^2} \tag{5-2}$$

where: T_{xy} is the transmittance at the across the junction of mediums x an y, for normal incidence

The model must also consider non-absorbed light in each medium and is defined by:

$$k_y = (1 - A_y) \tag{5-3}$$

Therefore, the total transmittance through medium y sandwiched by medium x that accounts for light lost at both surface junctions, as well as that absorbed internally, is defined by:

$$T_{xyx} = T_{xy} \cdot (1 - A_y) \cdot T_{xy} = (1 - A_y) \cdot T_{xy}^2 \tag{5-4}$$

Using the Equations 5-1, 5-2, 5-3 and 5-4, a model is now developed for an air-water-sample-glass-air interface used in the sample testing as shown in Figure 5-7. The measured transmittance through water and the tray, is given by:

$$T_{1245} = T_{12} \cdot (1 - A_2) \cdot T_{24} \cdot (1 - A_4) \cdot T_{45} \tag{5-5}$$

where: A_2 is the absorbance of light in water
A_4 *is* the absorbance of light in tray
T_{12} is the measured of light transmittance from air to water
T_{24} is the measured of light transmittance from water to tray
and T_{45} is the measured of light transmittance from tray to air

The measured transmittance through water, tray and *sample,* is defined by:

$$T_{12345} = T_{12} \cdot (1 - A_2) \cdot T_{23} \cdot (1 - A_3) \cdot T_{34} \cdot (1 - A_4) \cdot T_{45} \tag{5-6}$$

where: A_3 is the absorbance of light in sample
T_{23} is the measured of light transmittance from water to sample
and T_{34} is the measured of light transmittance from sample to tray

Using Equations 5-5, 5-6, and solving for the absorbance of the sample yields;

$$A_3 = 1 - \frac{1}{4} \cdot \frac{T_{12345}}{T_{1245}} \cdot \frac{(n_2 + n_3)^2 \cdot (n_3 + n_4)^2}{n_3^2 \cdot (n_2 + n_4)^2} \tag{5-7}$$

where: n_2 is the index of refraction of water
n_3 is the index of refraction of sample
and n_4 is the index of refraction of tray

Using A_3 for the sample, the expected transmittance, T_{135}, of the sample can be calculated as follows:

$$T_{135} = T_{13} \cdot (1 - A_3) \cdot T_{35} \tag{5-8}$$

where: T_{13} *and* T_{35} are the transmittance across the junction of air and the sample respectively, and are is further defined by:

$$T_{13} = T_{35} = \frac{4 \cdot n_3 \cdot n_5^{\,2}}{(n_3 + n_5)^2} \tag{5-9}$$

where: n_1 (= n_5) is the index of refraction of air

Using A_3 for the sample, the expected reflectance, R_{135}, of the sample in air alone can be calculated as follows:

$$R_{135} = R_{13} \cdot \left[1 + T_{13}^2 \cdot (1 - A_3)^2\right] \tag{5-10}$$

where: R_{13} is the expected transmittance of light from at an air/sample junction and is given by:

$$R_{13} = \frac{(n_1 - n_3)^2}{(n_1 + n_3)^2} \tag{5-11}$$

With reference to Figure 5-2, there are a number of additional assumptions required in using the above calculations for this model. Typically, there are multiple reflections for each surface that can affect both the assumed transmitted and reflected light.

A transmittance measurement includes light that has been reflected an even number of times at internal surfaces but at much reduced signal. Assuming light travels through the medium in a single pass, a transmittance of 90.9% is assumed (n = 1.585), using the model. The difference between the measured and assumed

transmittance is 0.1% and will be neglected for this model.

Similarly, a specular reflected light includes light that has reflects an odd number of times from the surfaces. For transparent materials, where the transmitted light is at least one order of magnitude stronger than specular reflection, only fundamental reflections will be assumed in the model.

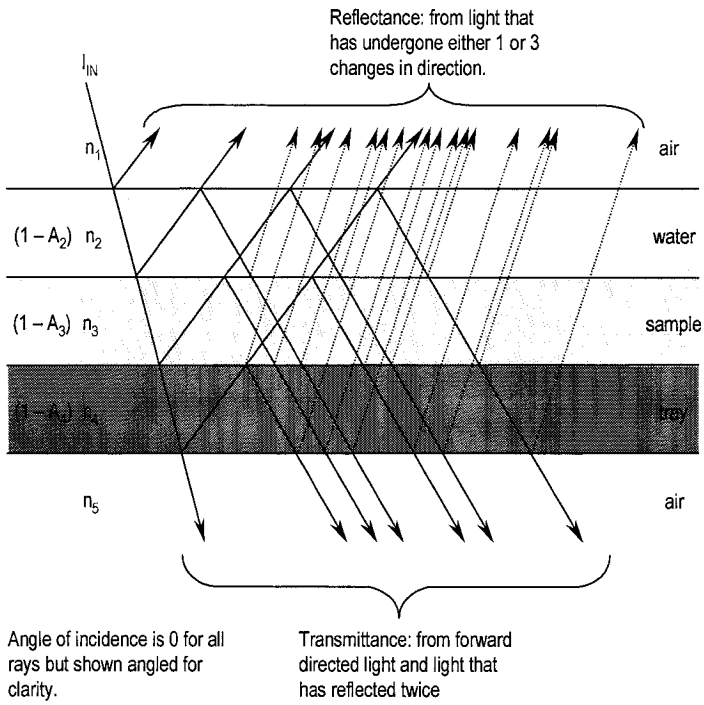

Figure 5-2: Multiple internal reflections

Light measured as transmitted light includes light that undergoes countless directional changes.

The measured non-absorbed light from the tray (MatTek Corporation) is 98.4%, using the visible spectrum, and is calculated from the sum of the four optical measurements. The predicted non-absorbed light using the model is 98.2%, resulting in a difference of 0.2%. The measured non-absorbed light in water is 1.000. This value compares favourably with the theoretical attenuation of light in water given by:

$$I = I_o \cdot e^{\alpha L} \tag{5-12}$$

where: α is 1×10^{-3} cm^{-1} (attenuation of water)
and L is 0.6 cm (height of water in the tray)

A control sample is then used to evaluate the efficacy of the above model using white light. This sample is chosen to be rigid, have homogeneous optical properties, and have a known index of refraction. Polystyrene was chosen as the control sample. The predicted non-absorbed light from the sample when placed in a water-filled tray using the above model is 99.7%. The polystyrene control was then measured in air alone and the non-absorbed light was measured as 99.3% resulting in an error of 0.4% of the predicted value when using the model. The value of transmittance of the control sample was predicted using the above model and found to be 89.7%. The measured value is 89.4% resulting in an error of 0.3%.

The combined value of transmittance (transmitted light + forward scattered light) for the sample, tray, and water is 91.3%. The corresponding predicted non-absorbed light from the sample is 90.9% when assuming a single pass of the transmitted light. These results show that the prediction is close to the actual to within 0.4%, and that the assumptions are sufficient for the intended applications.

The measured value of the specular reflection in air is 6.4% and the predicted value using the model is 6.5%. It is important to note that the model does not account for forward scatter or non-specular reflection from the sample. Therefore, this difference of 0.1% could be the value of the non-specularly reflected light.

The model assumes that the indices of refraction of the tray, water, air, and sample are known. As the sample index of refraction may have some variability, a tolerance analysis is required. The results in Table 5-1 show that the variation in error between the predicted and measured transmittance is due to the error in estimating n_3 of the sample.

Table 5-1: Tolerance Analysis of n_3

n_3	Expected Non-absorbed light ($1 - A_3$)	Calculate transmittance of control alone	Error
1.570	0.996	0.900	0.67%
1.575	0.996	0.899	0.56%
1.580	0.996	0.898	0.45%
1.585	0.997	0.897	0.34%
1.590	0.997	0.896	0.22%
1.595	0.998	0.895	0.11%
1.600	0.998	0.894	0.00%
1.605	0.998	0.894	0.00%
1.610	0.999	0.893	0.11%
1.615	0.999	0.892	0.22%
1.620	1.000	0.891	0.34%
1.625	1.000	0.890	0.45%
1.630	1.000	0.889	0.56%

Tolerance analysis to determine the error in estimating the value of n_3 of the sample.

The results of the modeling approach suggest that the approximation was good when the transmittance is 100% transmitted light with no forward scattered light, and that the reflectance is 100% with no, non-specularly reflected light. However, when forward scatter and non-specular reflection of a sample increase, the prediction of all four properties without the holder is less accurate. The system primarily focuses on accurately measuring *small* changes of the optical properties but can predict, with limitations, the absolute values of the optical properties of the sample by compensating for holder effects.

5.2 Testing Synthetic Materials

Several types of synthetic materials are tested including corneal constructs and corneal onlays. These materials can be easily damaged, especially if they are based on, or hosts living tissue, and generally require careful handling. Unless otherwise stated, all optical testing of the four measurands is performed with light

within the visible spectrum and at 450 nm, 500 nm, 550 nm, 600 nm, and 650 nm.

5.2.1 Optical Properties of Corneal Constructs

There are two types of corneal constructs available; the first type is thinner but more difficult to work with while the other type is thicker than a human cornea but more robust and is well suited for testing. The latter tissue's optical properties were tested. The corneal constructs were first rinsed in a buffered saline solution containing antibiotics and the initial optical properties were then measured at 650 nm to obtain baseline properties prior to treatment. Alcohol, (75%-75μL) was then placed on the tissue and the same optical properties were measured immediately, every minute for ten minutes, and then at 15 and 20 minutes thereafter.

The results from the testing of the corneal constructs subject to the application of alcohol demonstrates that there is a measurable response, as a change in all measurands as shown in Figure 5-3. Approximately five minutes after exposure, the Forward Scattered Light (FSL) increases by 14.8% compared to the untreated state and was relatively constant to the test-end, where it is 13.4% higher than at the untreated state. After 4 minutes, there is a reduction with no recovery in, Transmitted Light (TL) of 48.6%, Specularly Reflected Light (SRL) of 21.7%, and Non-Specularly Reflected Light (NSRL) of 32.0%. The increase in FSL is consistent with a decrease in TL.

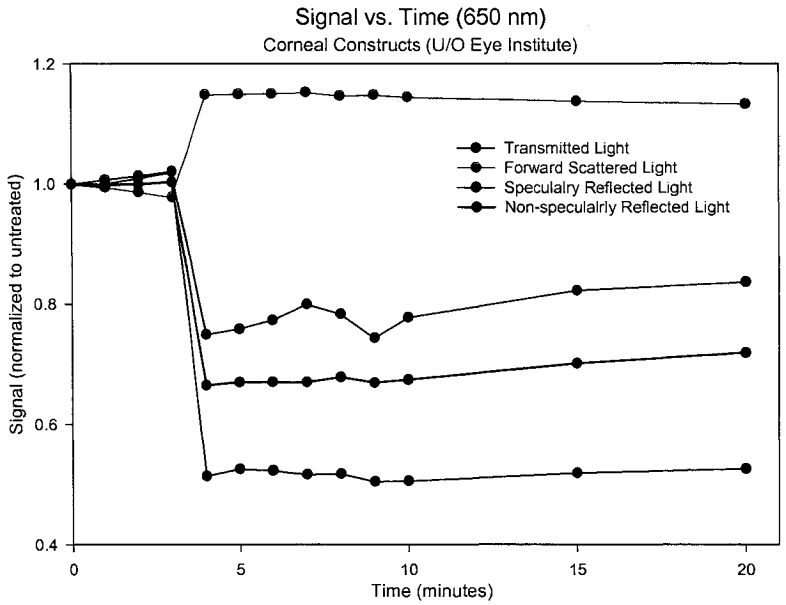

Figure 5-3: Change in Optical Properties - Corneal Construct

Typical response of a corneal construct to the application of a 70% ethanol solution.

5.2.2 Optical Properties of Engineered Tissues

Engineered tissues requiring optical testing were supplied as blinds samples[1]. TL and NSRL were measured using the precursor to the proposed system. As such, these samples proved useful in comparing the older design to new one. With the older design, the samples were tested in air, and as such, the correction as described in Section 5.1 is applied to properly compare the two sets of data. A problem encountered during testing is that the material can float when the solution is added. Therefore, the tissue was placed in the tray and allowed to dry out for 3 hours and adhere to the tray. A quantity of 10 ml of buffered saline solution (BSS) was added to the tray. Any tissues that float after adding fluid were rejected for optical testing. The optical properties were measured 5 times using the visible spectrum.

---

[1] Provided by Dr. Heather Sheardown of McMaster University

The optical properties are presented in the four graphs in Figure 5-4. Standard error bars show the tight tolerance in measurements of the new system. The raw data from the system includes the optical data from the holder and a correction factor must be used to factor out the effect of the holder to compare treatments to those from the precursor system. The results with the correction factor applied are presented in Table 5-2 and show that for 3 of the 4 samples, the adjusted TL is higher, by an average of 2.1%. The precursor design used tissue exposed to the air allowing it to dry out during the 10-15 minutes while the test is being conducted. Tissue that is allowed to dry out immediately starts to increase in opacity, reducing TL. The correlation between the data of the older design and the new system results in r = 0.643 (Pearson formula).

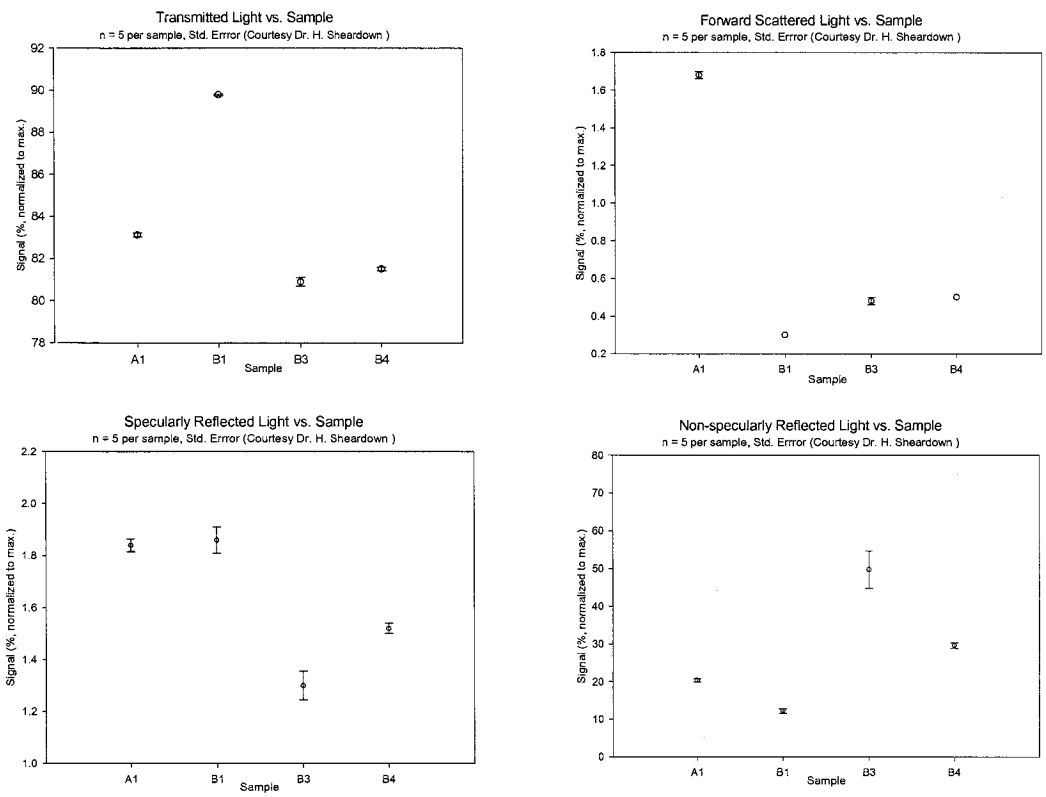

Figure 5-4:Optical Properties of Engineered Tissues

TL, FSL, SRL, AND NSRL of four engineered samples using the visible spectrum.

Table 5-2: Transmitted Light: Current Design vs. Older Design

Tissue Sample	Transmitted Light: Including Holder	Transmitted Light: Adjusted- holder excluded	Transmitted Light: *Older Design*
A1	83.1%	88.2%	80.7%
B1	89.8%	95.3%	91.4%
B3	80.9%	85.8%	87.8%
B4	81.5%	86.5%	82.8%
Mean	**83.8%**	**89.0%**	**85.7%**

Comparison of TL using the system and the older design (accuracy 2%).

5.2.3 Optical Properties of Corneal Onlays

Two groups of 3 corneal onlays were provided to determine if there was a difference in their respective optical properties[1]. The tissue optical properties were measured at 450 nm, 500 nm, 550 nm, 600 nm, 650 nm, and with visible light.

The fluid from the onlay vials was used to ensure sample health. The test was performed at room temperature and the total time for the testing of all samples is two hours. The holders were obtained from MatTek Corporation (part number P35G-0-14-C-gm) and were inspected for scratches and other defects, which might impact optical measurements.

TL is lowest at 450 nm, increases with increasing wavelength and is highest for 650 nm for all samples as presented in Figure 5-5. FSL for all but sample #5 is below 1.5% for all wavelengths as presented in Figure 5-6. SRL from all samples was lowest at 450 nm and highest at 600 nm as presented in Figure 5-7. All samples exhibit lower than 6% SRL. NSRL for all samples is below 18% with the highest NSRL at 450 nm and the lowest at 650 nm for all samples as presented in

[1] Provided by Dr. May Griffith of the University of Ottawa

Figure 5-8. All samples were of good quality.

Consideration of all optical properties reveals that sample #3 and #4 are better samples: TL varies from 84.0% to 90.5%, FSL varies from 0.3% to 0.6%, and NSRL varies from 0.7% to 5.2%. SRL is comparable for all samples.

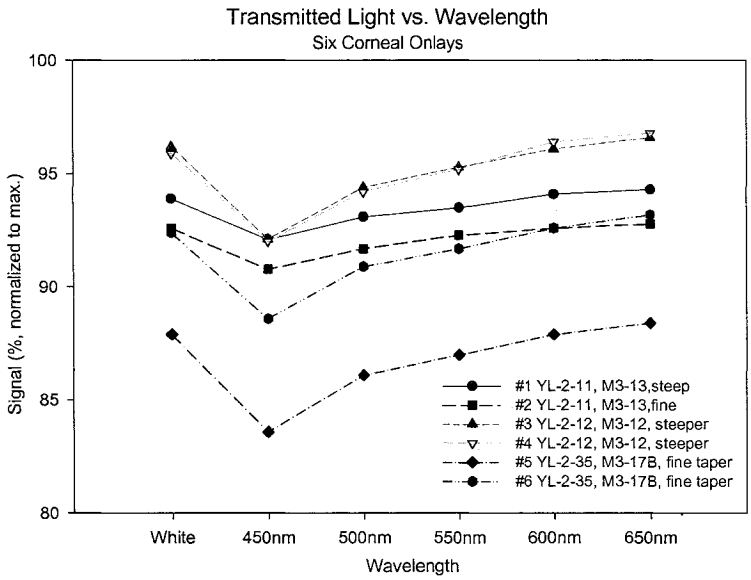

Figure 5-5: Transmitted Light - Onlays

TL for six spectral ranges (White = Visible Spectrum) using six corneal onlay samples.

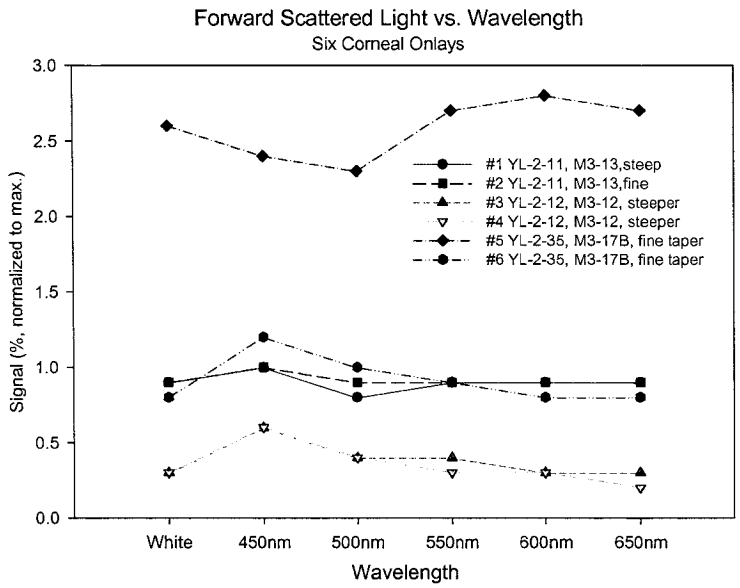

Figure 5-6: Forward Scattered Light - Onlays

FSL for six spectral ranges (White = Visible Spectrum) using six corneal onlay samples.

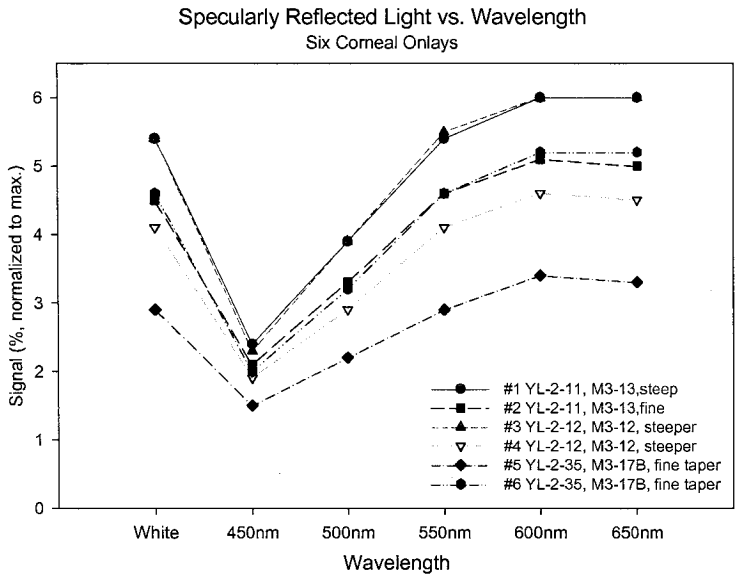

Figure 5-7: Specularly Reflected Light – Onlays

SRL for six spectral ranges (White = Visible Spectrum) using six corneal onlay samples.

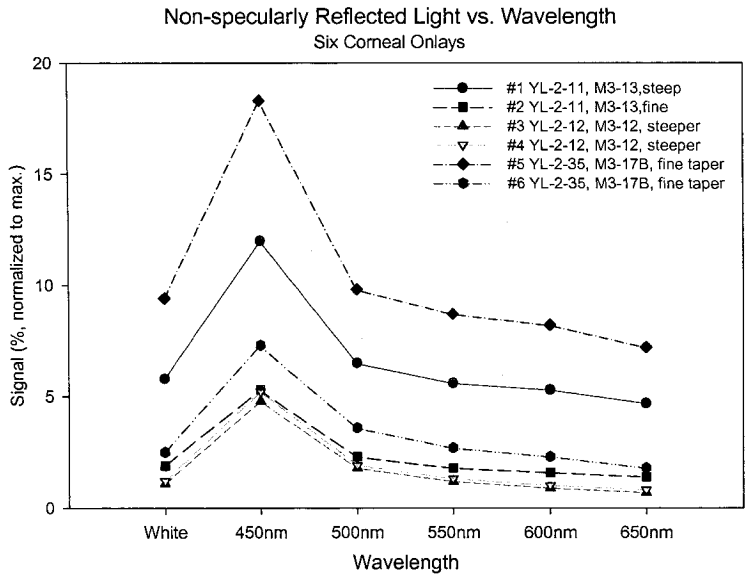

Figure 5-8: Non-specularly Reflected Light - Onlays

NSRL for six spectral ranges (White = Visible Spectrum) using six corneal onlay samples.

5.3 Testing Natural Materials

Natural materials tested in the course of this work include human, porcine, and bovine post mortem corneas and crystalline lenses.

5.3.1 Measuring a Cataract Effect in Porcine Lenses

When crystalline lenses are cooled to 4°C, an occlusion forms in its center and is described as a cold cataract effect as shown in Figure 5-9. This effect is reversible as the lens is warmed and can thus be the basis for a test to demonstrate the system's ability to monitor changing optical properties of tissues.

Whole porcine eyes were obtained and lenses (tissues) excised within two hours of death and stored in a pH-buffered saline solution (BSS) at 4° C for 24 hours. To prevent condensation on the tray from affecting the transparency, the tissue and accompanying fluid are transferred to an identical tray that was maintained at 21°. The optical properties were tested within 15 seconds of being

removed from the cold storage and then every second for 15 minutes thereafter.

The values of both SRL and NSRL are above the normal operating range of the system are presented in Figure 5-10. Therefore, absolute values are inaccurate, thus, the values normalized to the first measurement of the test are presented. Initially, the lens is completely opaque and TL and FSL are non-existent. As the lens warms up from 4° to 21°, and the opacity resolves there is an increase in both TL and FSL. The cataract effect is observed to completely disappear at approximately 10 minutes, which is consistent with the measured data.

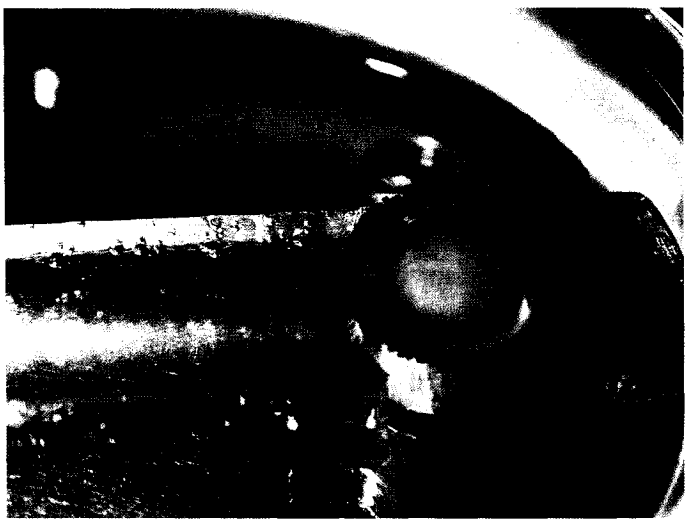

Figure 5-9: Cataract Effect - Porcine Lens

Cataract effect observed in porcine lens stored at 4° for 24 hours.

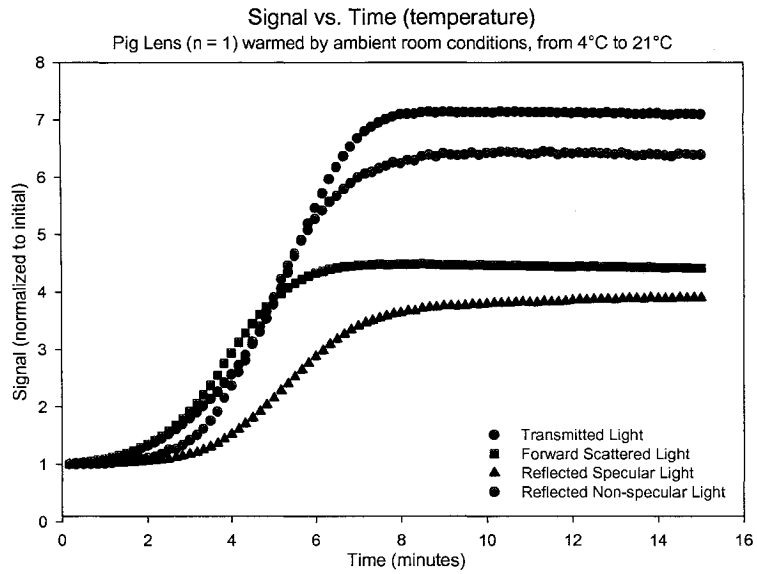

Figure 5-10: Optical Properties vs. Time - Porcine Lens

The change in optical properties as a porcine lens is warmed by ambient conditions from 4° to room temperature (21°) measured every 1 second.

5.3.2 Optical Properties of Porcine Lenses

The purpose of this test is to demonstrate equivalency to the back vertex distance (BVD) test used by Sivak *et al* (Sivak, 1997) and Bantseev *et al* (Bantseev, 2003). The lenses are exposed to three substances, a 70% ethanol solution (alcohol), sodium dodecyl sulphate (SDS), and a control, D-MEM-F12. The optical properties are measured for each sample, at 450 nm, 500 nm, 550 nm, 600 nm, 650 nm, and over the visible spectrum.

Whole eyes were obtained from a local butcher and they were dissected using biological protocols. Any damaged samples or those that would not be contained by the 4-part containment chamber as shown in Figure 5-11 were rejected after initial dissection and were allowed to sit in a nutrient medium for 24 hours. For each substance, 12 lenses were used (t-test, two-tailed, power = 0.80 and α = 0.10). The tissues were rinsed and drained three times and were placed in a four-part

containment chamber, which was in turn placed in a tray for optical testing with 13 ml of D-MEM/F12 (nutrient medium). The lenses were placed inside the chamber to prevent movement of the lenses, and the optical properties were then measured. Due to the variability in the readings observed in a pre-test, each optical property was measured three times, with re-centering of the sample before each measurement. The samples were then transferred to a tray for chemical exposure (reactant tray). A nylon containment ring was placed on each of the tissues as shown in Figure 5-12. This containment ring ensures that the chemical maintains contact with the lens and only in the confined area for the required time. A volume of 10 μl of the chemical was placed within the containment ring and the tissues were set aside for 30 minutes. The tissues were then rinsed and drained, without moving the washers, to minimize the impact of the chemical on the surrounding, unaffected tissue. The tissues were then transferred back to the optical trays. The optical test was performed every 15 minutes for the first hour, then every hour for the next 6 hours, and finally at 24 hours.

TL is presented normalized to the untreated condition in Figure 5-13. Immediately following the application of the alcohol (acute), TL decreases to 73% Relative to Untreated (RTU) and remains unchanged for the balance of the testing. Application of SDS results in an increase in TL 114% RTU at 3 hours and decreases to 78% RTU at test-end. Application of the control results in a decrease in TL to 93% RTU at test-end. One sample was rejected as TL for each of two tests (alcohol and SDS) as they differed from the other samples by more than 2 standard errors (SE) and because small bubbles were observed on the samples. For consistency, the data for these same samples was removed for the other three optical properties as well.

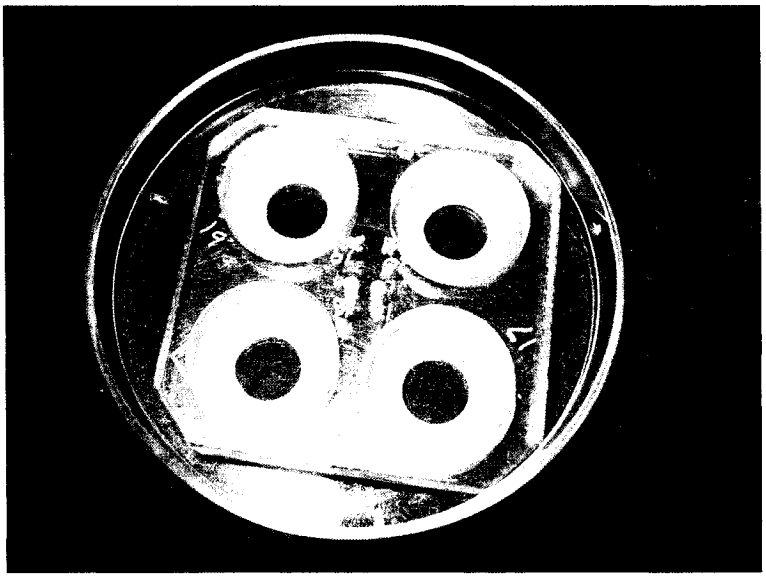

Figure 5-11: Tray and 4-Part Containment Chamber

The four part chamber used to isolate up to four lenses or corneas. Note that the fluid is not present.

The data for FSL is normalized to the untreated condition and is presented in Figure 5-14. Exposure to alcohol resulted in an increase in FSL to 164% RTU at the acute time point and remains constant throughout the test. SDS results increases FSL to 149% RTU at the acute condition followed by a gradual decrease to 123% RTU at 24 hours. Application of the control results in a gradual increase in FSL to 141% RTU at test-end. The increase in FSL is consistent with a decrease in TL.

Figure 5-12: Containment Ring shown with Porcine Lenses

Containment rings (6 mm ID) on porcine lenses (also for corneas) to ensure the substances remain in contact with the central part of the lens.

The results of the forward scatter of the porcine lenses are compared to the BVD test. The lens is an optical element that focuses all rays of collimated light entering the lens to the back focal plane. In this study by Bantseev et al (Bantseev, 2003) using the BVD test, the variability in the focal length of a bovine crystalline lens is measured before and after the application of sodium dodecyl sulfate (SDS). When a substance, such as an alcohol or surfactant, is applied to the lens, the index of refraction of the lens changes the focal point. While still a result of change in index, this system measures the aggregate forward scattered light in a single reading. Hartwick *et al* (Hartwick, 1997) observed a temporal profile of the forward scatter, when using Alcaine, a corneal anesthetic on a bovine lens. This result is consistent with the sharp increase followed by a subsequent drop in FSL observed in the first five hours of testing as shown in Figure 5-14. Although the magnitude and response time differ with respect to the BVD test, there are similar temporal trends between FSL and the focal length variability.

As with the previous measurands, SRL data is normalized to the untreated condition and is presented in Figure 5-15. Immediately after exposure to alcohol, SRL decreases to 89% RTU at the acute condition and increases to 96% RTU at 2.5 hours and then decreases to 80% RTU by 24 hours. Application of SDS results in

an increase in SRL to 106% RTU at 4 hours and a decrease to 95% RTU at test-end. Application of the control results in a gradual increase in SRL to 87% RTU at 4.5 hours, followed by an increase to 105% RTU at test-end.

The NSRL data is normalized, as with the previous measurands, to the untreated condition and is presented in Figure 5-16. With exposure to alcohol, NSRL increases at the acute condition to 179% RTU, recovers at 1.5 hours, and then increases again to 433% RTU at test-end. At 24 hours, five of the 12 data points vary by several orders of magnitude, with no corresponding visual indications. As well, the absolute NSRL is low, which results in abrupt relative changes. Therefore, these data points should be rejected. Application of SDS results in an increase in NSRL to 139% RTU at acute condition. NSRL then decreases to 117% RTU at test-end. Application of the control results in an abrupt increase in NSRL to 162% RTU at 4.5 hours, followed by a decrease to 108% RTU at test-end. The increase in SRL is consistent with a decrease in NSRL, for all substances and particularly so with the control.

In summary, this system can be used to observe a change in optical properties of crystalline lens when an irritant is applied. Application of alcohol produces the most dramatic change in all four optical properties, while the control exhibits changes that are more gradual. Monitoring the samples over time provides valuable data as to the possible recovery mechanisms that may exist.

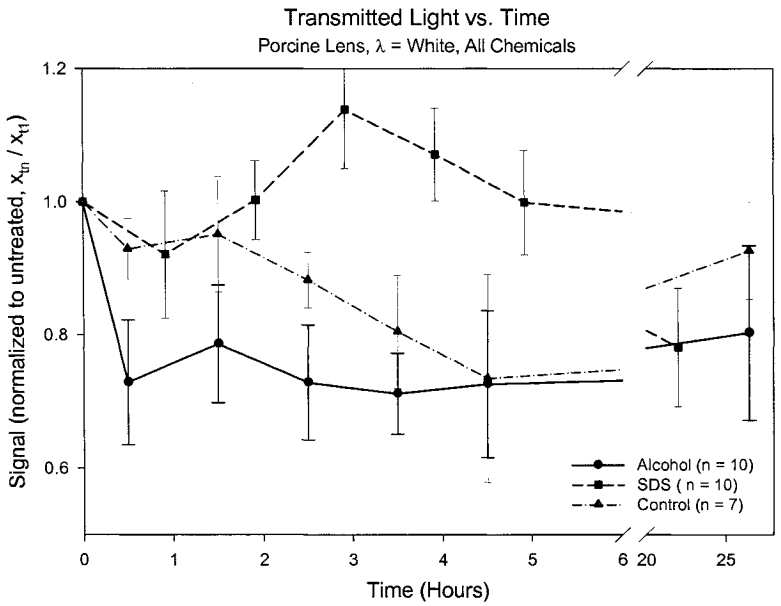

Figure 5-13: Transmitted Light vs. Time - Porcine Lens

TL normalized to untreated condition at t = 0 hours using alcohol, SDS, and a control.

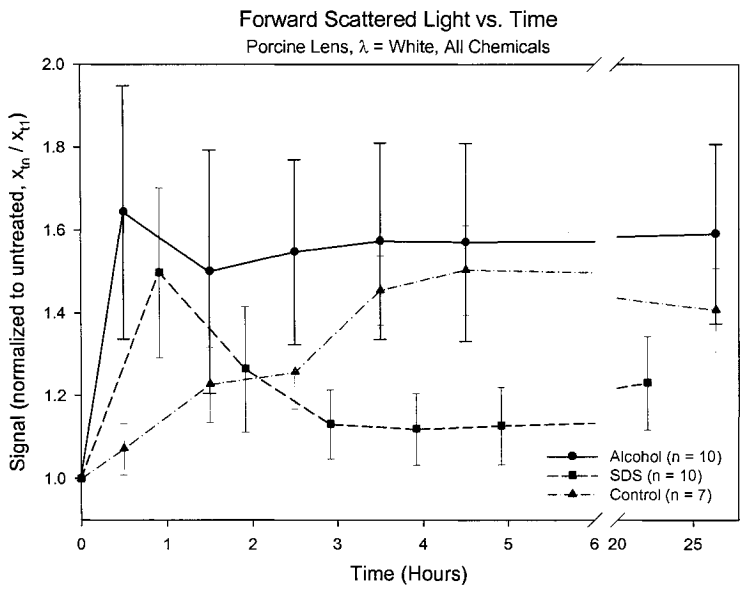

Figure 5-14: Forward Scattered Light vs. Time - Porcine Lens

FSL normalized to untreated condition at t = 0 hours using alcohol, SDS, and a control.

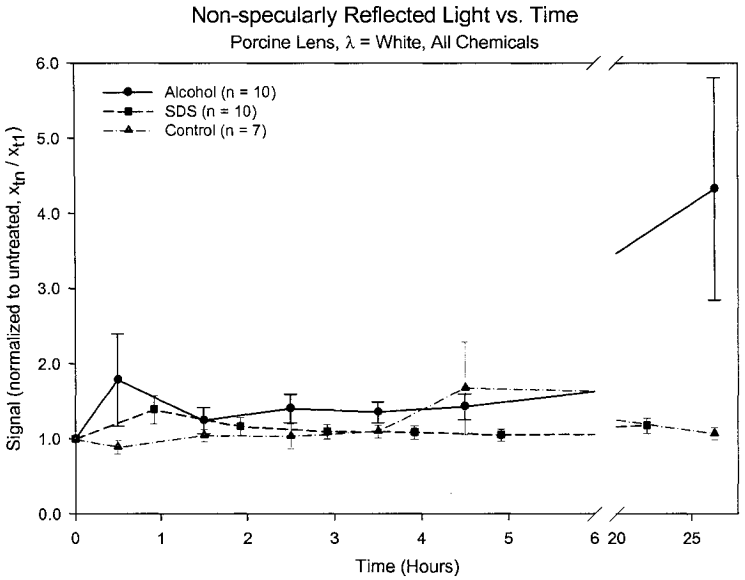

Figure 5-15: Specularly Reflected Light vs. Time - Porcine Lens

SRL normalized to untreated condition at t = 0 hours using alcohol, SDS, and a control.

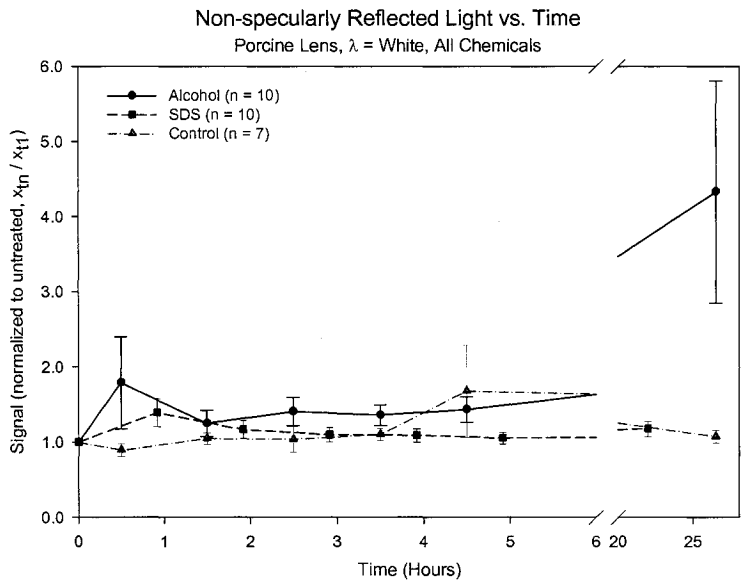

Figure 5-16: Non-specularly Reflected Light vs. Time - Porcine Lens

NSRL normalized to untreated condition at t = 0 hours using alcohol, SDS, and a control.

5.3.3 Optical Properties of Bovine Corneas

The purpose of this test is to observe changes in optical properties when three substances are applied to a bovine cornea. The three substances are: a 70% ethanol solution (alcohol), sodium dodecyl sulphate (SDS), and a control, D-MEM-F12. The corneal cells have a regenerative capability and the hypothesis is that this mechanism can be observed as a change in the optical measurement. Because of the large quantity of samples and the time required for testing, the tests were performed in two groups over a 24-hour period. As a result, two control groups were evaluated to determine if the time of death has any impact on the dynamic range of optical responses. This test is also used to determine the efficacy of the containment rings to control substance exposure for crystalline lenses previously used on bovine corneas, as is critical to keeping at least part of the corneal sample free of the applied substance.

Whole bovine eyes and divided into two equal-sized groups for which the time of death was known to within 2 hours. For the first group, the corneas were excised immediately, and for the second group the whole eyes were stored in a medium used by eye banks at 4° C and the corneas excised the following day. The first group was used to assess a 70% ethanol solution (alcohol) and a control, while the second group was used to assess the response of SDS and a second control. The treatment and measurement protocols are identical for both groups. Immediately after excision, the samples were placed in a four-part chamber, which were in turn placed in a tray as shown in Figure 5-11, and the entire tray was filled with 13 ml of D-MEM/F12 (nutrient medium). After the optical properties were measured (untreated), the tissues were then transferred to a tray (treatment tray) and a nylon containment ring (washer) placed on each of the tissues. A volume of 75 μl of the test substance was placed within the containment ring and the tissues were left for 10 minutes. The tissues were then rinsed and drained, without moving the washers, to minimize the impact of the test substance on the unaffected are of the tissue. The tissues were then returned to the optical trays and the optical test was performed every 30 minutes for a total of 3 hours.

Exposure to alcohol results in an abrupt decrease of TL from 70% to 31% at acute conditions with little long-term recovery as presented in Figure 5-18 and it can be observed in Figure 5-17 as a hazy area. Exposure to SDS results in a slight increase in TL followed by a gradual decrease over the 3-hour duration. Exposure to the first control results in an abrupt decrease in TL at acute condition from 77% to 55% compared with a more gradual overall decrease in TL as observed with second control. This data suggests that the fresher the sample, the more responsive it is to a substance, and that perhaps the control used was not a negative control.

Exposure to alcohol results in an abrupt increase in FSL from 4% to 27% at acute condition as presented in Figure 5-19. The increase in FSL is consistent with a decrease in TL. Exposure to SDS results in a gradual increase in FSL from 7% at acute condition to 10% at test-end. Exposure to first control results in an increase in FSL from 2% to 10% at acute condition compared with a more gradual overall decrease in FSL for second control for the same time.

Exposure to alcohol results in a decrease in SRL from 2.1% to 1.1% at acute condition as presented in Figure 5-20. Exposure to SDS results in little change in SRL, except for an increase at 0.5 hours to 2.8%. The first control remains unchanged after exposure, while the second control exhibits a decrease in SRL from 3% to 2% over the test duration. A higher initial SRL for the older samples is possibly related to their 24-hour storage in a growth medium.

Exposure to alcohol results in an abrupt increase in NSRL from 10% to 23% at the acute state as presented in Figure 5-21. Exposure to SDS results in a long-term increase in NSRL to test-end. Exposure of the sample to the both controls results in a long-term increase in NSRL.

Results from this test suggest that the response of the bovine cornea to the application of a chemical can be measured as a change in its optical properties. As

well, a partial recovery in some of the optical properties is consistent with the repair mechanism of the cornea assuming it is kept in a suitable environment. The initial TL for the group measured on the first day (73.5 %) is higher than that of the group tested on the second day (62.1 %), suggesting that the corneas deteriorate over the first 24 hours post mortem. A separate pre-test determined that TL decays from 80% on the first day to 65% on the second day and 45% on the third day. This result partially contradicts the results of Gautheron *et al* (Gautheron, 1992), who stated that fresh corneas and corneas preserved for 48 hours had similar optical properties. If the tissues deteriorate sufficiently, the dynamic response, or change in optical signal, will not be large enough to provide meaningful data. The results by Gautheron *et al* presented a possible reason why exposure to SDS resulted in an increase in TL, rather than the expected decrease as caused by other surfactants. Gautheron *et al* stated that the SDS is actually destroying the epithelial layer of the cornea, leaving the stroma, which does not become opaque.

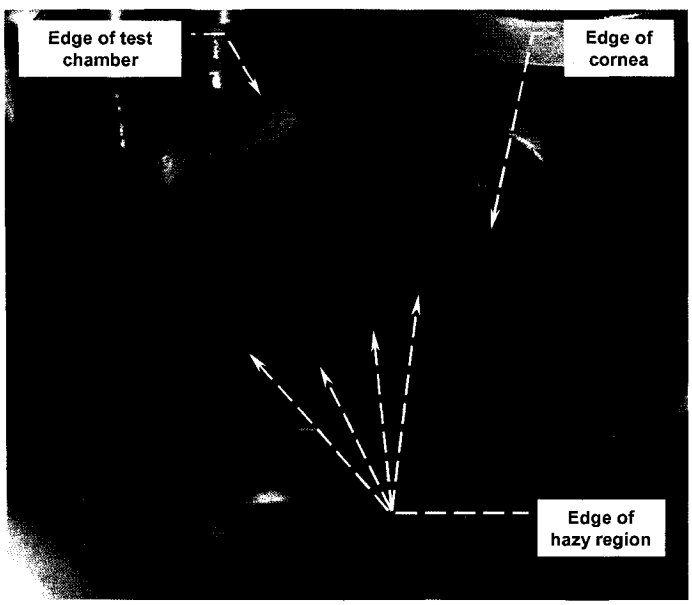

Figure 5-17: Haze-effect from alcohol exposure - Bovine Cornea

Exposure of bovine cornea to alcohol (hazy region) where the containment ring was able to confine the alcohol.

The results from this test can also be compared to the Draize toxicity test. The results presented in this work are not affected by the live-subject variability

previously described. In addition, measurements can be taken as often as every second with excellent repeatability compared with poor repeatability of the Draize test. The Draize test can only indirectly infer opacity and backscatter, and results are quantified using a coarse scale of 1 to 4. The Draize test also requires that a trained observer make this measurement, while this system has a large operating range and a greater sensitivity. As well, the tissue contact area can be modified using containment rings of varying sizes, a feature virtually impossible to achieve with a live animal subject.

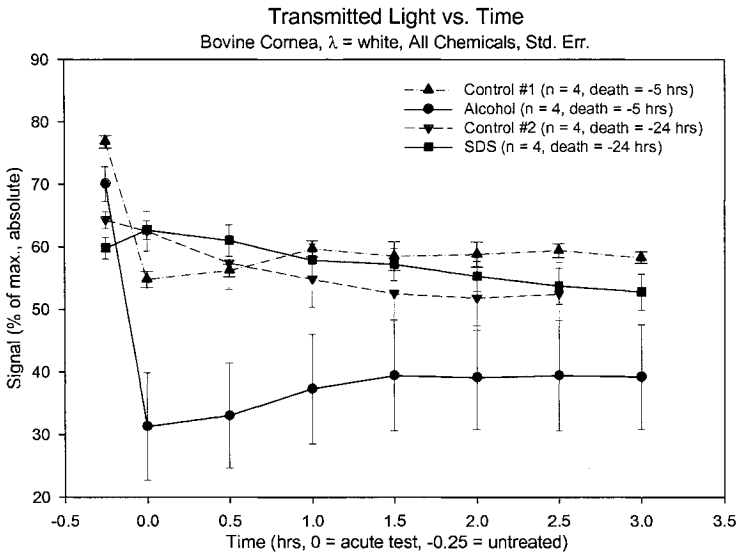

Figure 5-18: Transmitted Light vs. Time – Bovine Cornea

TL measured over a 3-hour period using alcohol, SDS, and 2 controls.

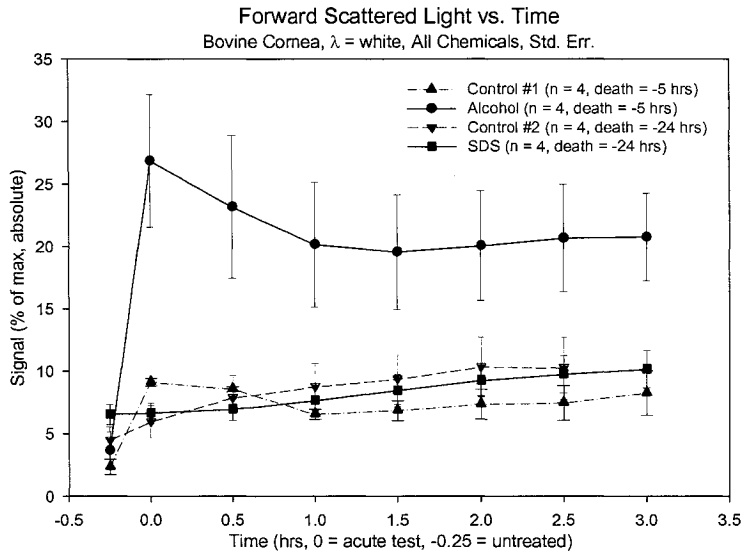

Figure 5-19: Forward Scattered Light vs. Time – Bovine Cornea

FSL measured over a 3-hour period using alcohol, SDS, and 2 controls.

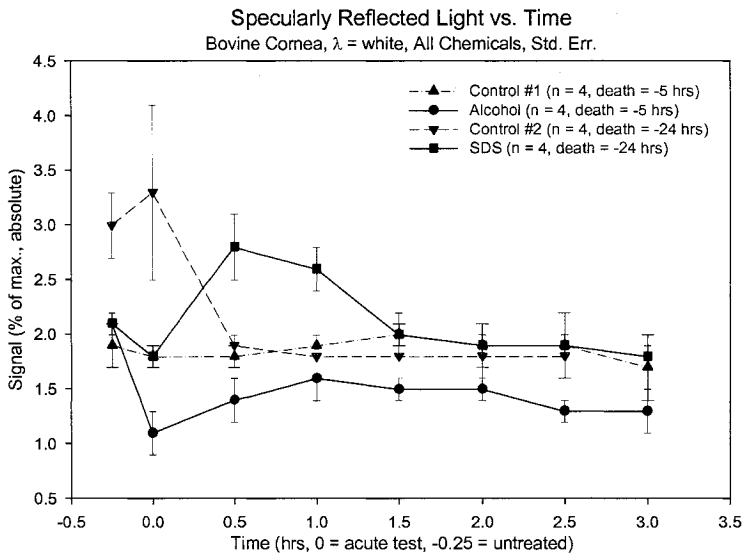

Figure 5-20: Specularly Reflected Light vs. Time – Bovine Cornea

SRL measured over a 3-hour period using alcohol, SDS, and 2 controls.

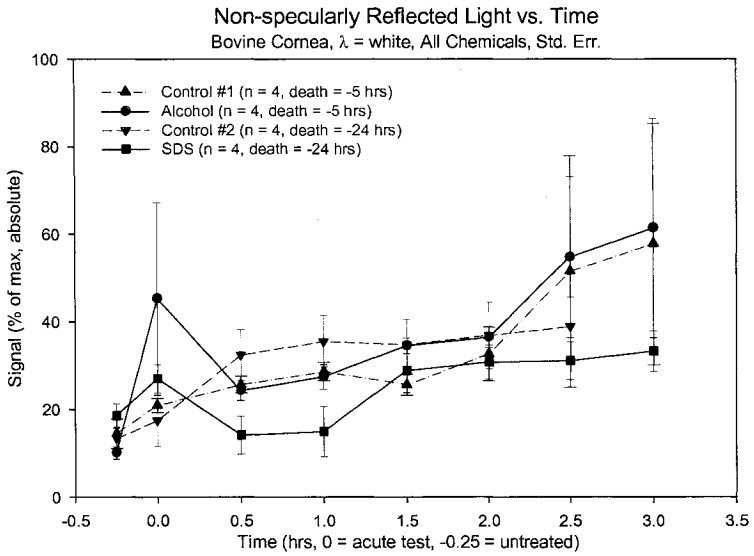

Figure 5-21: Non-specularly Reflected Light vs. Time – Bovine Cornea

NSRL measured over a 3-hour period using alcohol, SDS, and 2 controls..

5.3.4 Optical Properties of Human Corneas

The purpose of this test is to determine if human corneas can be used for toxicity screening testing. All whole eyes and corneas were obtained from cadavers destined for scientific research. The corneas were excised from the whole eyes immediately prior to testing.

After excision, the corneas were separated into two groups and tested using the same protocols as used with the bovine cornea. The first group of three samples was exposed to 10 μL of SDS using the containment ring described in previous sections, while the second group was not exposed to any substance. TL is measured using the visible spectrum for both groups prior to the exposure process, immediately afterwards, and then every 15 minutes for the first hour and then every hour for a total of three hours.

Only one of the controls (#303) exhibits a gradual decrease in TL and this same sample is the only one to have greater than 50% TL for the initial test as

presented in Figure 5-22. All of the tissues were 2 to 3 weeks old, and as a result do not perform well as toxicity test tissues. From previous testing with bovine corneas, it is known that corneas should be used no later than 48 hours from time of death. Another important factor in using human corneas for testing is that corneas are often only available after being rejected for human transplant surgeries or other research. For this reason, they are not recommended for any optically based screening tests.

5.4 Summary

Results of synthetic and natural material testing prove that the system is a useful tool in assessing the changes in optical properties of biological samples due to a stimulus. Numerous test results demonstrate that optical properties will change depending on the type of chemicals applied to stress the biological system. As well, some of the optical properties exhibit temporal variations. New methods and protocols have also been developed to further optimize the system's capability to be used with biological samples.

Equivalency to three established biological assay techniques was verified. The forward scatter measurement is comparable to the BVD test by Sivak, but also provides spectral data. Tissue transparency results are comparable to the BCOP test developed by Gautheron, but offer greater sensitivity and objectivity. The system's increased sensitivity to small changes suggests that corneal tissues have more subtle changes than stated by Gautheron *et al.* The quality and objectivity of the system's data is even more compelling when compared to the Draize toxicity test, not to mention the advantages of not requiring live test subjects.

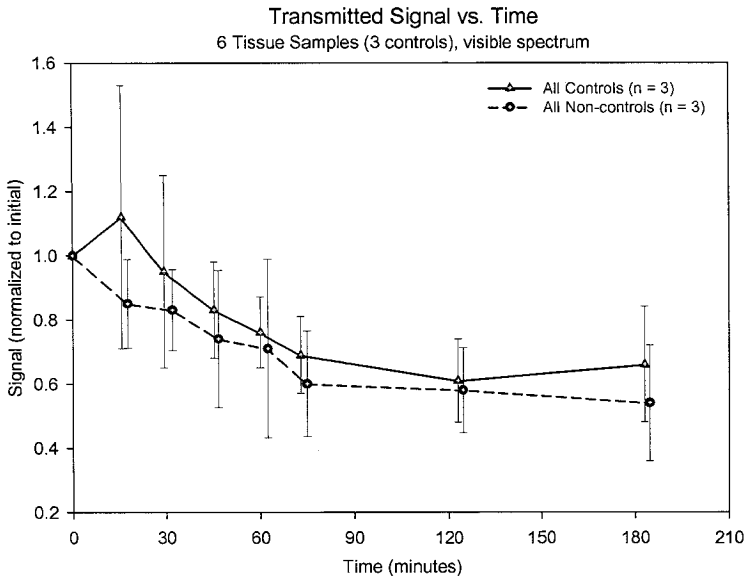

Figure 5-22: Transmitted Light (Normalized) vs. Time - Human corneas

Data normalized to initial values. With the exception of sample #178, relative TL decreased by 30-70% through to test-end.

6 Conclusion and Future Possibilities

There is an increasing need for assessing changes in biological systems in research and industry. Ideally, these assessment tools are non-invasive, allowing researchers to reduce sample quantity size and improve the quality of information. The hypothesis was that light could be used as an effective non-invasive probe. By designing, constructing, and testing it, a system that can measure transmitted light, forward scattered light, specularly reflected light, and non-specularly reflected light it is shown that light is an effective high quality probe to verify biological systems. The final version of this system was fully validated and it was demonstrated to have a repeatability of 0.02%, a reproducibility of 0.15%, a two-fold improvement in sensitivity over another system, and a threshold detection limit of 0.0063% of maximum signal. Protocols were developed and the light source drift was measured and accounted for in the calibration of the system.

Non-specularly reflected light was shown to be dependant on the position of the top surface of the sample as sample thickness is increased to 0.400". While this value is beyond the expected sample thickness, it can be corrected for using several possible design changes. A change in the upper surface location results in the light being less tightly focused on the detector. Therefore, a larger detector that is less sensitive to focusing changes (sample height) could be used. An alternate design could use a vertical translation stage to ensure a constant upper surface datum point, regardless of the sample thickness.

Finally, a testing regime was completed that utilized a wide variety of biological samples, both natural and synthetic for final validation. In completing this test plan, methodologies unique to optical testing of biological samples were also developed, verified, and implemented, which increased the overall confidence in the resulting measurands. Equivalency of the test results was established with several tests including the Draize irritancy test, the BCOP test, and the BVD test.

The system has proven in a research environment to be a valuable and reliable tool and is ready for additional opportunities in commercial and/or industrial laboratories. There are several applications for this system. Leaf optical property testing is one such area, where reflectance and transmittance are used to non-invasively monitor samples. Existing industrial paint quality systems uses more complex evaluation techniques, and thus could benefit from using this simple, robust, and precise system. Water turbidity is another possible area for this system because of the low cost compared to various laser-based techniques.

There are a number of areas for consideration for possible design improvements. Automated positioning and centering of the samples could further improve the reproducibility of the system. By using a linear or circular sample-mounting tray, the duration of the test could also be reduced. Detector mounting could be improved by reducing their mounting footprint and/or by placing automated shutters to eliminate specular reflection from the protective glass exterior of the detector. The absolute optical properties of the controls were determined using a lab-built integrating sphere. To improve the values of the absolute signal, a commercially available sphere should be utilized to verify these measurands.

Bibliography

1 P. Greenbaum, "Scanning the Emerging Areas," in *Engineering Dimensions*, vol. Nov-Dec 03, 2003, pp. 32-35.

2 European Communities, 2003, "European Parliament approves animal testing and marketing ban for cosmetics (76/768/EEC)", web site, http://www.eubusiness.com/imported/2003/01/100971/

3 "Replacing the Draize eye irritation test: scientific background and research needs," presented at Journal of Toxicology-Cutaneous & Ocular Toxicology, 1996.

4 K. R. Wilhelmus, "The Draize eye test," *Surv Ophthalmol*, vol. 45, pp. 493-515, 2001.

5 M. Johnson, "Remote turbidity measurement with a laser reflectometer," *Water Science and Technology*, vol. 37, pp. 255-261, 1998.

6 J. Jacquemoud and S. Ustin, "Leaf optical properties: A state of the art," presented at International Symposium Physical Measurements & Signatures in remote sensing, Aussois, France, 2001.

7 J. Scheers, M. Vermeulen, C. de Maré, and K. Meseure, "Assessment of Steel Surface Roughness and Waviness in relation with Paint Appearance," *International Journal of Machine Tools and Manufacture*, vol. 38, pp. 647-656, 1998.

8 P. Gautheron, M. Dukic, D. Alix, and J. Sina, "Bovine Corneal Opacity and Permeability Test: An In Vitro Assay of Ocular Irritancy," *Fundamental and Applied Toxicology*, vol. 18, pp. 442-449, 1992.

9 P. Gautheron, J. Giroux, M. Cottin, L. Audegond, A. Morilla, L. Mayordomo-Blanco, A. Tortajada, G. Haynes, V. J., R. Pirovano, E. Gillio Tos, C. Hagemann, P. Vanparys, G. Deknudt, G. Jacobs, M. Prinsen, S. Kalweit, and H. Speilman, "Interlaboratory assessment of the bovine corneal opacity and permeability (BCOP) assay," *Toxicol In Vitro*, vol. 8, pp. 381-392, 1994.

10 P. L. Casterton, L. Potts, and B. Klein, "A Novel approach to assessing eye irritation potential using the bovine corneal opacity and permeability assay," *Journal of Toxicology-Cutaneous & Ocular Toxicology*, vol. 15, pp. 147-163, 1996.

11 L. Bousse, C. Cohen, T. Nikiforov, A. Chow, A. R. Kopf-Sill, R. Dubrow, and J. W. Parce, "Electrokinetically Controlled Microfluidic Analysis Systems," *Annual Review of Biophysics and Biomolecular Structure*, vol. 29, pp. 155-181, 2000.

12 S. Burchiel, F. T. Lauer, D. Gurulé, B. J. Mounho, and V. M. Salas, "Uses and Future Applications of Flow Cytometry in Immunotoxicity Testing," *Methods*, vol. 19, pp. 28-35, 1999.

13 R. D. Jiji, "A simple, low-cost, remote fiber-optic micro volume fluorescence flowcell for capillary flow-injection analysis," *Analytical and Bioanalytical Chemistry*, vol. 374, pp. 385 - 389, 2002.

14 R. S. Gurjar, V. Backman, L. T. Perelman, I. Georgakoudi, K. Badizadegan, I. Itzkan, R. R. Dasari, and M. S. Feld, "Imaging human epithelial properties with polarized light-scattering spectroscopy," *Nat Med*, vol. 7, pp. 1245-8, 2001.

15 V. Bantseev, D. McCanna, A. Banh, W. W. Wong, K. L. Moran, D. G. Dixon, J. R. Trevithick, and J. G. Sivak, "Mechanisms of ocular toxicity using the in vitro

bovine lens and sodium dodecyl sulfate as a chemical model," *Toxicological Sciences*, vol. 73, pp. 98-107, 2003.
16 A. Hartwick, J. G. Sivak, and K. L. Herbert, "Relative toxicity of three corneal anesthetics measured in vitro with the cultured bovine lens," *Journal of Toxicology-Cutaneous & Ocular Toxicology*, vol. 16, pp. 253-266, 1997.
17 J. G. Sivak and K. L. Herbert, "Optical damage recovery of the in vitro bovine ocular lens for alcohols, surfactants, acetates, ketones, aromatics, and some consumer products: A review," *Journal of Toxicology-Cutaneous & Ocular Toxicology*, vol. 16, pp. 173-187, 1997.
18 R. Farrell, R. McCally, and P. Tatham, "Wave-length Dependencies of Light Scattering in Normal and Cold rabbit corneas and their Structural Implications," *J. Physiol.*, vol. 233, pp. 589-, 1973.
19 O. Kostyuk, O. Nalovina, T. M. Mubard, J. W. Regini, K. M. Meek, A. J. Quantock, G. F. Elliott, and S. A. Hodson, "Transparency of the Bovine Corneal Stroma at Physiological Hydration and its Dependence on Concentration of the Ambient Anion," *J Physiol (Lond)*, vol. 543, pp. 633-642, 2002.
20 D. Priest and R. Munger, "A New Instrument for Monitoring the Optical Properties of Corneas," *IOVS Poster Presentation*, vol. 39, pp. S352, 1998.
21 Labsphere Inc., "A Guide to Integrating Sphere Theory and Applications", web, Mar 2004, http://www.labsphere.com/tech_info/docs/IS_Theory_Application.pdf
22 J. Zwinkels, "Spectrophotometry," *Seminar on Photometry*. Ottawa: National Research Coucil (Canada), 1989, pp. 107-122.
23 A. Nussbaum and R. Phillips, 1976, *Contemporary Optics for Scientists and Engineers*, 3 ed, Prentice-Hall.
24 X. Fuentes-Arderiu, "Glossary of ISO metrological and related terms and definitions relevant to clinical laboratory sciences." http://www.westgard.com/isoglossary.htm
25 *The Oxford Reference Dictionary*, Oxford University Press, Oxford, UK.
26 D. Sliney and M. Wolbarsht, 1980, *Safety with Lasers and Other Optical Sources*, 4 ed, Plenum Press, New York.
27 W. T. Welford, 1986, *Aberrations of Optical Systems*, IOP Publishing, Bristol, England.

Appendix A: Equipment List

Item	*Detailed*	*Manufacturer*	*Model/Part number*
Culture Chamber	Transwell-Clear	Corning Costar Corp.	3450, 3650
Culture Chamber	Glass bottom	MatTek Corp.	P35G-0-14-C
Culture Chamber	Polystyrene	Corning Life Sciences	430165
Culture Medium	Modified Eagle Medium with L-glutamine, pyridoxine HCl, without Herpes buffer, without phenol red	Gibco BRL	D-MEM/F12 (cat # 21041-025)
Digital Multimeter	(s/n 0941919)	Keithley	2000
Digital Multimeter	(s/n US36080909)	Hewlett Packard	34401
Filter (optical)	Set of six, broadband, 40nm wide, 450-,500-, 550-, 600-, 650nm	Ealing	unknown
GPIB Cable	(s/n 0156327B)	Amphenol	488-C156327B
Lens 1	achromatic lens, f = 10cm, dia = 25 cm	Melles Griot	unknown
Lens 2	achromatic lens, f = 100cm, dia = 30 cm	Edmund Scientific	F32-500
Lens 3	achromatic lens, f = 100cm, dia =30 cm	Edmund Scientific	F32-500
Light Source	250W halogen light source	Carl Zeiss	KL Series
Mirror	Parabolic mirror	Perkin Elmer	PB-117
Opal Diffuser	25mm ∅	Edmund Scientific	H43-717
Photo Detector	Si Photodiode	Hamamatsu	S2386-45k
Scanner Card	For digital multimeter	Keithley	2000/2000-SCAN-

Item	*Detailed*	*Manufacturer*	*Model/Part number*
			10
Spectrophotometer	400 – 800 nm grating-based, < 3 nm, 1 μs integration time	Thorlabs	SP1
Tissue Culture Dish	60x15mm polystyrene	Becton Dickinson Laboratories	35-3002
Laser Power Meter	400 – 1064nm, 10mW	Coherent – Auburn Group	Laser Check

Appendix B: Optical Concepts

Imaging vs. Non-imaging System

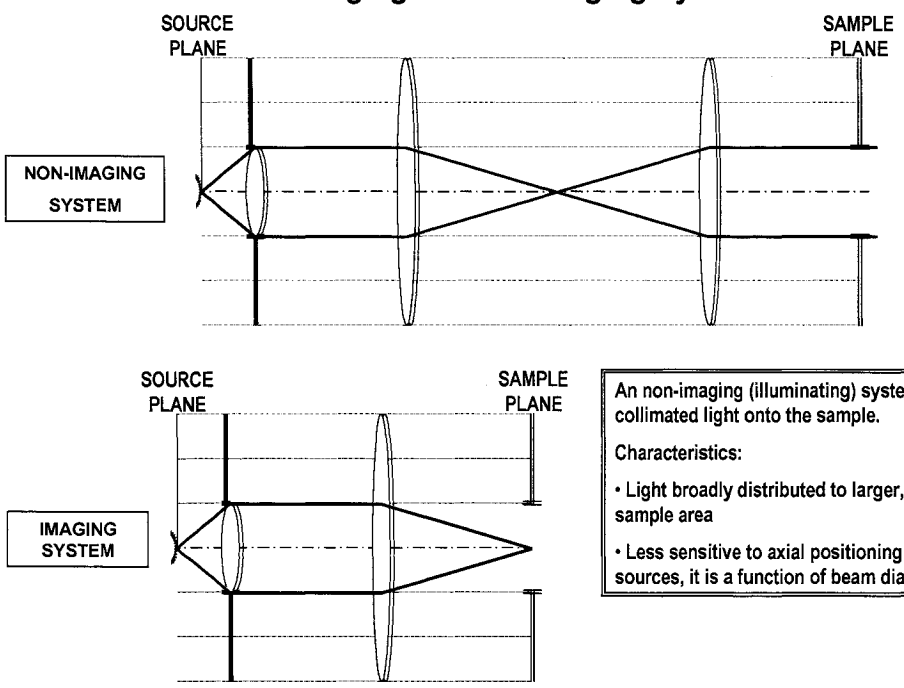

An non-imaging (illuminating) system projects collimated light onto the sample.

Characteristics:

- Light broadly distributed to larger, definable sample area
- Less sensitive to axial positioning (for extended sources, it is a function of beam diameter)

Magnification/Minification of Beam Size

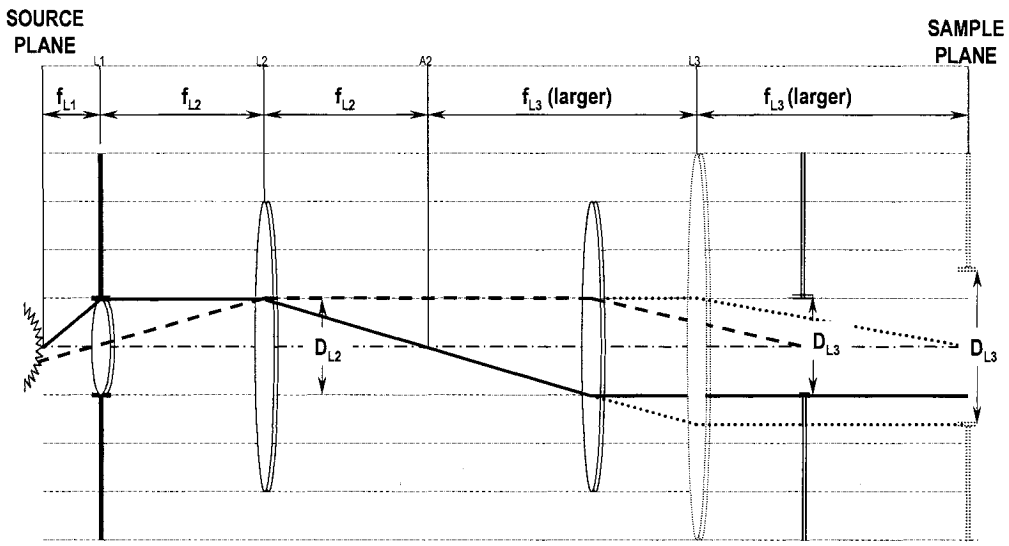

Magnification of beam diameter from L2 to sample plane is defined by the focal length ratio $M = F_{L3} / F_{L2} = D_{L3} / D_{L2}$. Note that overall track length is also affected.

3 Lens System

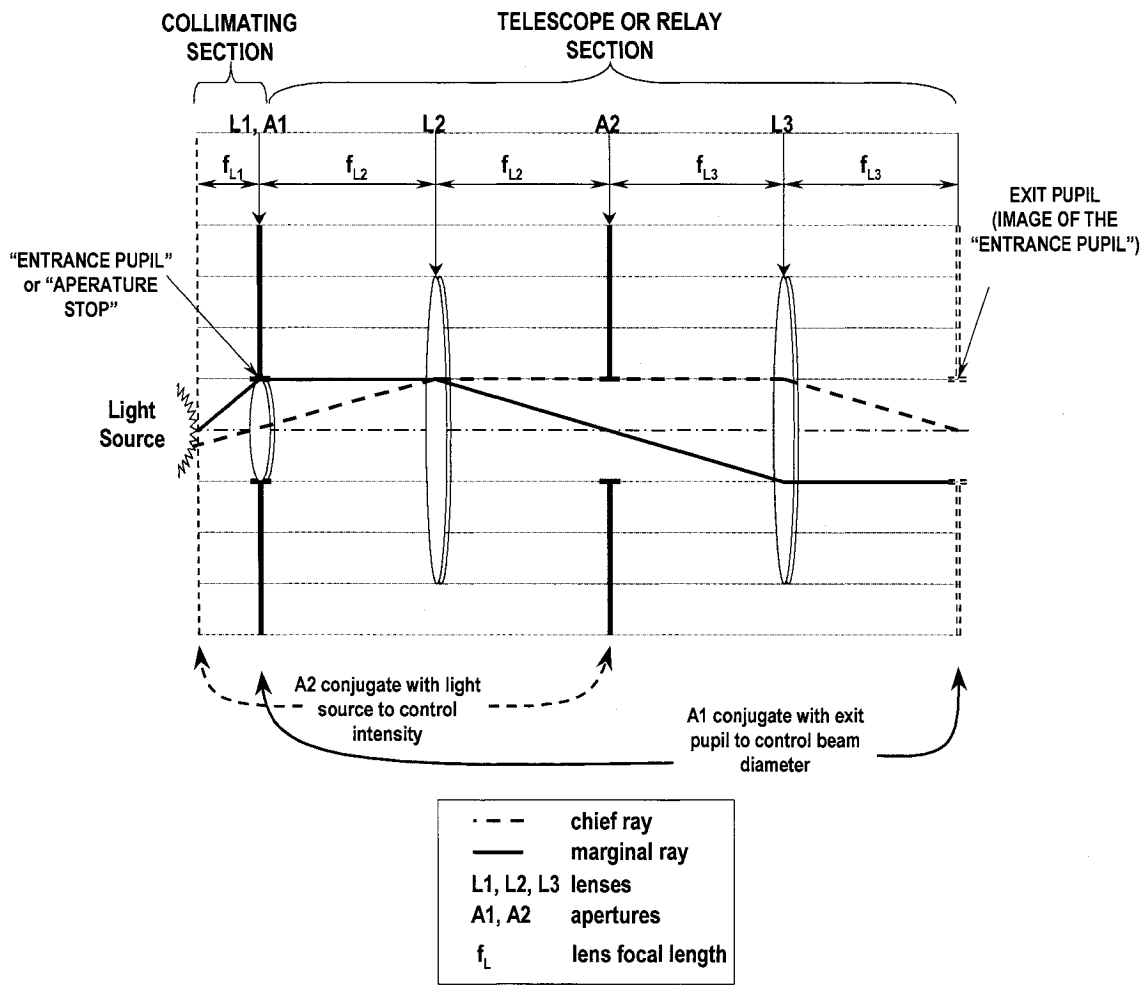

The three-lens system is used to collimate and magnify the light from an extended source onto the sample plane. The 1st lens collimates the light while the remaining 2 magnify the light from the extended source (fiber tip) to the sample plane (exit pupil).

Beam size change using Aperture 1

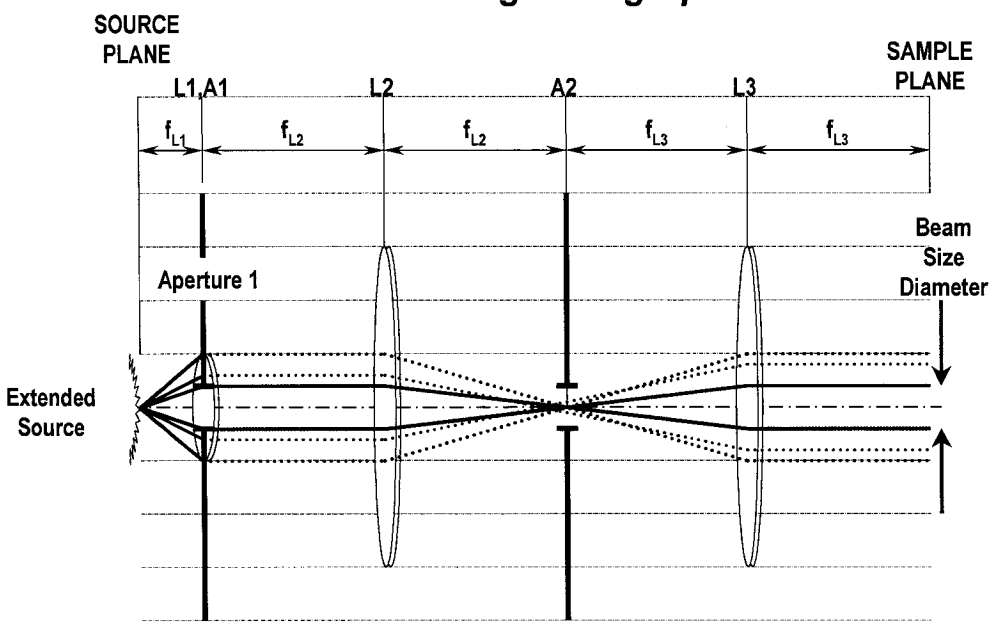

Variation of the diameter of aperture 1 (A1) changes beam diameter at the sample plane (exit plane – secondary focal plane of L3), independent of intensity (power per unit area) changes.

Intensity change using Aperture 2

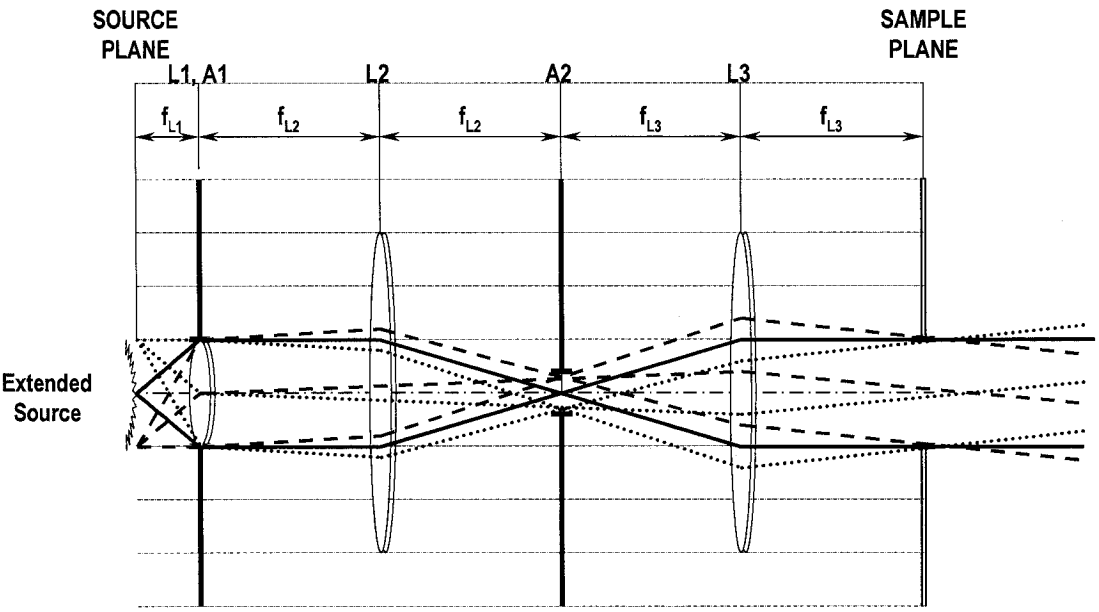

Variation of the diameter of aperture 2 (A2) changes beam intensity at the sample plane (exit plane), independent of beam diameter changes.

Appendix C: Design Schematic

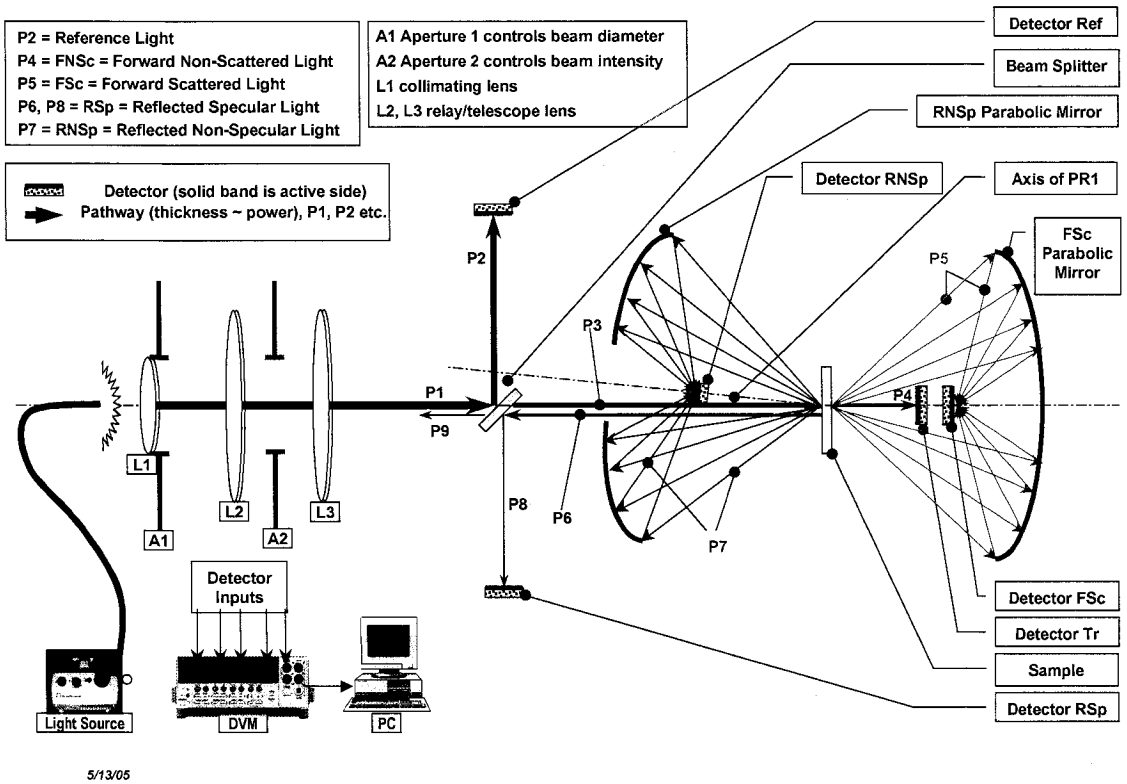

Appendix D: Detector Mounting Details

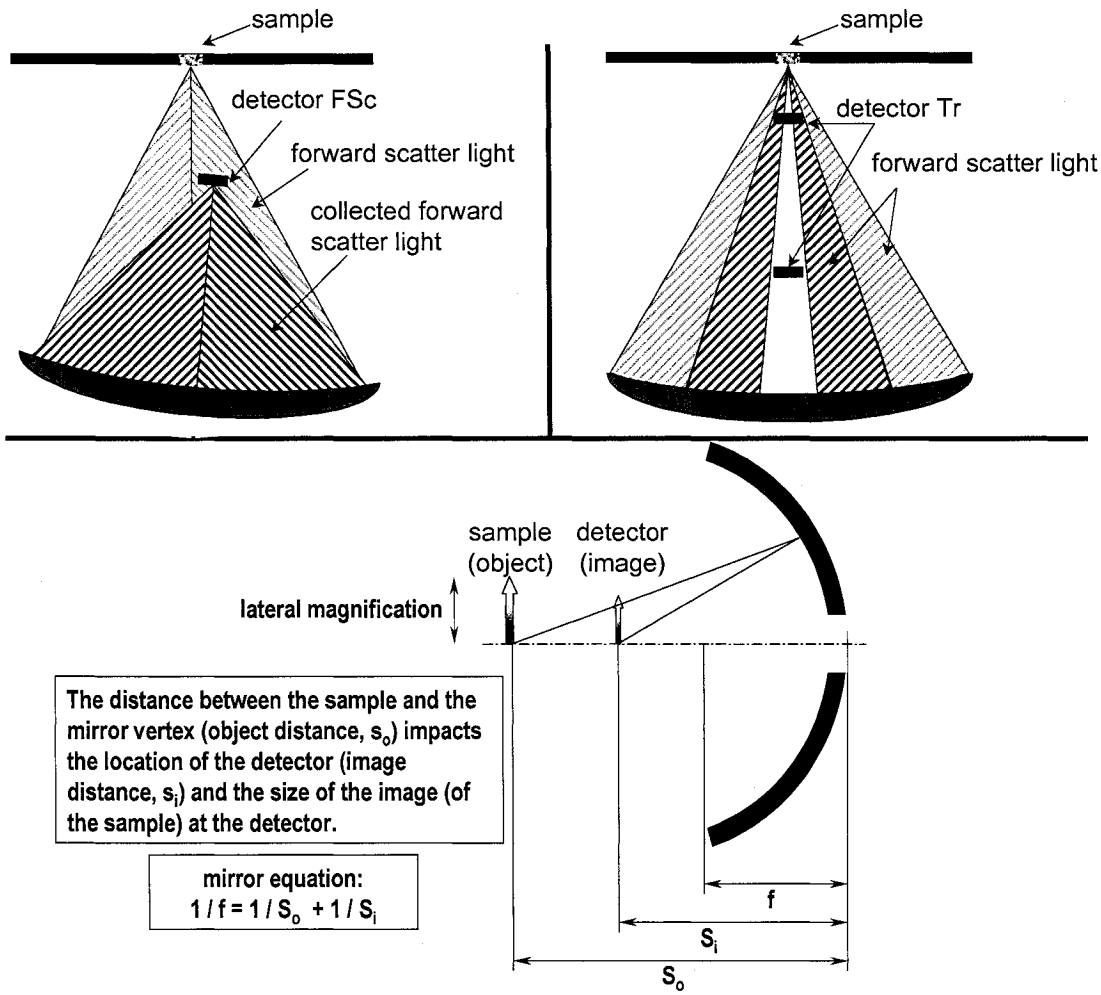

The upper left image shows that the detector for forward scatter captures the scattered light and is angled away from the central axis as the detector would otherwise be too close to the detector for transmitted light (Tr). The upper right image shows that if the detector is placed too close to the sample, the detector captures unwanted scattered light as well as blocks this scattered light from reaching FSc detector. The lower image applies to both the upper mirror (non-specularly reflected light) and the lower mirror (forward scattered light) and shows that the placement of the mirror defines the lateral dimensions of the imaged light at the detector (and thus the signal strength detected) as well as axial location of the detector.

Appendix E: Optical Layout Drawing

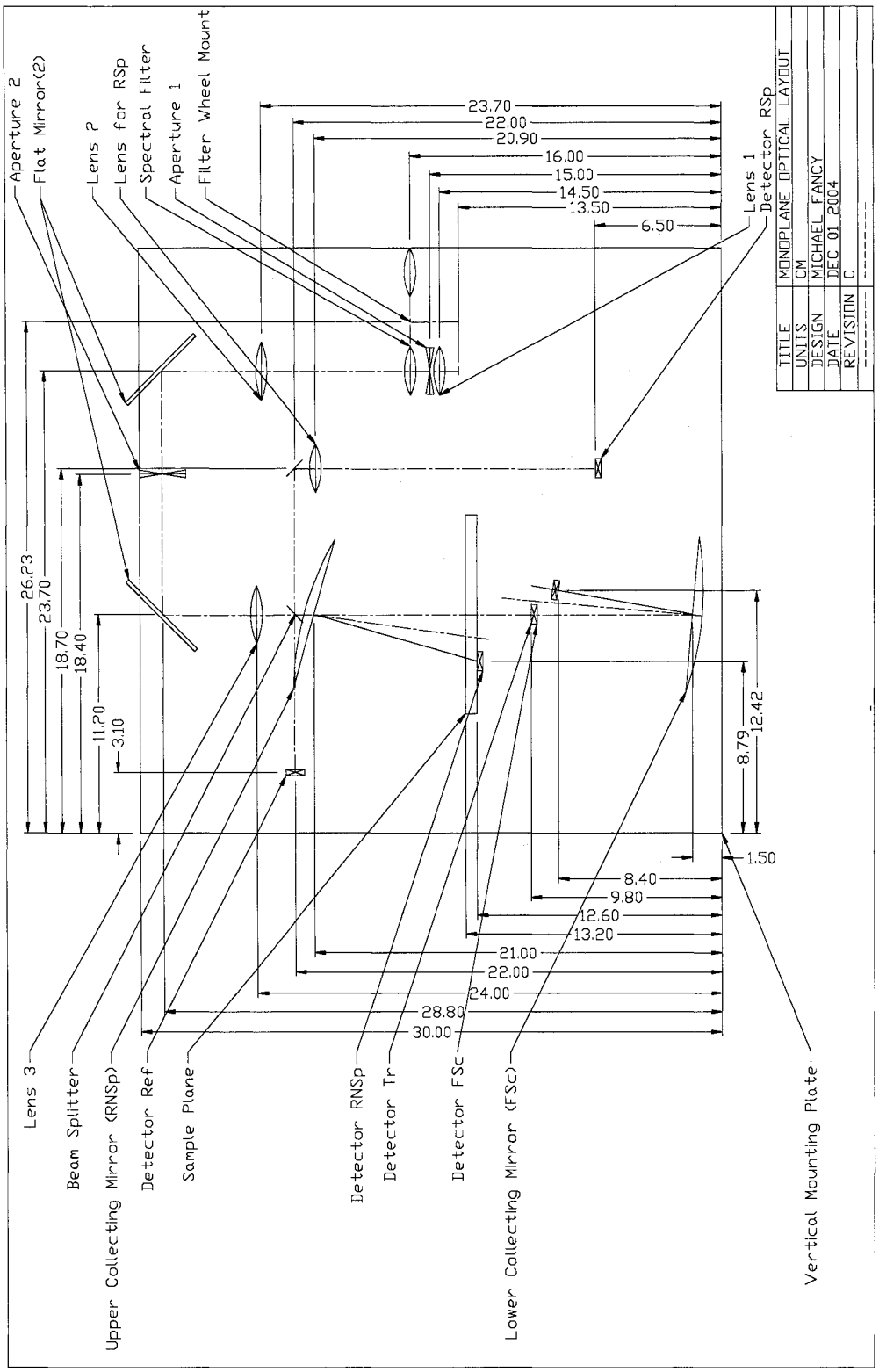

Appendix F: Beam Splitter Optimization

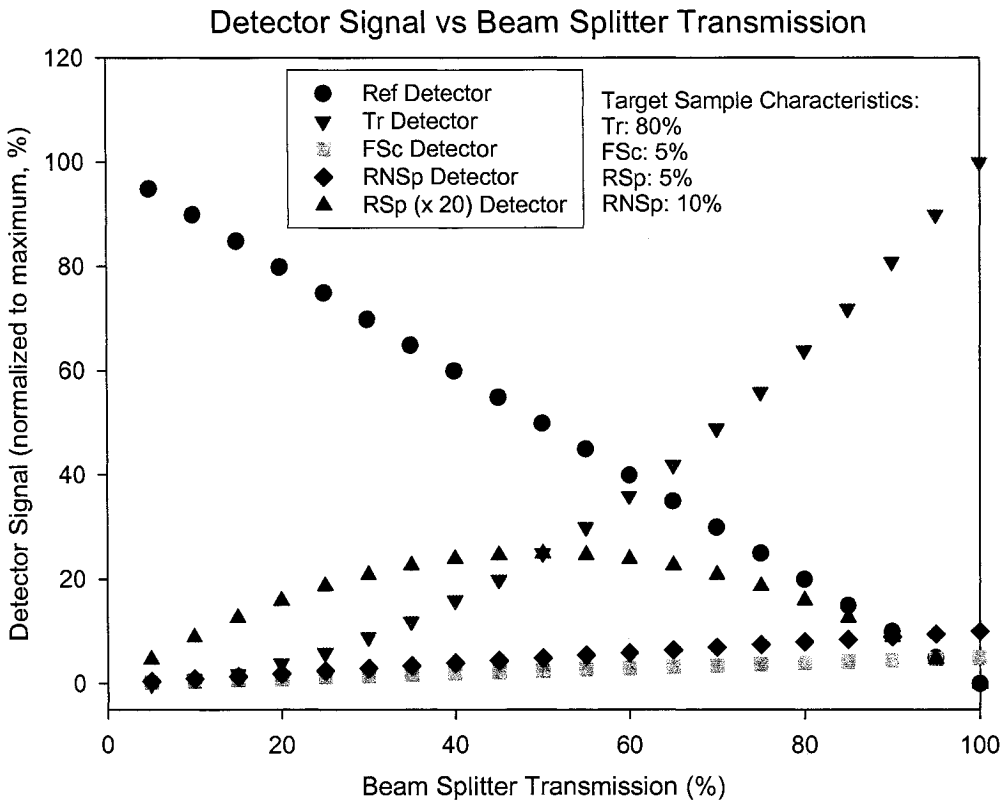

Various beam splitter designs and the resulting impact on the four detectors assuming an ideal target sample. The weakest of the five system signals is at the RSp detector (0% to 1.3%) and therefore is the critical variable with a peak using a beam splitter with 50% transmission (50% reflected) is used.

Appendix G: Ray Tracing Program

The author completed a special studies course as part of the academic requirements for the Masters Degree Program. As a component of the course, a software program was created to specifically consider which conic type (ε) best maximizes the light gathering efficiency of the collecting mirrors. The program also considers the impact of sample size and detector size on the collecting efficiency. Variables include the collecting mirror diameter, mirror focal length, mirror conic, mirror tilt angle, location (x, y, z) and size of test sample and detector, and sample scatter angle.

The test sample is represented optically as an extended object using a grid of 5 x 5 points. The sample is the round region illuminated by the light source, but for ease of programming, a square grid is chosen. Each of the 25 points in turn produces scatter approximated by a cone defined by four boundary quadrant vectors and one central vector. These 125 rays (vectors) are directed to the collecting mirror and reflected to the detector. The location for the detector is optimized to capture the greatest percentage of the 125 vectors, which defines the system collection efficiency, and is proportional to the expected light intensity.

The following physical dimensions are those used in the system (unless otherwise indicated): mirror size - 70 mm X 70 mm square (actual 80 cm ∅), mirror focal length (f_m) - 41 mm, sample size of 2.1 mm x 2.1 mm (actual 2 to 6 mm ∅), detector size - 6.4 mm ∅ (actual 3.9 mm x 4.6 mm), and a mirror tilt angle of 5°. The lateral location of the detector is optimized as a function of ε. The axial distance to the mirror of the detector (image plane) and the sample (object plane) are 84mm, which is 2 x f_m, and close to that used in the actual setup. The model does not consider the variation in signal intensity as a function of the angle measured from the surface normal, which often follows Lambert's law [26]. As well, using only four vectors to define the boundary of the cone of scatter resulting in data that is not as smooth observed in the actual setup. The

code is based on an algorithm created by W.T Welford [27] and the programming language is MatLab ®. This particular algorithm does not utilize any paraxial approximations. As well, it is based on vector equations, greatly simplifying the programming. A summary of the key variables is shown in Appendix Figure 1.

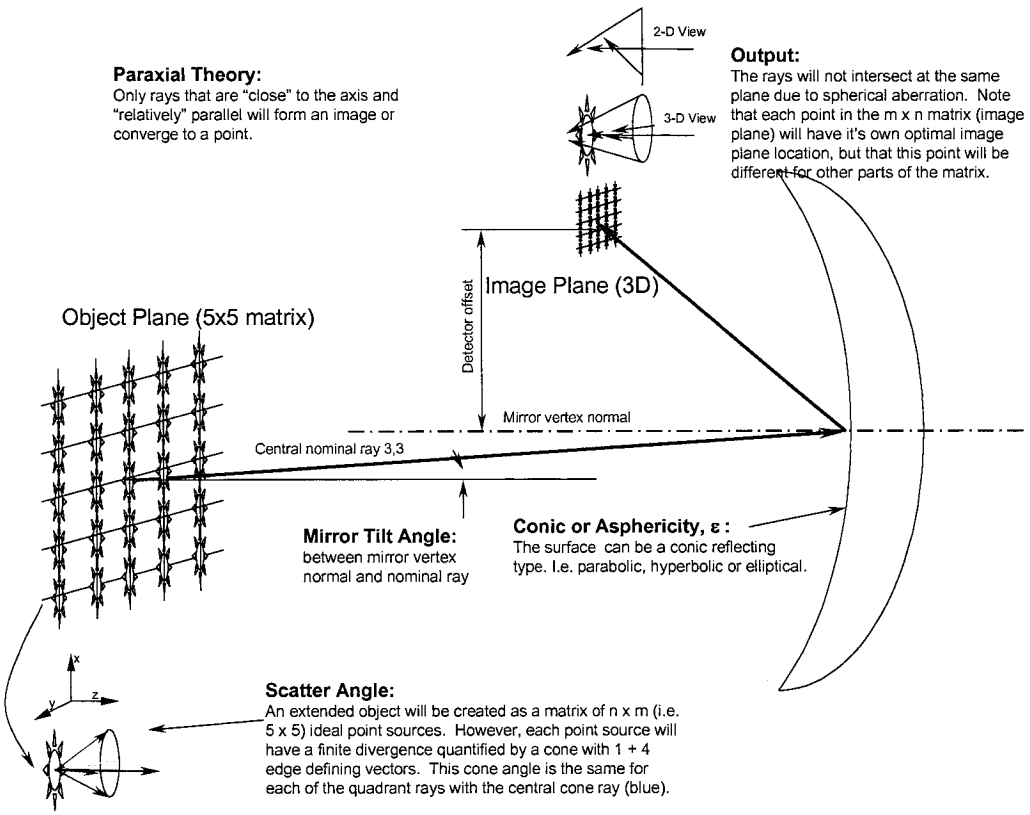

Appendix Figure 1: Algorithm Variables

Key variables in the algorithm are represented in graphical format. The sample is defined as a matrix of 25 points. Each point emits scatter with an angle measured from the surface normal and forming a cone defined by four quadrant vectors as well as one central vector. Vectors from each of the 25 points are reflected by a mirror of conic ε to the detector (image plane). The mirror collecting efficiency is defined by the percentage of original rays leaving the source that intersect the image plane and confined to the lateral dimensions of the detector.

Graphical results using a parabolic mirror (paraboloid), the parameters defined

above, and scatter angles from 5° to 20° are presented in Appendix Figure 2. Increasing the scatter angle, which tests the image quality at the detector, decreases the mirror collecting efficiency from 86% to 40%. Results of varying both ε and scatter angle are presented in Appendix Figure 3. Maximum efficiency of 89.6% is achieved with scatter less than 6° for all conics (ε = -2.0 to 1.25). However, as scatter angle increases to 20°, the mean efficiency for all conics reduces to 58%, more acutely with hyperboloids and oblate ellipsoids. Both the paraboloid (ε = 0) and the oblate ellipsoid (peak ε = 0.75) are less sensitive to increased scatter: over the scatter range of 5° to 20°, paraboloid efficiency is 76.7% while oblate ellipsoid (ε = 0.75) efficiency is 82.8%; over the scatter range of 5° to 10°, paraboloid efficiency is 88.2% while oblate ellipsoid (ε = 0.75) efficiency is 84.4%. Therefore, both the paraboloid and ellipsoid conics provide the best overall mirror collecting efficiency.

Some of the data set does not vary smoothly, and is possibly the result of the low number of scatter vectors defining the extended object. Ideally, the program is modified to increase the flexibility of the code to allow for more realistic scatter profiles. However, not all conics are available as off-the-shelf components, and as such, their purchase would have added to the logistical challenges of this project. However, the results did indicate that the parabolic collecting mirror was an ideal selection, and helped validate the design process.

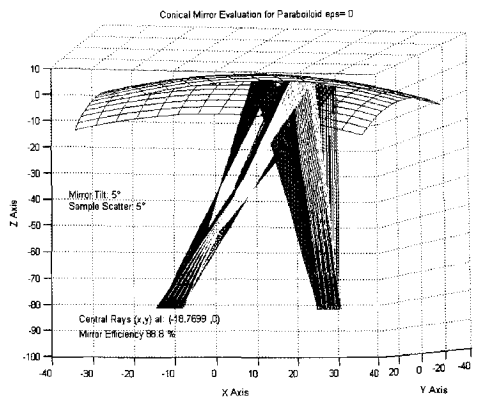

Sample Scatter Angle: 5°

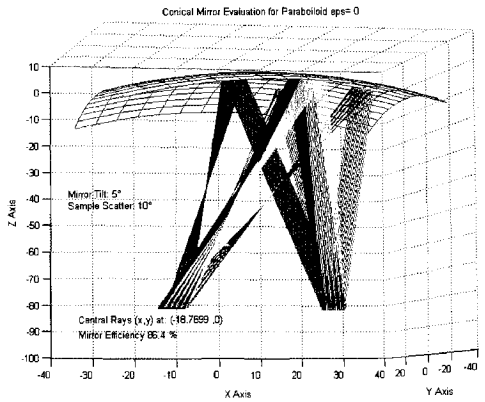

Sample Scatter Angle: 10°

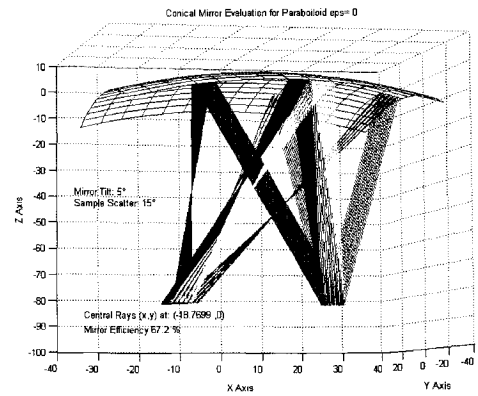

Sample Scatter Angle: 15°

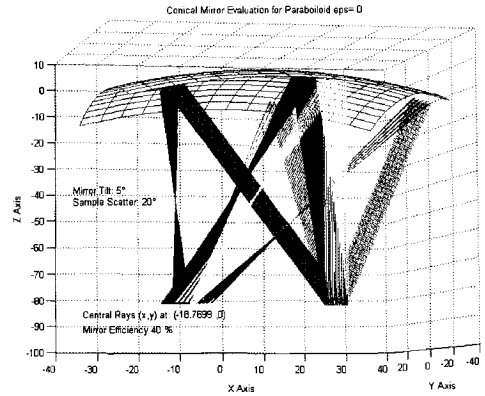

Sample Scatter Angle: 20°

Appendix Figure 1: Collection Efficiency vs. Scatter Angle

Results from MatLab® routine written by the author to predict mirror collection efficiency. The rays originate from a sample 7mm square composed of a 5 x 5 finite grid representing and 'extended object'. The scatter from each one of the 25 source points (collectively creating an extended object) is approximated by a cone defined by 4 quadrant vectors (central vector is coloured dark blue). The rays reflect off the conic surface (paraboloid shown above) and end at the detector plane measuring 7.2mm ∅, representing the 'image plane'. As the scatter angle is progressively increased from 5° to 20°, while other variables are kept constant, the efficiency decreases from 88.8% to 40%.

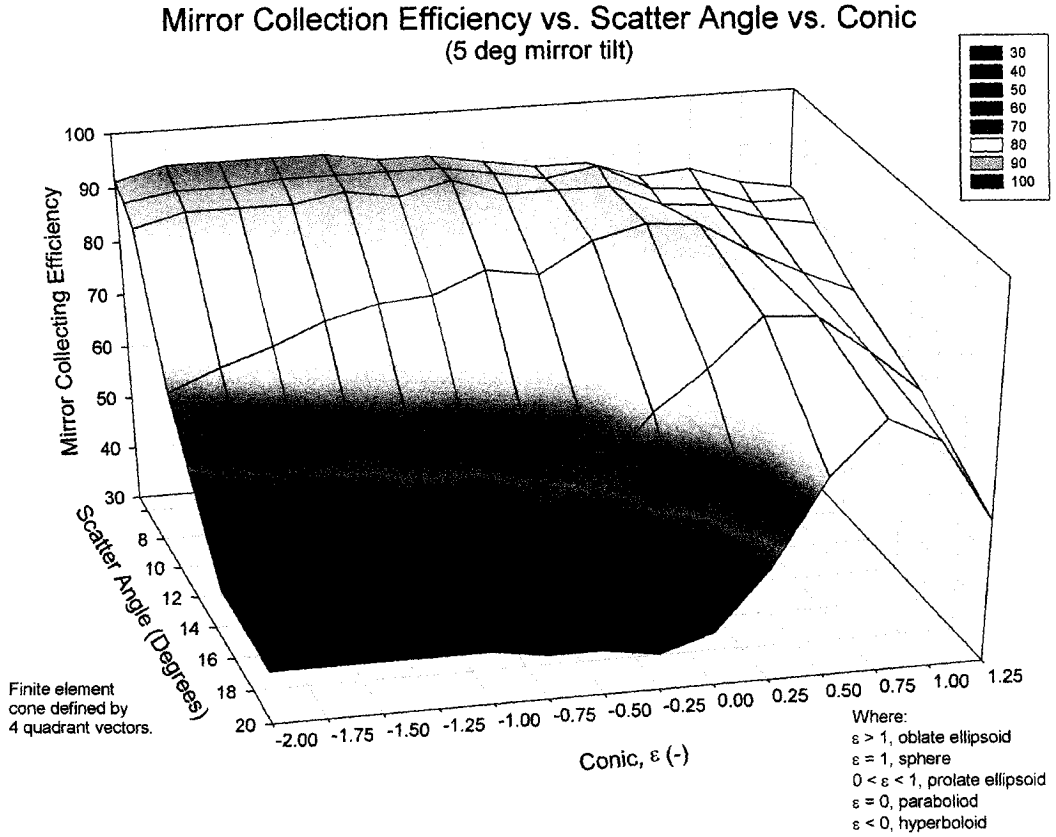

Appendix Figure 2: Collection Efficiency vs. Scatter Angle vs. Conic

The mean mirror collection efficiency is representative of light intensity. The efficiency for all conics (ε) is 89.6% for low scatter (≤6°). Higher scatter of 15% reduces the conic mean efficiency to 58%, and particularly for hyperboloids and oblate ellipsoids. Paraboloids maintain 76.7% over the scatter range of 5-20° scatter but a mean efficiency of 82.8% is achieved for the same scatter range using an oblate ellipsoid (ε = 0.75).

Appendix H: System Calibration Flow Chart